

# **Fabrication of Polymersomes using Microfluidic Devices**

**DOCTORAL THESIS  
(Dissertation)**

to be awarded the degree of Doctor rerum naturalium (Dr. rer. nat.) at  
the Faculty of Biology, Chemistry and Earth Sciences, University of  
Bayreuth

submitted by

**Dipl. Chem. Julian Thiele**

from Hamburg

Bayreuth, 2011



The work described in this thesis was carried out at the Institute of Physical Chemistry at the University of Hamburg and the University of Bayreuth under the supervision of Prof. Stephan Förster as well as at the School of Engineering and Applied Sciences/Department of Physics at Harvard University under the supervision of Prof. David A. Weitz from September 2008 to January 2011.

Thesis submitted: 04/15/2011

Date of scientific colloquium: 11/16/2011

Jury:

Prof. Stephan Förster (Chief reviewer)

Prof. Thomas Pfohl (Second reviewer)

Prof. Thomas Scheibel (Third reviewer)

Prof. Axel Müller (Chairman)



*The Road not Taken*

from "Mountain Interval", Robert L. Frost, **1916**.



# Table of Contents

<b>Abbreviations, symbols and chemical structures .....</b>	<b>1</b>
<b>Summary .....</b>	<b>6</b>
<b>Zusammenfassung.....</b>	<b>8</b>
<b>1 Introduction.....</b>	<b>10</b>
1.1 Microfluidic devices - design, fabrication and application.....	11
1.1.1 PDMS-based microfluidic devices .....	13
1.2 Polymersomes - vesicular self-assemblies of diblock copolymers .....	20
1.2.1 Microfluidic polymersome fabrication techniques.....	29
1.3 Fluid flow in microchannels - manipulation and simulation .....	35
1.4 Motivation, objective and strategy of this thesis .....	47
1.5 References.....	51
<b>2 Thesis Overview .....</b>	<b>60</b>
2.1 Fabrication of polymersomes using flow focusing .....	61
2.2 Patterning microfluidic device wettability.....	64
2.3 One-step formation of multiple emulsions.....	68
2.4 Fabrication of polymersomes from double-emulsion templates.....	73
2.5 Appendix: Development and application of a microfluidic spray dryer .....	76
2.6 Individual contribution to joint publications.....	80

<b>3</b>	<b>Preparation of Monodisperse Block Copolymer Vesicles via Flow Focusing in Microfluidics .....</b>	<b>83</b>
<b>4</b>	<b>Patterning Microfluidic Device Wettability using Flow Confinement.....</b>	<b>95</b>
<b>5</b>	<b>One-step Formation of Multiple Emulsions in Microfluidics.....</b>	<b>111</b>
<b>6</b>	<b>Fabrication of Polymersomes using Double-Emulsion Templates in Glass-Coated Stamped Microfluidic Devices .....</b>	<b>126</b>
<b>7</b>	<b>Appendix: Early development drug formulation on a chip: Fabrication of nanoparticles using a microfluidic spray dryer ..</b>	<b>141</b>
<b>8</b>	<b>List of Publications.....</b>	<b>163</b>
8.1	Non-peer-reviewed publications .....	165
8.2	Conference presentations .....	167
<b>9</b>	<b>Acknowledgements .....</b>	<b>168</b>
<b>10</b>	<b>Declaration / Erklärung .....</b>	<b>169</b>



## Abbreviations, symbols and chemical structures

### Abbreviations

AA	Acrylic acid
AFM	Atomic force microscopy
API	Active pharmaceutical ingredient
APS	Ammonium persulfate
CAD	Computer-aided design
CFD	Computational fluid dynamics
CLSM	Confocal laser scanning microscopy
Cryo-TEM	Cryo-transmission electron microscopy
DLS	Dynamic light scattering
EDX	Energy dispersive X-ray analysis
EPR	Enhanced permeability and retention
FEM	Finite element method
FITC	Fluorescein isothiocyanate
HFE	Hydrofluoroether
HFF	Hydrodynamic flow focusing
IPA	Isopropyl alcohol
LSM	Level set method
MC	Main channel
MEMS	Microelectromechanical system
MF	Microfluidic
O/W/O	Oil/water/oil
PAA	Poly(acrylic acid)
PDE	Partial differential equation
PDMS	Poly(dimethylsiloxane)
PDI	Polydispersity index
PEG	Poly(ethylene glycol)
PSD	Particle size distribution
PVA	Poly(vinyl alcohol)
SC	Side channel

SBRP	Simulation-based rapid prototyping
SEM	Scanning electron microscopy
TEMED	Tetramethylethylenediamine
W/O/W	Water/oil/water; chapter 1.2.1, 2.4 and 6: water/organic solvent/water
XRD	X-ray diffraction

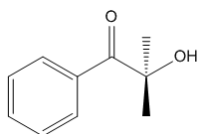
### Symbols

$c$	Concentration
$Ca$	Capillary number
$D$	Diffusion coefficient
$d$	Drop size
$E_{adhesion}$	Adhesion energy
$f_R$	Flow rate ratio (center stream : side stream)
$H$	Mean curvature
$h/w$	Microchannel aspect ratio (height/width)
$K$	Gaussian curvature
$M_N$	Number average molecular mass
$M_W$	Weight average molecular mass
$P$	Packing parameter
$Pe$	Péclet number
$R_H$	Hydrodynamic radius
$Sc$	Schmidt number
$T$	Shell thickness
$t$	Time
$U$	Volumetric flow rate
$u$	Velocity vector
$We$	Weber number
$x_f$	Flow length
$\gamma$	Surface tension
$\lambda$	Slip length
$v$	Flow velocity

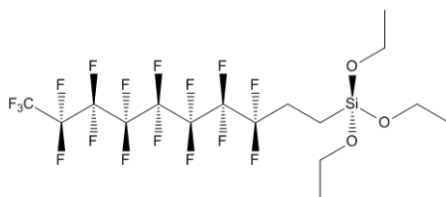
$\rho$	Density
$\theta$	Contact angle
$\tau$	Shear stress

### Important chemical compounds

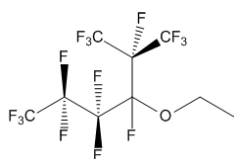
Darocur<sup>®</sup> 1173      2-Hydroxy-2-methyl-1-phenylpropan-1-one



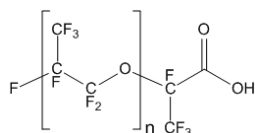
Fluorosilane      (Heptadecafluoro-1,1,2,2-tetrahydrodecyl)triethoxysilane



HFE-7500      3-Ethoxy-1,1,1,2,3,4,4,5,5,6,6,6-dodecafluoro-2-(trifluoromethyl)-hexane

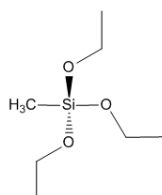


Krytox<sup>®</sup> 157 FSL<sub>14</sub>      Perfluoropolyether carboxylic acid,  $M_N = 2500 \text{ g mol}^{-1}$



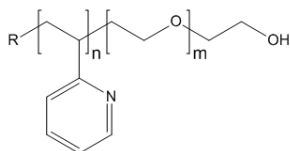
MTES

Methyltriethoxysilane



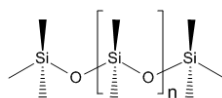
P2VP<sub>47</sub>-*b*-PEG<sub>29</sub>

Poly(2-vinylpyridine)-*block*-poly(ethylene glycol),  
 $M_W = 6400 \text{ g mol}^{-1}$



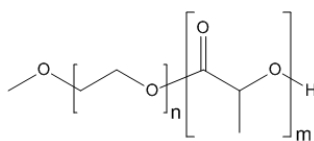
PDMS

Poly(dimethylsiloxane)



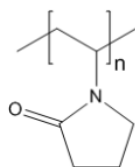
PEG<sub>114</sub>-*b*-PLA<sub>35</sub>

Poly(ethylene glycol)-*block*-poly(lactid acid),  $M_W = 10000 \text{ g mol}^{-1}$



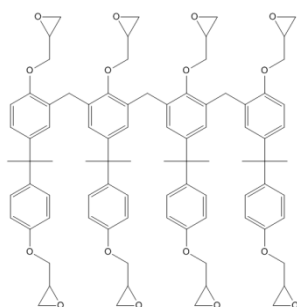
PVP-10K

Poly(vinylpyrrolidone),  $M_W = 10000 \text{ g mol}^{-1}$



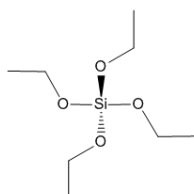
SU-8

Negative photoresist<sup>a</sup>



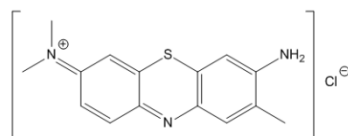
TEOS

Tetraethyl orthosilicate



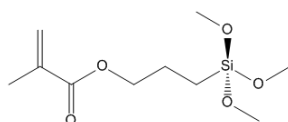
Toluidine Blue

(7-Amino-8-methyl-phenothiazin-3-ylidene)-dimethyl-ammonium chloride



Grafting silane

3-(Trimethoxysilyl)propyl methacrylate



<sup>a</sup> IUPAC-compliant name determined using ACD/Name, v10.0: Bis(2-(oxiran-2-ylmethoxy)-3-(2-(oxiran-2-ylmethoxy)-5-(2-(4-(oxiran-2-ylmethoxy)phenyl)propan-2-yl)benzyl)-5-(2-(4-(oxiran-2-ylmethoxy)phenyl)-propan-2-yl)phenyl)methane

## Summary

The fabrication of diblock copolymer vesicles, so-called polymersomes, from poly(2-vinylpyridine)-*block*-poly(ethylene glycol) (P2VP-*b*-PEG) and poly(ethylene glycol)-*block*-poly(lactid acid) (PEG-*b*-PLA) by means of microfluidics is described. The experiments were performed in microfluidic devices made by soft lithography in poly(dimethylsiloxane) (PDMS). To gain insight into the fluid dynamics in the microfluidic devices, 2D and 3D simulations based on the finite element method (FEM) were performed. This allowed for optimization of the microchannel geometry, and thus precise control over the formation process and properties of the polymersomes, which were extensively characterized by dynamic light scattering (DLS), confocal laser scanning microscopy (CLSM) and cryo-transmission electron microscopy (cryo-TEM). Two distinct approaches to control the vesicular self-assembly of copolymer molecules into polymersomes were studied: the undirected self-assembly using hydrodynamic flow focusing (HFF) and the directed self-assembly using copolymer-stabilized water/organic solvent/water (W/O/W) double emulsion templates.

In the former case, the formation of polymersomes occurred at the interface of a flow-focused, copolymer-loaded solvent stream and a selective solvent in a simple microchannel cross junction. Investigations revealed that the polymersome size is in proportion with the flow rate ratio of polymer solution and the selective solvent; a nucleation and growth model explaining the observed relation between flow conditions and polymersome size was proposed.

In the latter case, the formation of polymersomes was directed by W/O/W double emulsions during evaporation of the organic solvent in which the copolymer was dissolved.

The formation of vesicles from diblock copolymers in microfluidic devices not only enables continuous fabrication of polymersomes with controlled size and narrow polydispersity (PDI), but also offers the ability to tune the polymersome size over several orders of magnitude from less than 50 nm using HFF to more than 100  $\mu\text{m}$  using double-emulsion templates.

To allow for the aforementioned studies, preliminary work focusing on increasing the resistance of PDMS towards swelling due to organic solvents was performed. By using a glass-like coating based on sol-gel chemistry, the swelling of PDMS was decisively decreased. Analyses of coated devices by scanning electron microscopy (SEM) illustrated that the coating could be homogeneously distributed even in complex microfluidic devices as employed for the preparation of double-emulsion templates. To simplify the fabrication of microfluidic devices with patterned wettability as required for the formation of double emulsions, a novel method to spatially pattern the surface properties of microchannels using flow confinement was developed.

For a better understanding of the formation of double emulsions, a fundamental investigation of multiple emulsion formation in microfluidic devices in general was performed. Results show that, depending on the number of dripping instabilities present in the device, multiple emulsions can either be formed in a sequence of emulsification steps or in a one-step process. It was furthermore demonstrated that one-step formation of multiple emulsions provides a novel way to create emulsions from liquids, which otherwise cannot be emulsified controllably, such as viscoelastic polymer solutions or liquids exhibiting a low surface tension.

Finally, the development of a novel microfluidic spray dryer based on a conventional microfluidic device for forming double emulsions was presented and its application for fabricating drug nanoparticles from hydrophobic active pharmaceutical ingredients (APIs) was demonstrated.

## Zusammenfassung

Die Herstellung von Blockcopolymer-vesikeln, sogenannten Polymersomen, unter Verwendung der Blockcopolymer-Poly-2-vinylpyridin-*block*-polyethylenoxid (P2VP-*b*-PEO) und Polyethylenoxid-*block*-polylactid (PEO-*b*-PLA) mittels Mikrofluidik wurde untersucht. Die Durchführung der Experimente erfolgte in mikrofluidischen Bauelementen, die mittels „weicher“ Lithographie (engl. soft lithography) unter Verwendung des Elastomers Polydimethylsiloxan hergestellt wurden. Um Einblick in die Fluidodynamik in den mikrofluidischen Bauelementen zu erhalten, wurden 2D- und 3D-Simulationen auf Basis der Finiten-Elemente-Methode durchgeführt. Dies ermöglichte die Optimierung der Mikrokanalgeometrie und erlaubte somit eine genaue Kontrolle des Bildungsprozesses der Polymersomen sowie ihrer Eigenschaften. Diese wurden mittels dynamischer Lichtstreuung, konfokaler Laserrastermikroskopie und kryo-Transmissionselektronenmikroskopie eingehend charakterisiert.

Zwei verschiedene Ansätze zur Kontrolle der Vesikelbildung von Blockcopolymer-Molekülen wurden untersucht: die ungerichtete Assoziation mittels hydrodynamischer Strömungsfokussierung sowie die gerichtete Assoziation unter Verwendung von Blockcopolymer-stabilisierten Doppemulsionen der Form Wasser/Organisches Lösungsmittel/Wasser, welche als Template dienen.

Im ersten Fall erfolgte die Bildung der Polymersomen an der Grenzfläche einer hydrodynamisch fokussierten Blockcopolymerlösung und eines selektiven Lösungsmittels in einem einfachen mikrofluidischen Kanalkreuz. Untersuchungen zeigten, dass die Größe der Polymersomen proportional zum Volumenstromverhältnis von Blockcopolymer-Lösung und selektivem Lösungsmittel ist. Ein entsprechendes Nukleations- und Wachstumsmodell, welches den beobachteten Zusammenhang zwischen Strömungsverhältnissen und Polymersomengröße herstellt, wurde entwickelt.

Im letzteren Fall ließ sich die Bildung von Polymersomen mit Hilfe von W/O/W-Doppemulsionen durch Verdunstung der organischen Phase, in der das Blockcopolymer molekular gelöst war, steuern.



Beide hier beschriebenen Ansätze ermöglichen nicht nur die kontinuierliche Herstellung von Polymersomen kontrollierter Größe und niedriger Polydispersität. Sie erlauben darüber hinaus die Größe der Polymersomen in einem mehrere Dekaden umfassenden Bereich von weniger als 50 nm unter Anwendung hydrodynamischer Strömungsfokussierung bis zu mehr als 100  $\mu\text{m}$  unter Verwendung von Doppelemulsionstemplaten genau einzustellen.

Um die vorstehend genannten Untersuchungen durchführen zu können, wurden zunächst Möglichkeiten zur Erhöhung der Resistenz von PDMS gegenüber organischen Lösungsmitteln untersucht; unter Verwendung einer Glas-ähnlichen Beschichtung, hergestellt mittels Sol-Gel-Chemie, konnte die Stabilität der Mikrokanäle entscheidend verbessert werden. Ferner wurde eine neuartige Methode zur orts aufgelösten Strukturierung von Oberflächeneigenschaften in Mikrokanälen durch kontrollierte Beschränkung von Fluidströmen entwickelt. Dies stellt eine entscheidende Vereinfachung der Herstellung von mikrofluidischen Bauelementen beispielsweise zur Bildung von Doppelemulsionen dar.

Zum besseren Verständnis der Herstellung von Doppelemulsionen wurde eine grundlegende Untersuchung zur Bildung multipler Emulsionen in mikrofluidischen Bauelementen durchgeführt. Deren Ergebnisse weisen darauf hin, dass multiple Emulsionen in Abhängigkeit von der Anzahl im Bauelement vorhandener hydrodynamischer Instabilitäten, die zur Tropfenbildung führen, entweder in einer Abfolge einzelner Emulsifizierungsschritte oder in einem einstufigen Prozess gebildet werden. Die einstufige Herstellung multipler Emulsionen kann darüber hinaus auch zur Bildung von Emulsionen aus solchen Flüssigkeiten verwendet werden, die sich andernfalls nicht kontrollierbar emulsifizieren lassen, wie am Beispiel viskoelastischer Polymerlösungen sowie Flüssigkeiten mit extrem niedriger Oberflächenspannung gezeigt werden konnte.

Schließlich wurde ein neuartiger mikrofluidischer Sprühtrockner auf Basis eines herkömmlichen Bauelementes zur Darstellung von Doppelemulsionen entwickelt und erfolgreich zur Herstellung von Nanopartikeln aus hydrophoben Arzneiwirkstoffen eingesetzt.

# 1 Introduction

Over the last two decades, microfluidics has emerged as an interdisciplinary technology with a wide range of applications in chemistry, biotechnology and physics, capable of controlling fluid flow and reaction conditions with unprecedented accuracy. Compared to conventional bulk processes, the consumption of reagents and the production of waste are reduced, due to the small dimensions of the microchannels, enabling cost-efficient operation and the handling of precious samples down to the femtoliter range.

In the following, a brief survey of recent trends in microfluidics is given with regard to fabrication techniques and practical implementations as well as key challenges that have been encountered in design, engineering and application of microfluidic devices, and how PDMS-based microfluidics has the potential to address these issues. In addition, computational fluid dynamics is introduced as a versatile tool to facilitate the efficient design and improvement of microfluidic devices. In this context, fluid flow simulations based on the finite element method are presented which have been developed to optimize the microfluidic devices in the present work.

As a major part of this thesis is dedicated to the fabrication of copolymer-based vesicles, so-called polymersomes, a short overview over conventional fabrication techniques, formation mechanisms as well as the application of vesicles in biology and medicine is given thereafter. Special attention is drawn to the evolving vesicle preparation techniques on the micron scale, which serve as a basis to implement PDMS-based microfluidic devices as a novel platform to fabricate polymersomes.

### 1.1 Microfluidic devices - design, fabrication and application

*Microfluidics* refers to platforms and methods for controlling and manipulating the fluid flow in quasi-two- and three-dimensional channels with a characteristic length scale in the micrometer range.<sup>1</sup> The basic concept of microfluidics has evolved from solid-state electronic circuits, which is why the counterparts of many active components in microfluidic devices can be found in electronic devices as well.<sup>2</sup> Starting with the theoretical description of a miniaturized total analysis system ( $\mu$ -TAS) by Manz et al. in 1990,<sup>3</sup> the concept of a *lab on a chip* has evolved tremendously, leading to the miniaturization and integration of valves, electrodes, mixers, switches, sensors or heaters in microchannel networks.<sup>1,4,5,6,7,8</sup> As all operations can be combined on a single device, the need for larger and expensive laboratory equipment is eliminated, and the development of mobile lab applications is facilitated. This reduces energy consumption and waste production and ultimately production costs.

The most obvious advantage provided by microfluidic devices is the superior control over flow conditions and fluid volumina therein. Thereby, a microchannel network enables handling and manipulation of fluid volumes down to the femtoliter range and, therefore, extremely low sample consumption. This feature is especially important when dealing with precious biological samples or samples that are unavailable in large enough quantities to be properly studied.<sup>7,9</sup> It also enables trapping, detection and manipulation even of single molecules or cells, circumventing the less-accurate measurement of averaged properties in bulk.<sup>10,11,12,13</sup>

In addition, the miniaturization of reaction vessels by means of microfluidics features fast and uniform heat distribution due to the small thermal mass of the device and its high surface-to-volume ratio, and improves the control over and safety of exothermic reactions.<sup>14,15</sup> In addition, even rapid reactions kinetics can be controlled at the exact reaction stage by adapting the design according to the reaction, nucleation and growth mechanism and the number of reaction steps, as desired in the fabrication of nanomaterials, for instance.<sup>16,17</sup> Apart from these general advantages, the confinement of fluids in micron-scale dimensions enables access to fluid flow phenomena that are not observable in macroscopic systems. Owing to this so called scaling effect, viscous

dissipation and pressure effects dominate over inertia, resulting in a laminar, turbulence-free flow,<sup>13,18,19</sup> as further elaborated in chapter 1.3.

Due to the customizability and performance of microfluidic devices, the number of promising applications is growing quickly. They range from the production of pharmaceuticals, cosmetics, nutrition, and agricultural products over the preparation of smart polymer capsules, (Janus-) micro<sup>20,21,22,23,24</sup> and nanoparticles<sup>16,25,26</sup> with a large diversity of morphologies and physicochemical properties with respect to size, shape, surface charge and amphiphilicity,<sup>27,28</sup> to the miniaturization and improvement of conventional analytical processes, such as free-flow electrophoresis, polymerase chain reaction (PCR) and blood sample analysis.<sup>29,30,31</sup> In addition, while biological samples degrade when exposed to high-energy radiation, preventing a detailed characterization on the nanoscale, their investigation applying high-resolution characterization methods using X-ray or synchrotron radiation is greatly facilitated in microfluidic devices, owing to the short residence times therein.<sup>32,33</sup>

Another important task that can be performed in microfluidic devices, is the formation of droplets, or the generation of segmented flow in general, as independent reaction vessels and templates in self-assembly processes.<sup>28,34,35,36,37</sup> Libraries of droplets are also applicable as platforms for high-throughput screening of aptamers and enzymes in drug discovery and protein crystallization studies, for instance, overcoming the limitations of conventional screening techniques in combinatorial chemistry and biotechnology, which usually require large amounts of consumable materials for performing the same tasks.<sup>38,39,40,41</sup>

The development of microfluidic devices has greatly benefited from the mature state of microelectromechanical system (MEMS) fabrication using silicon and glass.<sup>27</sup> Although being chemically inert and resistant to high temperatures, both materials have drawbacks. They are porous and hard to manipulate, and the implementation of switchable components is thus a challenging task. Moreover, their processing usually requires a cleanroom environment and caustic chemicals like hydrofluoric acid. Also, silicon is not optically transparent limiting online process tracking. Soft materials, which are easy to form and manipulate, are able to overcome these limitations, albeit for applications that usually require temperatures lower than 200 °C.<sup>16,42,43</sup>

The technique of choice for processing soft materials in microfluidic device fabrication is soft lithography, specifically casting, molding and hot embossing.<sup>27,44,45,46</sup> A great variety of polymers can be used in soft lithographic fabrication techniques, most notably perfluoropolyethers,<sup>47,48,49</sup> and fluorinated terpolymers (e. g. Dyneon™ THV),<sup>50</sup> polyimides,<sup>51,52</sup> polyurethanes,<sup>53</sup> poly(methyl methacrylates)<sup>54,55</sup> and the elastomer PDMS, which is nowadays strongly linked with soft lithographic rapid prototyping and replica molding, as the following chapter will show in detail. Although polymer-based soft lithography is dominating the field of microfluidic device fabrication, the search for new manufacturing techniques and materials is still the target of ongoing investigations. Most recently it was demonstrated that even office equipment - paper and adhesive tape – can be used to fabricate sophisticated devices at extremely low cost, suitable for healthcare and water analysis in the third world,<sup>56,57</sup> which underlines the diversity of current research in this area.

Despite the promises made by microfluidics and recent improvements in device fabrication, the manufacturing of complex devices, in particular with integrated mechanical components remains a complex procedure and it is not unusual that the device materials require extensive modifications to match the needs for reaction conditions as well as educt/product properties and applied characterization techniques, which is why microfluidics is considered to be in the state of academic research, yet.<sup>58,59</sup>

### **1.1.1 PDMS-based microfluidic devices**

Although microfluidics greatly facilitates the handling of small sample volumes, the product output of a single microfluidic experiment is small as well. This diminishes the promises of microfluidics to supplant conventional industrial bulk processes in the near future. Due to the ease of fabrication of stamped devices, this limitation might be overcome by massive parallelization of single microfluidic devices using soft lithography.<sup>60,61</sup> Founded by Whitesides et al. in 1997, soft lithography using elastomeric polymer molding has grown to the most important technique in microfluidic device manufacturing.<sup>44,45,46,62</sup> It enables rapid prototyping of microfluidic devices with micro-

### 1.1.1 PDMS-based microfluidic devices

---

and even nano-sized channels of squared or circular shape,<sup>63,64</sup> that can be engineered with high aspect ratios of  $h/w = 10:1$  and higher, depending on the device material.<sup>65</sup>

PDMS and related siloxane-based polymers are widely used for making molds and stamps using soft lithography as they combine a large number of properties that are interesting for microfluidic devices.<sup>66,67</sup> PDMS provides excellent optical transparency from 240 to 1100 nm,<sup>68</sup> low toxicity and is highly permeable to gases, which is particularly interesting for cell culturing and growth studies in micro chambers. As the elasticity of PDMS can be controlled by the ratio of the PDMS oligomer and cross-linker using commercially available preparation kits (e.g. Dow Corning's Sylgard 184), the fabrication of sophisticated devices for applications requiring chaotic mixers or pneumatically activated pumps and valves is facilitated.<sup>8,62,69</sup> In addition, PDMS is like most other polymers electrically insulating, thus enabling the integration of electrodes for manipulating fluid flow by electric fields.

To manufacture a microfluidic device by rapid prototyping in PDMS, a master structure containing the positive relief of the desired microchannel network is fabricated via conventional photolithography using commercially available photoresists, such as SU-8,<sup>70,71</sup> as shown in Figure 1. The most important feature of the device master is that it is reusable and can be replicated over many cycles, allowing rapid prototyping at low cost. A detailed description of the master preparation can be found in chapter 4.

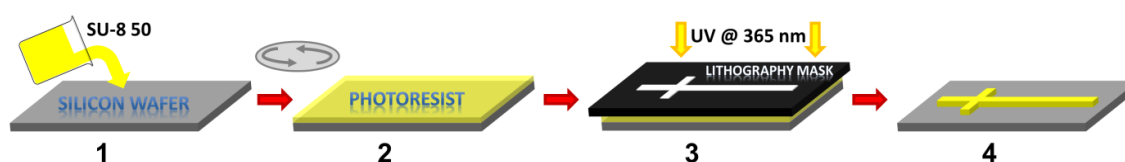


Figure 1: Manufacture of a microfluidic device master by means of photolithography. (1) Typically, a polished silicon wafer is used as substrate, (2) on which a layer of SU-8 is spin-coated. (3) The wafer is exposed to UV light through a photomask, designed in a computer-aided design (CAD) program, e.g. AutoCAD. (4) The microchannel structure is yielded by subsequent polymerization and development of the photoresist.

To characterize the patterned surface of the device master, SEM is the method of choice. It can be applied to determine the exact channel height and to identify defects, which could be imparted to the PDMS replica and disrupt the laminar microflow at worst. The SEM analysis of a microfluidic device designed for forming polymersomes via HFF is shown in Figure 2.

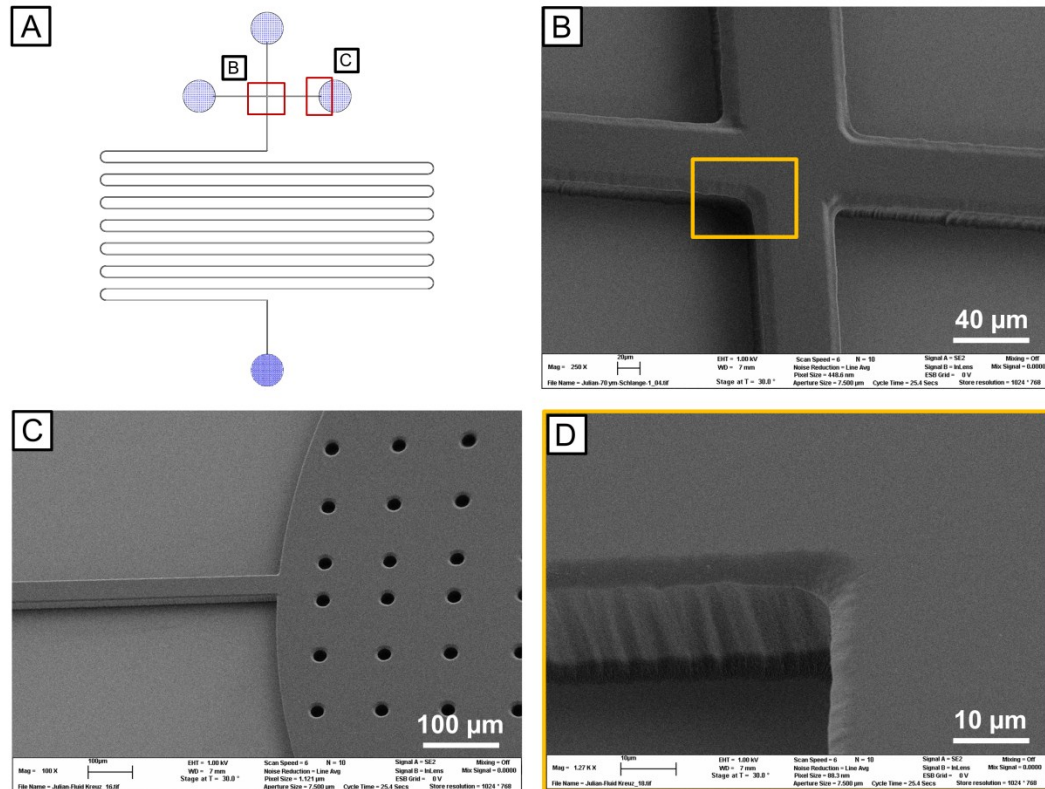


Figure 2: SEM characterization of a device master for fabricating microchannel replica in PDMS. (A) To-scale schematic drawn in AutoCAD 2008; the microchannel geometry is optimized for the preparation of polymersomes using HFF. (B) Cross junction with three inlet channels and one larger channel leading to the meander-shaped mixing zone. (C) Microchannel with basin as a punch target; by introducing holes in the master, the large basin will be stabilized by posts in the later PDMS replica. (D) Wavelike profile of the side walls due to the limited resolution of the lithography mask. The dark layer at the bottom of the SU-8 structure is an optical effect arising from the limited depth of field of the secondary electrons that are detected.

Despite the high resolution that is achievable using SEM, SU-8 is susceptible to electron beam damage. This can cause shrinkage of the photoresist during the imaging process,

### 1.1.1 PDMS-based microfluidic devices

especially when analyzing high-aspect-ratio features at high acceleration voltage.<sup>72</sup> Moreover, the non-conductive polymer easily builds up surface charges that diminish the image quality. A novel alternative for topographic mapping of the device master is the use of confocal laser scanning microscopy (CLSM) in the reflective mode, as shown in Figure 3.

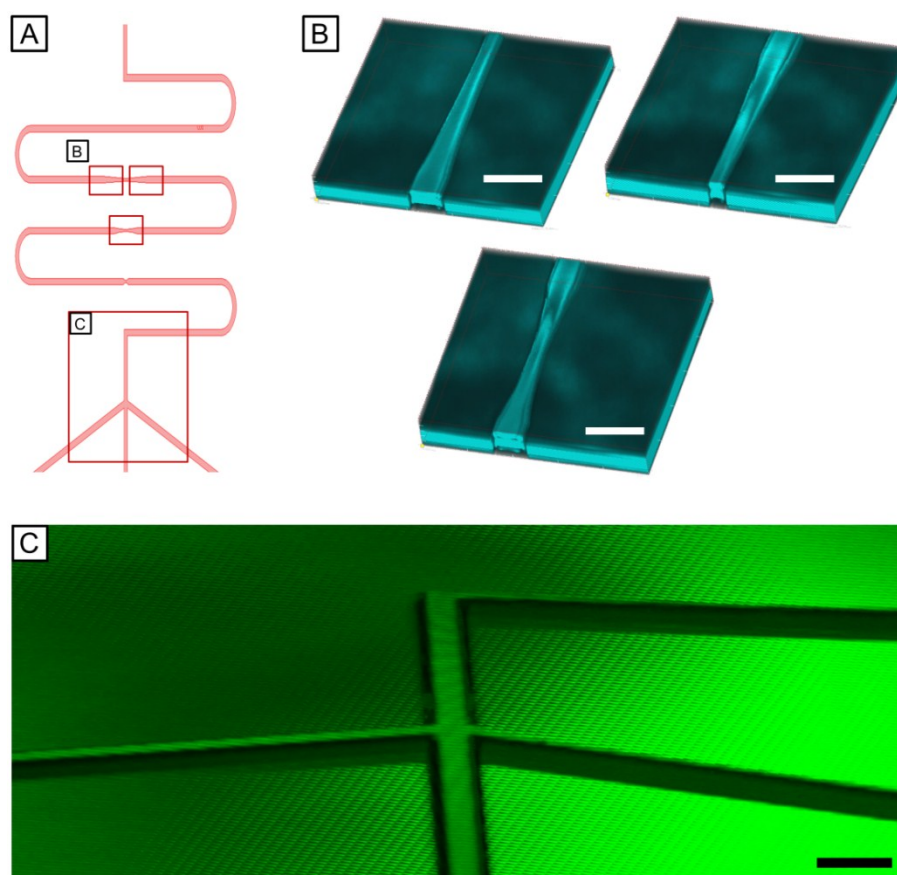


Figure 3: Characterization of microstructures using CLSM in the reflective mode. (A) Schematic of a microfluidic device designed for investigating the shear-induced orientation of poly(isoprene)-*b*-poly(ethylene glycol) cylinder micelles in curved and tapered microchannels. (B, C) 3D reconstruction of 2D slices of the corresponding device master. Due to the limited scanning area of 1.3 x 1.3 mm, the upper constriction is analyzed in two steps. Scale bars denote 100  $\mu\text{m}$ .

In contrast to SEM, CLSM is non-destructive and can be therefore also applied for the characterization of sensitive biofilm-coated surfaces in biological MEMS applications, for instance. Although the reflectance of silicon, approximately 28 %, is rather low,<sup>73</sup> the



reconstruction of z-stacks of individual confocal images enables high-resolution imaging of the patterned master that is comparable with the maximum resolution of the photo patterning masks.

Along the rapid prototyping process, the microchannels are formed in PDMS by replica molding, as sketched in Figure 4. As PDMS shrinks only minimal during curing ( $< 1\%$ ) device features down to the nanoscale can be replicated. Thereafter, the open PDMS replica is sealed with a glass slide that is covalently bonded to the PDMS surface in a condensation reaction between silanol groups on the PDMS and glass surface that have been previously generated in an air or oxygen plasma.<sup>74</sup> Instead of using a glass slide, the PDMS replica can also be sealed with polyimide foils (Kapton<sup>®</sup>), that are X-ray transparent.<sup>75</sup> This approach enables the combination of microfluidic technology with state-of-the-art X-ray analysis methods and the *in-situ* investigation of structure formation and orientation changes of colloids, polymers or proteins under strain in flow fields with micron-scale resolution.<sup>33,76</sup>

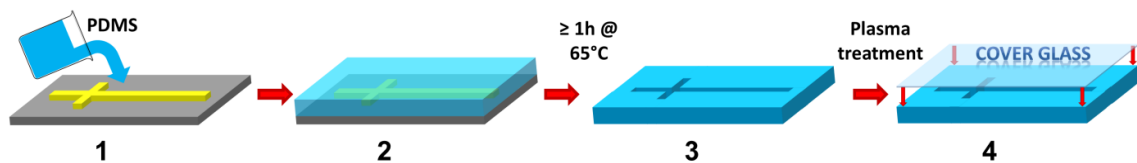


Figure 4: Soft lithographic replication of the master structure. (1, 2) The PDMS oligomer and cross-linker are mixed at a typical ratio of 10:1 and poured onto the master. (3) PDMS is cross-linked at approximately 65 °C for at least 1 h and peeled-off the master structure. (4) The PDMS replica is sealed with a cover glass slide after air or oxygen plasma treatment.

Despite its many advantages in fabrication and physical properties, PDMS has at least two significant drawbacks.<sup>68</sup> Issues related with PDMS include the unspecific adsorption of biomolecules, which can foul the hydrophobic PDMS surface and reduce the device performance. Moreover, the application of bare PDMS is limited to aqueous solutions and a small number of polar organic solvents. As PDMS is a hydrocarbon itself, organic solvents that are soluble in hydrocarbons can swell PDMS, which causes deformation, or even collapse of the microchannel structure.<sup>68,77</sup>

One way to reduce the swelling of PDMS and the adsorption of hydrophobic compounds is to minimize the surface contact with the channel walls. This can be achieved by using circular-shaped microchannels, in which a three-dimensional coaxial flow pattern forms. Using multiple phase flow, the compound or solvent of interest is surrounded by a protective sheath flow and the contact with the microchannel walls is minimized, as shown in chapter 2.5 and 7. Other approaches to reduce the swelling of PDMS utilize solvent-resistant materials, such as glass-like coatings based on sol-gel chemistry,<sup>78,79</sup> organic/inorganic hybrid polymers,<sup>80</sup> and parylenes.<sup>81,82,83</sup> However, as parylenes only allow limited surface functionalization, and hybrid polymers usually require extensive synthesis, sol-gel coatings are usually applied. In a typical coating process, liquid silicon alkoxide precursors (e.g. TEOS) are hydrolyzed and deposited on the surface of the microchannels, where the condensed silica species gels upon heating, forming a three-dimensional glassy network.<sup>84</sup> Due to the variety of silicon alkoxides and alkyl-substituted ethoxysilanes (e.g. MTES and fluorosilanes), the stiffness, porosity, wettability and surface functionalization of sol-gel coatings can be precisely controlled.<sup>85</sup>

Microchannel wettability is crucial for controlling the fluid flow in microfluidic devices.<sup>86</sup> While the plasma treatment that is used to activate the PDMS/glass surface in the bonding process renders the intrinsically hydrophobic PDMS hydrophilic only temporarily, post bonding methods such as the grafting of hydrophilic polymers to sol-gel-coated microchannels or layer-by-layer deposition of polyelectrolytes turn the device permanently hydrophilic.<sup>87,88,89</sup> However, a large number of applications requires spatial resolution of the microchannel wettability. Local wettability modification can be achieved by utilizing the permeability of PDMS for oxygen that can diffuse from near-by reservoirs into the microchannels and inhibit the polymerization of hydrophilic monomers on the microchannel surface with spatial control.<sup>90</sup> Yet other methods use localized microplasma treatment or a spatially controlled UV light that triggers a photochemically induced polymerization reaction on the microchannel surface.<sup>91,92</sup>

Summarizing, rapid prototyping of microfluidic devices using soft lithography in PDMS is a simple and versatile tool for fabricating sophisticated devices at low cost. Although the application of PDMS-based devices beyond simple aqueous media in biomedical use requires additional processing steps specific to the application, rather simple and scalable surface modifications are available to enhance the chemical and physical resistance of

PDMS and broaden the application of microfluidics beyond its current state of academic research.

## **1.2 Polymersomes – vesicular self-assemblies of diblock copolymers**

The delivery of active pharmaceutical ingredients to specific biological sites is one of the most important aspects in the design of an effective drug therapy. However, previous studies on lipid vesicles, also referred to as liposomes, as capsules for drug protection, delivery and release have revealed certain limitations. Lipids as the building blocks of liposomes are usually obtained from natural sources with inconsistent composition, quality and limited structural variety.<sup>93</sup> Moreover, undirected hydrolysis and oxidation of lipids in solution can cause leakage of the liposomes explaining their short shelf-life. On this account, polymeric vesicles, so called polymersomes, have been under extensive investigation as biomimetic phospholipid analogues for improving encapsulation and delivery of imaging agents, drugs, proteins and genes for almost two decades with the first publication in 1995.<sup>94,95,96</sup> Polymersomes are self-assembled spherical structures with an aqueous core that is enclosed by a bilayer membrane usually composed of diblock copolymer amphiphiles, as shown in Figure 5.<sup>97,98,99</sup> Polymersomes combine the unique ability to encapsulate hydrophobic compounds in the bilayer and hydrophilic actives in the aqueous interior at the same time.

In contrast to the limited diversity of lipids, synthetic polymer analogs, which are inspired by the small natural amphiphiles, offer almost infinite options to control the structural and physicochemical variety of membranes and vesicles. Various copolymer architectures are able to form bilayer membranes including AB, ABA, ABABA, ABC and ABCA copolymers, with AB diblock copolymers being the most extensively studied and applied building unit.<sup>94</sup> Diblock copolymers exhibit an order of magnitude larger molecular weight as well as increased length and conformational freedom allowing for the formation of vesicles with thicker, highly entangled membranes. For this reason, polymersomes offer an improved structural toughness as well as decreased permeability as predicted by Fick's first law, and are inherently more stable than liposomes, even being able to survive autoclaving.<sup>100</sup> This facilitates a more effective protection of entrapped actives in the polymersome's aqueous interior from degradation upon arrival at the designated target cell.<sup>101,102</sup>

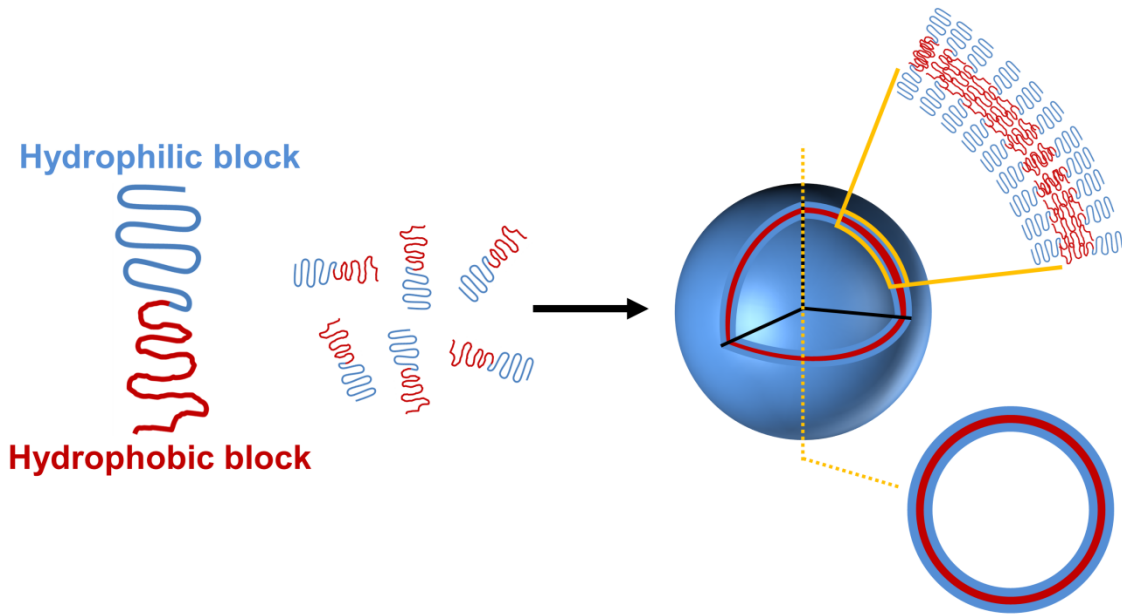


Figure 5: Self-assembly of amphiphilic diblock copolymers into polymeric vesicles, so-called polymersomes. The copolymer molecules arrange into a macromolecular bilayer enclosing a spherical compartment.

To increase the biocompatibility of polymersomes for applications in cellular targeting and cytoplasmic delivery of biologically relevant substances, chains of poly(ethylene glycol) (PEG) are often incorporated into the copolymer architecture to impart their biocompatibility to the polymersome bilayer and mimic the exo-facial glycocalix of cells.<sup>103,104</sup> In addition, *in vitro* and *in vivo* experiments have revealed that PEG-based copolymers, with the molecular weight of the PEG block  $M_{PEG}$  (equation 1-1), minimize the adhesion of the corresponding polymersomes to foreign surfaces and exhibit a much longer blood circulation half-life  $\tau_{1/2}$  than non-PEGylated liposomes.<sup>100,105,106</sup>

$$\tau_{1/2} \sim M_{PEG}^{0.43} \quad (1-1)$$

In addition, PEG-based polymersomes provide binding sites to attach ligands or antibodies to the vesicle surface to mimic viral targeting mechanisms of cells by molecular recognition, thus tailoring *in vivo* behavior to specific therapeutic needs.<sup>107,108,109,110</sup> Moreover, polymersomes are able to amplify the activity of drugs or genes by encapsulating and confining actives and directing their release at the specific

target compared to the undirected delivery of the free species. A prominent example in nanomedicines are polymeric vesicles bearing chemotherapeutic agents such as doxorubicin and paclitaxel for targeted drug delivery in clinical cancer therapy.<sup>96,111,112,113,114</sup>

However, to enhance the bioavailability of a drug, drug carriers have to combine targetability *and* stimuli responsiveness.<sup>104</sup> This can be achieved by using polymersomes, which offer a variety of controlled release mechanisms to disassemble in response to specific external stimuli. The most frequently applied mechanisms make use of enzymatic or hydrolytic degradation of hydrophobic ester blocks such as PLA or poly(caprolactone) (PCL),<sup>96,106,115,116</sup> redox- and pH-sensitive triggers,<sup>117,118</sup> or temperature-responsive copolymers.<sup>119</sup> This may be compared to the limited number of mechanisms that liposomes offer, like hydrolytic and thiolytic cleavage of lipid membranes.<sup>120</sup>

Despite the extensive use and diverse application of polymersomes and vesicles in general, their formation mechanism is not yet understood in its entirety, and thus the objective of ongoing research. The formation of polymersomes is usually viewed as a two-step process.<sup>121</sup> Analogous to studies on liposomes by Lasic et al. predicting a disk-like lipid micelle as an intermediate structure,<sup>122</sup> copolymer molecules self-assemble into lamellar, sheet-like aggregates in the first step, that subsequently curve and close up to form vesicles, as shown in Figure 6A. The process is driven by the energy loss owing to surface tension, which increases with the size of the planar bilayer, thus favoring spherical bilayers over flat ones.<sup>99,123</sup> In recent years, two alternative mechanisms have been proposed based on theoretical calculations.<sup>124</sup>

In the first case, spherical micelles rapidly form from a homogeneous copolymer solution. They then grow by the uptake of further copolymer molecules into their interior in a condensation-evaporation process forming bilayered large micelles, so called semi-vesicles, as shown in Figure 6B.<sup>124</sup> However, semi-vesicles are energetically unfavored and lower their energy by taking up solvent, which results in the formation of the desired vesicular structures.<sup>125</sup>

In the second case, spherical micelles serve, again, as a starting point. After their rapid formation, they slowly coalesce evolving into larger cylindrical or open disk-like micelles, which then curve to give rise of vesicles, as shown in Figure 6C.<sup>126,127,128,129</sup>

Indeed, similar intermediates have been found in experiments using detergent depletion to elucidate the formation mechanism of phospholipid vesicles.<sup>122</sup> By steadily removing detergent from a solution of phospholipids dissolved in detergent micelles, the mixed micelles grow into aggregates by fusion from which the desired liposomes evolve.

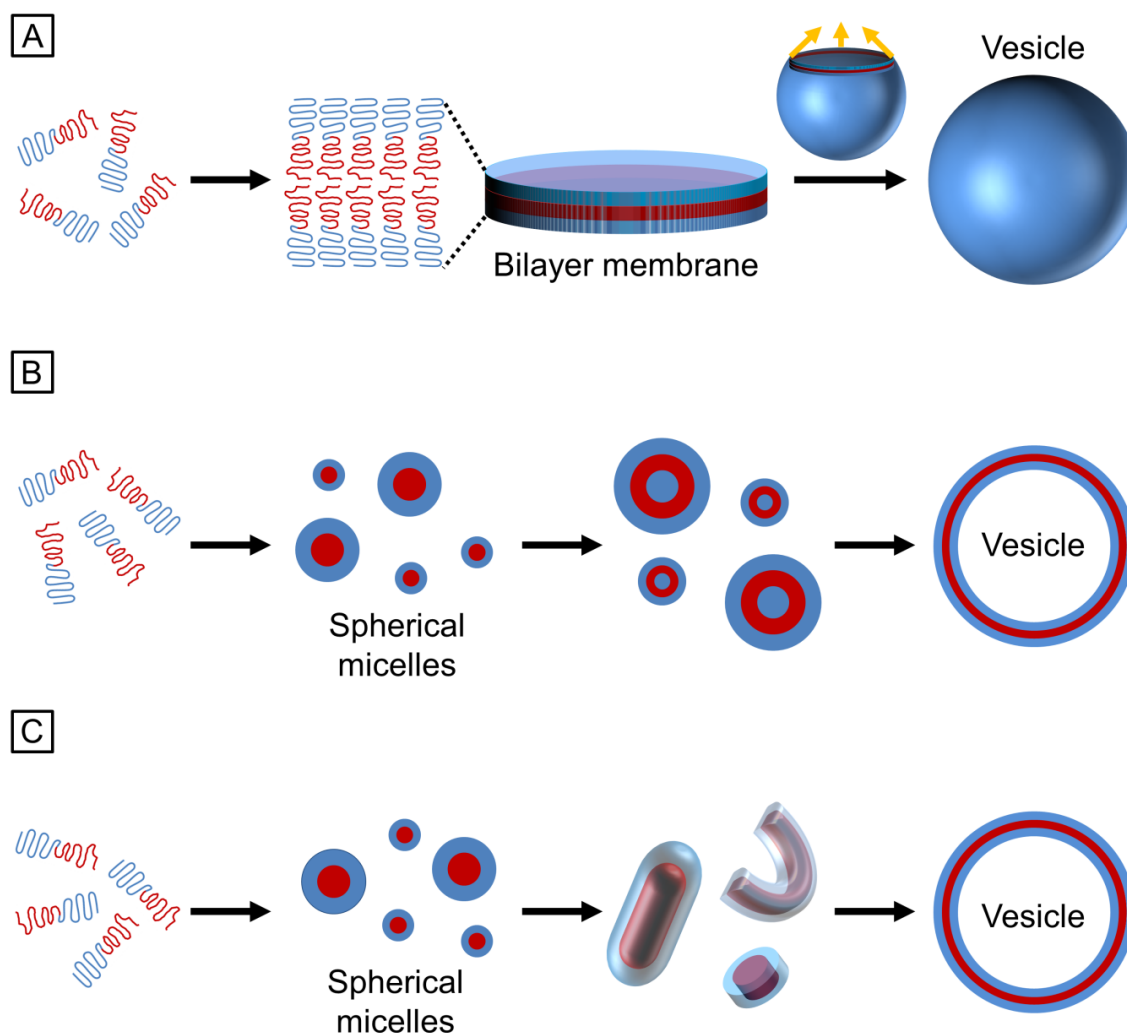


Figure 6: Schematic representation of different polymersome formation mechanisms.<sup>121,124</sup> A homogenous copolymer solution is assumed as a starting point. (A) Widely accepted two-step process involving the formation of a diblock copolymer bilayer followed by its closure to give a hollow vesicle structure. (B, C) Proposed mechanisms of polymersome formation based on molecular dynamics simulations,<sup>126</sup> external potential dynamics simulations<sup>125</sup> and density functional simulations<sup>127</sup> as well as dissipative particle<sup>128</sup> and Brownian dynamics studies,<sup>129</sup> respectively. (B) Spherical micelles grow by the uptake of copolymer molecules through an evaporation-condensation-like process into bilayered micelles, so called semi-vesicles, which take solvent into their inside to reach the energetically more favorable vesicular shape. (C) Spherical micelles coalesce to cylindrical and interconnected worm-like micelles as well as open disc-like structures. Close-up of these structures give rise to the formation of vesicles, as seen in experiments.<sup>130</sup>

Apparently, not all copolymers are able to self-assemble into vesicles, as certain prerequisites for composition and structure of copolymers exist. The dimensionless packing parameter  $P$  dictates the molecular shape of copolymer molecules in solution, and thus the morphology of the corresponding self-assembled copolymer aggregate upon phase separation of the hydrophobic and hydrophilic block. It is defined as the size of the hydrophobic block relative to the hydrophilic moiety.<sup>121</sup>

$$P = \frac{v}{a \cdot l} \quad (1-2)$$

where  $v$  is the volume of the hydrophobic block,  $a$  the hydrophilic-hydrophobic interfacial area, and  $l$  the hydrophobic block length normal to the interface, as illustrated in Figure 7. With increasing values of  $P$ , the morphology is tuned from spherical structures over toroidal to cylindrical aggregates, as exemplarily shown in Table 1.<sup>120,131</sup> Whether vesicles form or not is additionally determined by the effective interaction parameter  $\chi$  of water with the hydrophobic block.<sup>132</sup>

Shape	$P = \frac{v}{a \cdot l}$	$r_1$	$r_2$	$H$	$K$
Sphere	$\frac{1}{3}$	$r$	$r$	$\frac{1}{r}$	$\frac{1}{r^2}$
Cylinder	$\frac{1}{2}$	$r$	$\infty$	$\frac{1}{2r}$	0
Bilayer	1	$\infty$	$\infty$	0	0

Table 1: Packing parameter  $P$  of different aggregated structures as well as their corresponding mean curvature  $H$  and Gaussian curvature  $K$ , which can be expressed by the two radii of curvature  $r_1$  and  $r_2$ .

As the vesicle shape is mainly determined by interfacial curvature, the packing parameter can also be described by the mean curvature  $H$ , and Gaussian curvature  $K$  of the interfacial surface with the two radii of curvature  $r_1$  and  $r_2$ .<sup>131,133</sup>

$$P = 1 - Hl + \frac{Kl^2}{3} \quad (1-3)$$

$$P = 1 - \frac{l}{2} \left( \frac{1}{r_1} + \frac{1}{r_2} \right) + \frac{l^2}{3r_1 \cdot r_2} \quad (1-4)$$



In the case of cylinders,  $K = 0$ , and  $H = \frac{1}{2r} \Rightarrow \frac{1}{2l}$ . Insertion into (1-3) gives 0.5, as shown in Table 1:

$$P = 1 - \frac{l}{2l} + 0 = \frac{1}{2} \quad (1-5)$$

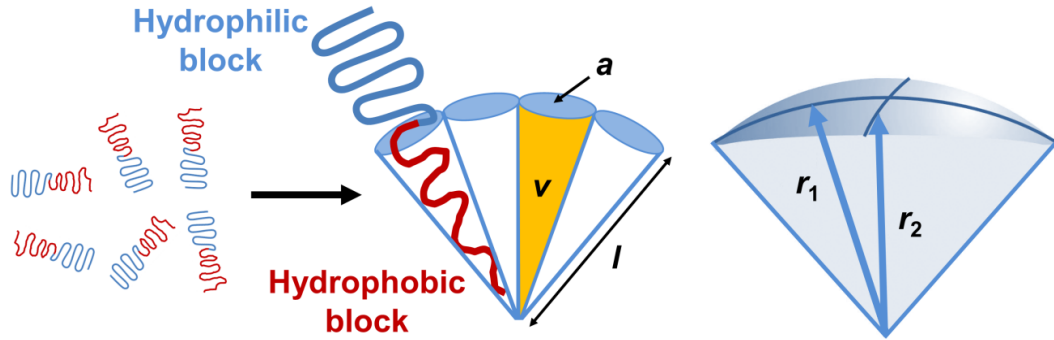


Figure 7: Illustration of the packing parameter  $P$  in terms of the interfacial area  $a$ , the hydrophobic volume of the copolymer  $v$  and the chain length normal to the interface  $l$  (left), as well as its relation to the interfacial mean curvature and Gaussian curvature, described by the curvature radii  $r_1$  and  $r_2$  (right). Adapted from <sup>121</sup>.

The size of the hydrophobic block, which dictates the bilayer thickness of the polymersome and thus the elasticity and stability of the membrane, provides a simple scaling of the copolymer membrane thickness  $d$ ,

$$d \sim (M_h)^b \quad (1-6)$$

where  $b$  is a parameter describing the folding state of the polymer chain with  $b = 1$  for a fully stretched polymer chain,  $b = 0.5$  for an ideal random coil, and  $b \approx 0.55$  in a polymersome, and  $M_h$  the mean molecular weight of the hydrophobic block, which can be estimated from the number average molecular weight  $M_N$  and the hydrophilic fraction  $f$ .<sup>101</sup>

$$M_h \sim M_N(1 - f) \quad (1-7)$$

As the number of amphiphiles on the inner and outer surface of the polymersome bilayer is trapped in a non-equilibrium state in the fabrication process, the bilayer spontaneously curves to minimize the bending energy for a given difference in the number of amphiphiles between the inner and outer copolymer monolayer.<sup>99</sup> This, in turn, allows for tailoring of vesicle size and morphology by the preparation method and the experimental conditions, resulting in a diverse ensemble of polymersomes, where each geometry represents a state of minimal bending energy. Applying the area difference between the inner and outer bilayer surface,  $A_{in}$  and  $A_{out}$ , respectively,

$$\Delta A = A_{in} - A_{out} \quad (1-8)$$

and the volume-to-area ratio  $V^*$

$$V^* = \frac{V}{\frac{4}{3}\pi R_A^3} \quad (1-9)$$

with  $R_A = \left(\frac{A}{4\pi}\right)^{\frac{1}{2}}$  and  $V^* = 1$  for spherical vesicles, the different vesicle shapes can be mapped in a phase diagram, as shown in Figure 8.

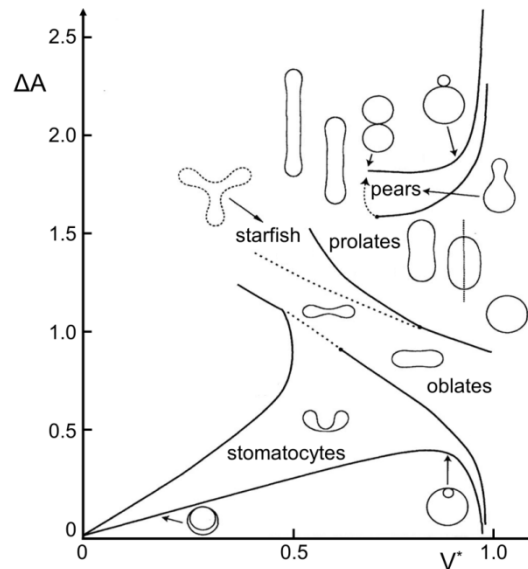


Figure 8: Phase diagram of theoretical polymersome shapes. The dimensionless volume-to-area ratio  $V^*$  is plotted as a function of the area difference between inner and outer bilayer. Adapted from <sup>121,135,136</sup>.

Depending on the number of bilayers that are interlaced with one another, it is broadly distinguished between unilamellar, oligolamellar and multilamellar structures, as shown in Figure 9.<sup>134</sup> Unilamellar vesicles are further classified as small, large or giant vesicles; vesicles encapsulated within vesicles are defined as multivesicular vesicles.

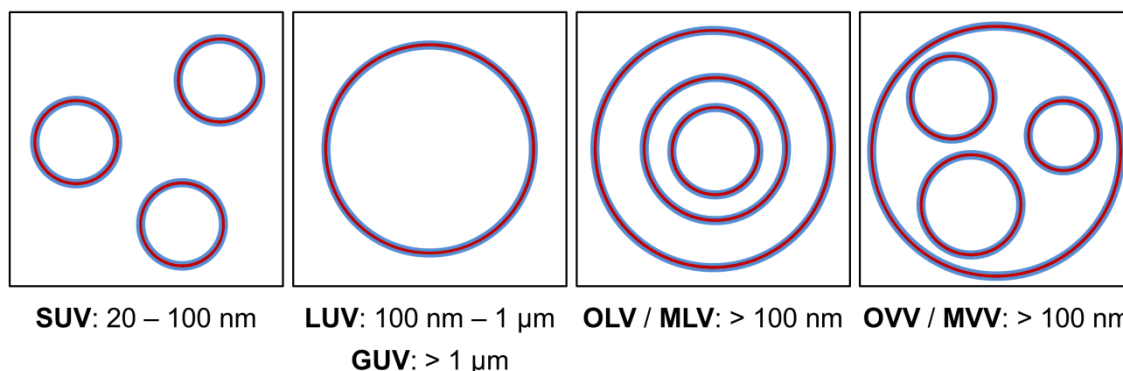


Figure 9: Classification of vesicle structures. Depending on the number of nested bilayers and the vesicle size, a distinction is made between small unilamellar vesicles (SUV), large unilamellar vesicles (LUV) and giant unilamellar vesicles (GUV) as well as oligolamellar vesicles (OLV) and multilamellar vesicles (MLV). Vesicles that are encapsulated within vesicles are specified as oligovesicular vesicles (OVV) and multivesicular vesicles (MVV), respectively.

To fabricate polymersomes, numerous laboratory- and industrial-scale fabrication techniques common to liposomes are available, each yielding vesicles with characteristic size, lamellarity and shape.<sup>2,84,180,179</sup> Larger vesicles can be produced by electroformation,<sup>103,137,138</sup> or by subjecting dispersions of smaller vesicles to ultrasound inducing vesicle-vesicle fusion,<sup>94</sup> while smaller vesicles are obtained by high-pressure extrusion through (polycarbonate) membranes, for instance.<sup>139,140,141</sup> Multilamellar vesicles, on the other hand, are yielded by transformation of unilamellar SUVs and LUVs in repeated dehydration-rehydration and freeze-thawing cycles. Novel methods for preparing polymersomes with narrow size distribution involve the use of modified inkjet printers for spraying copolymer-loaded drops into an aqueous solution.<sup>142,143,144</sup>

However, as the bilayer of polymersomes is less flexible than liposome membranes, the formation of polymersomes can be more challenging and time-consuming applying conventional approaches. In addition, despite recent advances on the rehydration of dried

copolymer films for fabricating polymersomes by using templates of copolymer patterned surfaces,<sup>145</sup> the undirected self-assembly usually yields vesicles with large size distributions.<sup>146,147,148</sup> A promising alternative to current preparation techniques is the use of microfluidics, providing an environment with extremely fast mixing times and unique control over self-assembly processes, as further described in chapter 1.2.1.

Summarizing, polymersomes offer great structural variety as well as widely tunable membrane properties and mechanical stability due to recent advances in block copolymer chemistry, hence representing a valuable advancement of current encapsulation and delivery approaches. Thereby, the same reasons which have been argued for using liposomes as delivery vehicles by Storm and Crommelin - *direction, duration, protection, internalization* and *amplification* - are also applicable to polymersomes.<sup>134</sup> However, despite the fact that most publications derive the advantages of polymersomes for encapsulation and delivery applications from comparisons with liposomes, it should be noted that viral capsids are increasingly recognized to be a more appropriate system for comparative studies, as both, polymersomes and viral capsids are composed of long-chain building blocks with similar molecular weight and physico-mechanical properties.<sup>120</sup>

So far, only a few fabrication techniques are known that yield polymersomes with the desired low polydispersity and controlled size.<sup>142</sup> While the development of novel polymersome fabrication techniques is thus one of the key motivations of this thesis,<sup>149,150</sup> current research on drug encapsulation and targeted delivery systems is not solely restricted to polymersomes. In search of alternatives to vesicles from copolymer building blocks, libraries of supramolecular structures from Janus-like dendrimers have recently been shown to be an interesting approach to form complex architectures by self-assembly, including vesicles, so called dendrimersomes.<sup>151,152</sup> Although dendrimer membranes are considerably stronger than their copolymer-based equivalents, dendrimersomes can as easily be lysed as polymersomes and liposomes. In addition, conventional vesicle fabrication techniques can be applied to fabricate uniform, long-term stable capsules.

## 1.2.1 Microfluidic polymersome fabrication techniques

### Hydrodynamic flow focusing

As mixing is dominated by diffusion, it is therefore inefficient to achieve homogeneous distribution of two fluids in a macroscopic system by passively waiting.<sup>153</sup> The mixing process can be accelerated by actively inducing turbulence.<sup>154</sup> However, the reaction kinetics of many processes at liquid-liquid interfaces, the folding of proteins, for instance, are on a time scale of milliseconds, and thus difficult to control even though using the fastest conventional turbulent mixers available, such as high-speed spray nozzles.<sup>12,155</sup>

To circumvent the limitations of turbulent mixing and enhance mixing rates, one needs to reduce the length scale on which the fluids mix.<sup>b</sup> This can be achieved in a microfluidic device.<sup>156,157</sup> The most common device design in PDMS-based microfluidics involves four perpendicular channels, of which three serve as inlets and one as the outlet channel, as shown in Figure 10.

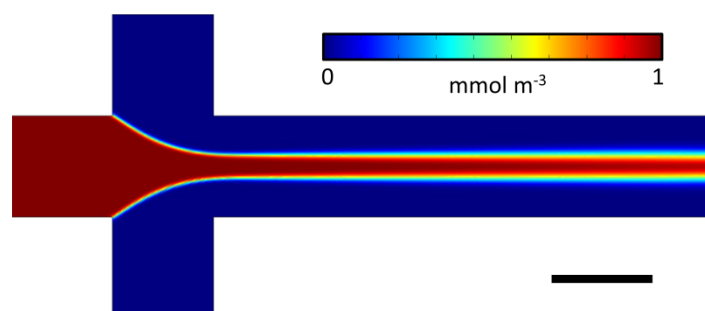


Figure 10: 2D simulation of the diffusion-based mixing of a flow-focused fluid stream in a microfluidic cross junction. The scale bar denotes 100 μm.

A solvent containing the compound of interest, such as a protein, copolymer or the like, is injected into the center inlet and narrowed into a jet by the solvent streams injected into both side channels. At their interface, the desired reaction is initiated by molecular diffusion. By tuning the flow rate ratio  $f_R$  between the center stream and the side streams, the width of the flow-focused jet can be adjusted over several orders of magnitude,

<sup>b</sup> A detailed theoretical background is provided in chapter 1.3.

allowing the controlled formation of stable fluid jets with diameters down to tens of nanometers, and thus controlled mixing times of microseconds.<sup>19</sup>

Due to its ability to control fluid flows on the same length scale as self-assembly processes, hydrodynamic flow focusing has opened up a wide field of applications. This includes the fabrication of organic and inorganic nanoparticles by nanoprecipitation,<sup>158,159,160,161,162</sup> or the preparation of polymer microspheres containing camptothecin for cancer therapy.<sup>163</sup> Like all other microfluidic technologies, HFF only requires small sample volumes. This facilitates the investigation of material properties of precious biomacromolecules such as proteins or DNA as well as their mechanical manipulation making use of the influence of geometric constraints on the flow at the fluid interfaces.<sup>155,164,165,166</sup> In addition, HFF can also be applied for fabricating vesicles. However, the majority of investigations has focused on liposome formation.<sup>167,168,169,170</sup> Only one very recent publication has reported the vesicular self-assembly of copolymers using HFF, though without elucidating the control over the vesicle size.<sup>118</sup> On this account, HFF was studied in the present work as a method for fabricating pH-sensitive polymersomes with tailored size for potential biomedical application. Special attention was drawn to form polymersomes in the size range of 50-150 nm, which is the optimal size to be applied for tumor-targeted drug delivery benefiting from the enhanced permeability and retention (EPR) effect<sup>c</sup> and to preserve the cell viability.<sup>104,107,113,171</sup>

### **Double-emulsion templates**

In conventional industrial processes, emulsions are typically formed using porous membranes or shear cells.<sup>172,173</sup> However, these techniques usually create emulsions with large size distributions. It is therefore difficult to control the encapsulation efficiency and amount of active ingredients in each droplet. Therefore, encapsulation for compartmentalization and triggered release of actives is still an insufficiently solved challenge for many formulations. Hence the investigation of novel encapsulation technologies is in the focus of current formulation research.

---

<sup>c</sup> EPR refers to the accumulation of nanoparticles in a tumor due to low lymphatic drainage of the surrounding interstitial fluid and high permeability of the tumor's vascular system.

Instead of forming many drops with poor control, in microfluidic devices, each drop is formed with unrivalled control. Unlike the microfluidic experiments discussed earlier using a *continuous* flow, droplet-based microfluidics creates and manipulates *discrete* volumes using immiscible fluids in a *segmented* flow. A single droplet can be interpreted as an independent microreactor, that enables rapid mixing, and thus short reaction times.<sup>37,41,157</sup> Each emulsion droplet can be individually loaded with actives, mixed, sorted, fused with other droplets or analyzed, being fabricated at rates of several kilohertz and almost quantitative encapsulation efficiency.<sup>5,37,174,175,176</sup>

Various channel designs are feasible to form drops. The most common channel geometries are flow-focusing junctions,<sup>177,178</sup> T-junctions,<sup>179,180,181</sup> and co-flowing junctions.<sup>182,183,184</sup> However, droplet microfluidics is not limited to single emulsions. By repeating one emulsification step, higher order emulsions can be formed as well, where each compartment is tunable with the same precision as a single emulsion droplet.<sup>185</sup> The most prevalent type are double emulsions, which are drops of one fluid encapsulated inside drops of a second immiscible fluid; they are either formed in a two-step or in a one-step process.<sup>186,187</sup> While O/O/W and W/W/O double emulsions are marginally stable,<sup>188,189</sup> water-in-oil-in-water (W/O/W) and oil-in-water-in-oil (O/W/O) double emulsions are widely used as a versatile tool for fabricating nanoparticles,<sup>190,191</sup> core-shell microcapsules and Janus-like particles with compartments that can be individually tuned with respect to size, composition and physical properties.<sup>192,193</sup> Such particles can be applied as electronic paper ink or optical sensors, for instance. Yet other applications focus on the formulation and delivery of drugs with acoustically triggered release mechanism, or nutrients in reduced-fat products.<sup>194,195,196,197</sup>

As double emulsions provide a highly controllable architecture, they are also a promising tool for the directed self-assembly of rather sophisticated structures like phospholipid vesicles,<sup>198</sup> as well as single and multicompartiment polymersomes using copolymer-stabilized double-emulsion templates.<sup>199,200</sup> Up to date, the fabrication of these templates is performed in microfluidic glass capillary devices.<sup>201</sup> However, the scale of control provided by capillary devices comes at cost as only small quantities can be prepared. To produce larger quantities, the glass capillary devices need to be parallelized. Their parallelization is difficult though due to their complex fabrication process. As each device requires shaping and manual alignment of several microcapillaries, large-scale production

and potential industrial application is severely restricted. To overcome the issues related with the use of glass capillary microfluidics is thus one of the aims of this thesis, as further elaborated in chapter 1.4.

To form polymersomes from double-emulsion templates, water/organic solvent/water (W/O/W) double emulsions are fabricated with a copolymer dissolved in the middle phase. By using a mixture of a good solvent and a bad solvent, the solubility of the copolymer as well as the density and evaporation rate of the organic solvent mixture can be precisely controlled, thus preventing destabilization of the double emulsion upon the templated vesicular assembly of the copolymer molecules. In the actual experiments, it was found that the stability of double-emulsion templates and the resulting polymersomes is further enhanced by addition of the homopolymer PLA. It is assumed that the homopolymer is incorporated in the vesicle bilayer.<sup>202</sup>

Inside the double emulsion, the copolymer migrates to the W/O and O/W interface of the double emulsion droplet, respectively, and stabilizes the emulsion due to its surfactant-like nature. A crucial aspect is the copolymer concentration. If the number of copolymer molecules at the inner/middle (W/O) and middle/outer (O/W) interface of the double-emulsion droplet is lower than the minimum amount to fully cover the two interfaces, the inner drop coalesces with the outer aqueous phase. Stable double-emulsion templates, however, undergo the desired emulsion-to-polymersome transition, with the shell of organic solvents dewetting from the inner drop, as shown in Figure 11.



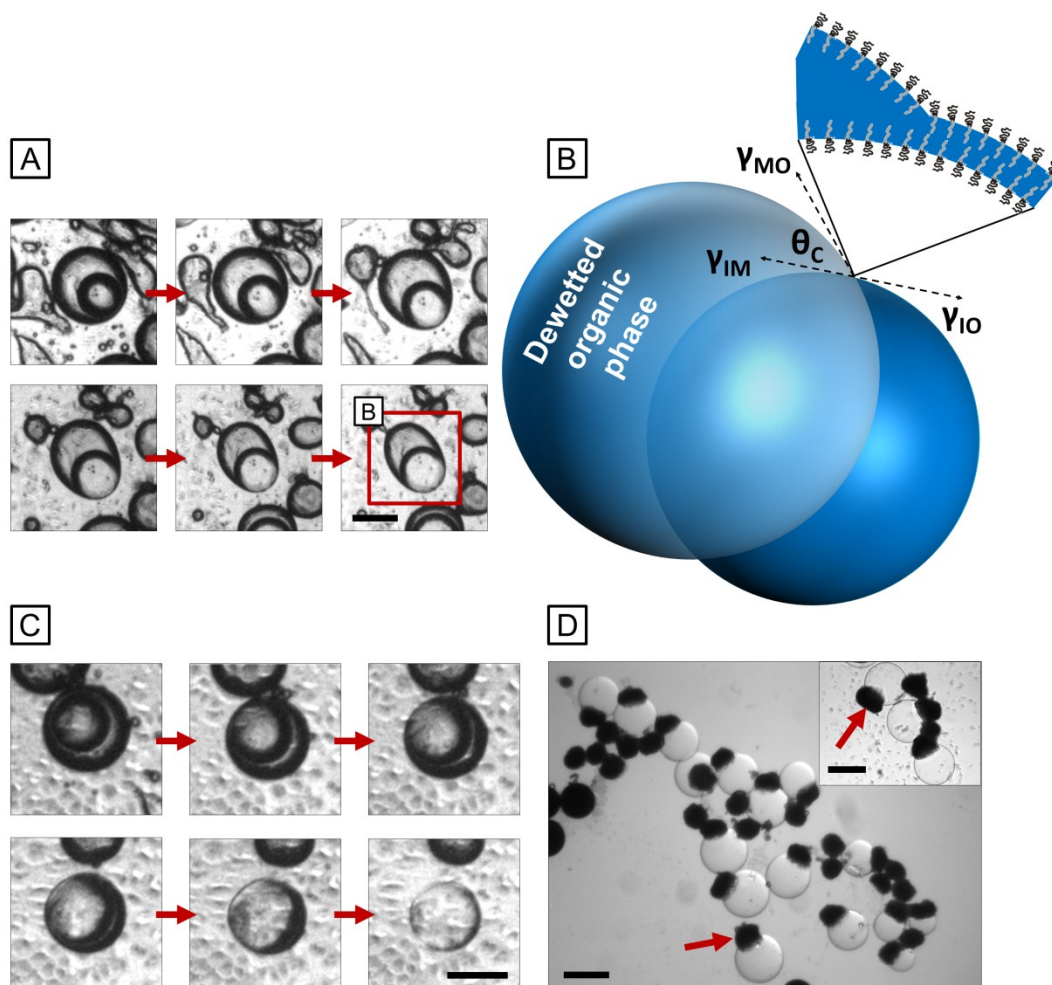


Figure 11: (A) Bright-field microscopy image sequence of the dewetting transition of a copolymer-stabilized W/O/W double emulsion droplet. The inner phase is composed of a solution of glucose (100 mM), surrounded by a shell of toluene and chloroform, 2:1 by volume, with PEG-*b*-PLA<sup>206,207</sup> at 120 mg mL<sup>-1</sup> and PLA at 40 mg mL<sup>-1</sup>. The continuous phase is a 10 wt% poly(vinyl alcohol) (PVA) solution. As the double emulsion is left in air, most of the double emulsion droplets burst upon transition. The time frame is 21.1 s. (B) Corresponding schematic of the dewetting transition. Adapted from<sup>201</sup>. (C) Bright-field microscopy image sequence of the dewetting of a PEG-*b*-PLA-stabilized W/O/W double emulsion droplet with an organic solvent shell containing 60 mg mL<sup>-1</sup> copolymer and 20 mg mL<sup>-1</sup> homopolymer. The time frame is 21.0 s. At lower initial polymer concentrations, smaller contact angles are observed during solvent evaporation (lower row). (D) After complete solvent evaporation, a patch of excess copolymer and homopolymer usually remains on the bilayer surface of the polymersomes, as indicated by the arrows. Scale bars denote 50  $\mu$ m.

The dewetting transition is driven by the adhesion energy between the inner and outer organic solvent/water interfaces with adsorbed polymer monolayers due to depletion

### 1.2.1 Microfluidic polymersome fabrication techniques

---

interactions, similar to the ones known from mixtures of hard spheres and solvated polymer chains:<sup>203</sup>

$$\gamma_{IO} = \gamma_{IM} + \gamma_{MO} - E_{adhesion} \quad (1-10)$$

with the interfacial energy of the bilayer  $\gamma_{IO}$ , the surface tension of the inner/middle and middle/outer interface,  $\gamma_{IM}$  and  $\gamma_{MO}$ , respectively, and the adhesion energy  $E_{adhesion}$ , which scales with the copolymer concentration, as shown in Figure 11A and C.<sup>204</sup> Assuming  $\gamma_{IM} = \gamma_{MO}$ , the contact angle  $\theta_c$  between the W/O and O/W interfaces, and thus the morphology of the equilibrium structure of the state of wetting, can be directly determined using the Young-Duprè equation.<sup>205</sup>

$$E_{adhesion} = 2\gamma_{IM}(1 - \cos \theta_c) \quad (1-11)$$

In the example shown in Figure 11B, the dewetting transition results in an acorn-like state of partial wetting of the organic solvent drop on the surface of the just formed polymersome bilayer. The drop of organic solvents continues to evaporate to give rise of the final polymersome with a dried aggregate of excess copolymer attached to its surface, as shown in Figure 11D. The size of the aggregate, which occasionally detaches from the bilayer surface, is controlled by the initial copolymer concentration.

### 1.3 Fluid flow in microchannels – manipulation and simulation

The complexity of microfluidic devices has grown to a stage where further development and improvement requires simulations of the fluid flows therein to enable an efficient device design process, and to model situations, which are otherwise difficult to test in reality. A simulation tool was therefore applied to optimize the microfluidic devices in the present work to gain insights in the fluid dynamics.

Computational fluid dynamics (CFD) is the standard tool for modeling fluid flow using numerical methods to solve partial differential equations (PDEs) that describe the transport of mass, momentum, and energy in moving fluids.<sup>208</sup> Numerous methods have been described in literature for approximating PDEs by discretization of the respective fluid dynamics problem. The most common are the finite element method (FEM), the finite difference method (FDM) and the finite volume method (FVM).<sup>209,210,211</sup> While CFD has been dominated by FDM and FVM in the last decades due to limited computational capacity, FEM has evolved as a powerful simulation tool due to recent advances in computer power, enabling high-accuracy modeling by handling complex mesh structures, and has therefore been chosen in the present work.

The mathematical model of any fundamental problem in fluid dynamics is governed by the Navier-Stokes equations, a set of two PDEs.<sup>211,212,213,214</sup> The first equation describes the velocity field in a Newtonian fluid by applying Newton's second law of motion<sup>d</sup> to a finite element of a fluid.

$$F + \eta \nabla^2 u - \nabla p = \rho \frac{\partial u}{\partial t} + \rho(u \cdot \nabla)u \quad (1-12)$$

with the velocity vector of the fluid flow  $u$ , the dynamic viscosity  $\eta$ , the fluid density  $\rho$ , and the long-range force per unit volume  $F$ , which can be gravity, for instance. The term  $\eta \nabla^2 u - \nabla p$  expresses the stress forces per unit volume due to a pressure gradient  $\nabla p$  and the viscosity  $\eta \nabla^2 u$ . In terms of Newton's law, the left-hand side of (1-12), which represents the total force that affects the fluid flow in a finite element, is equal to the

---

<sup>d</sup> If mass  $m$  is subject to force  $F$ , it undergoes an acceleration  $a$  with the same direction as  $F$  and a magnitude that is proportional to  $F$  and inversely proportional to  $m$ :  $F = ma$ .

acceleration per unit volume times the mass, while the right-hand side is obtained by expressing the acceleration in terms of the velocity field.

Assuming that a liquid is incompressible, which is a good approximation for the liquids used in the microfluidic experiments in this thesis, and neglecting the molecular nature of a liquid, thus treating it as a continuum, the second of the Navier-Stokes equations is obtained, referred to as the continuity equation.

$$\nabla \cdot u = 0 \quad (1-13)$$

It implies that the mass of a liquid flowing into a finite element over a period of time must be balanced by the same mass flowing out.

If the characteristic length of the fluid flow decreases to the size of the fluid transport system, a fundamental change in hydrodynamics occurs; viscous forces start to dominate over inertial forces, and the flow pattern is governed by laminar, turbulence-free flow. The Reynolds number is a measure for laminar flow and relates the magnitude of the inertial term  $\rho(u \cdot \nabla)u$  and the viscous term  $\eta \nabla^2 u$ .

$$Re = \frac{|\rho(u \cdot \nabla)u|}{|\eta \nabla^2 u|} = \frac{\rho v}{\eta} l \quad (1-14)$$

where  $l$  is a characteristic length (here the channel diameter) and  $v$  the flow velocity.<sup>213,215</sup>

In a microfluidic device, the inertial term can be neglected, because the flow velocity varies on the scale of the channel length  $l$ , hence  $Re \ll 1$ .<sup>19,216</sup> As the long-range force  $F$  is assumed to be uniform on a microscopic scale, it can be included in the pressure term  $\nabla p$  that becomes the modified pressure  $\nabla p'$ . This transforms the nonlinear Navier-Stokes equations into a set of linear PDEs, known as the Stokes equations.<sup>213</sup>

$$\eta \nabla^2 u = \nabla p' \quad (1-15)$$

$$\nabla \cdot u = 0 \quad (1-16)$$

Unlike (1-12), (1-15) contains no time derivative, since all fluid motions are symmetric in time at  $Re \ll 1$ .<sup>214</sup> Another important consequence of low-Reynolds-number flow is that

mixing is dominated by diffusion.<sup>19,157</sup> This can be elucidated by comparing the mixing time  $t_{mixing}$  with the diffusion time  $t_{diffusion}$ .

$$t_{mixing} = \frac{l}{v} \quad (1-17)$$

$$t_{diffusion} = \frac{l^2}{D} \quad (1-18)$$

where  $v$  and  $D$  denote the flow velocity and the diffusion coefficient, respectively.<sup>214</sup> As mentioned in chapter 1.2.1, the mixing time scales linearly with the characteristic length  $l$ , which is why mixing is dominated by convection in large geometries. On the contrary, the diffusion time scales as the square of  $l$ . Thus, diffusion becomes very important, when reducing the characteristic length to the micron scale. To describe diffusion at a given point in the microfluidic device, Fick's second law is used, giving the relation between the concentration gradient  $\nabla c$  and the rate of change of concentration by diffusion.<sup>217</sup>

$$\frac{\partial c}{\partial t} = -\nabla \cdot J = \nabla \cdot (-D\nabla c) \quad (1-19)$$

where  $J$  is the diffusive flux that measures the amount of substance moving through an area per time interval.

In order to fully describe a flow-focusing experiment in a microfluidic device using CFD simulations, the Navier-Stokes equations describing the physics of the fluid flow, (1-12) and (1-13), need to be coupled with Fick's law for diffusion, (1-19), which determines the local concentration and concentration changes in the microfluidic device. The concentration profile in a microfluidic flow-focusing device is exemplarily shown in Figure 12A. Since all fluid motion is stationary at low-Reynolds numbers, the concentration of the copolymer molecules or fluorescent dyes in the flow-focused fluid jet can be precisely determined at any point of the reaction as the time evolution of the reaction is separated spatially in the outlet channel of the device, as shown in Figure 12B. This enables time-resolved monitoring of the diffusion-based mixing with a resolution of a microsecond per micron channel length. Thereby, temporal resolution is extended by several orders of magnitude compared to conventional time-resolved measurements using HFF in a microfluidic device.<sup>153,155</sup>

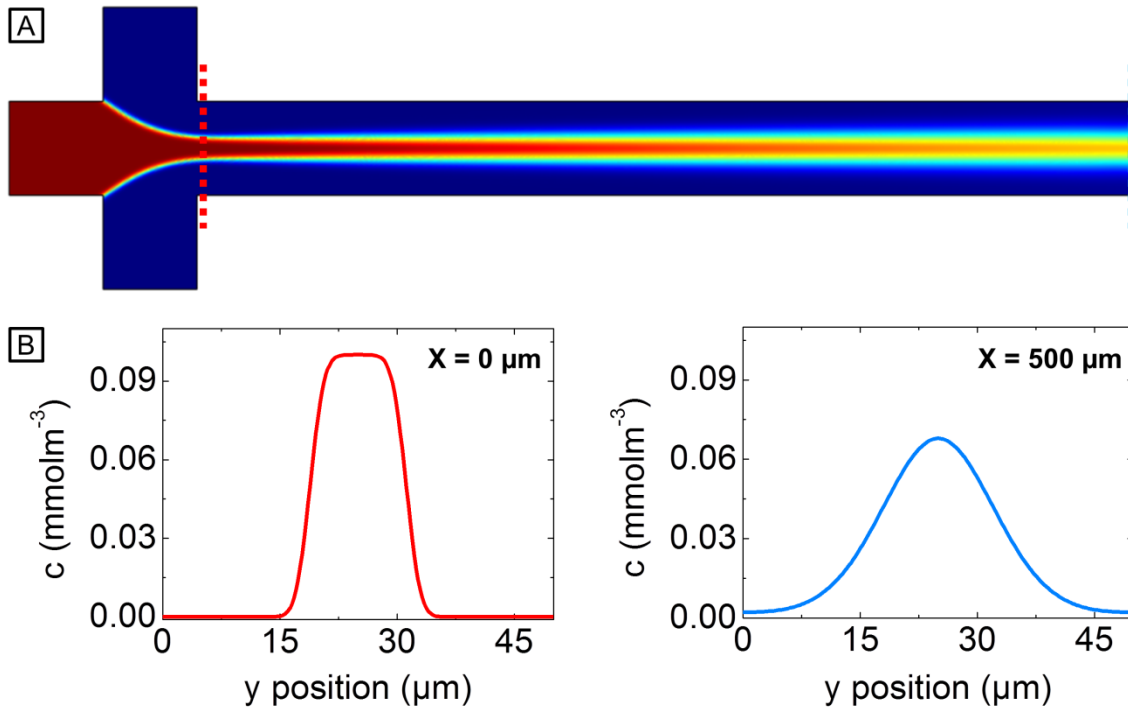


Figure 12: FEM-based simulation showing diffusion-based mixing of a flow-focused fluid jet in a microfluidic channel cross. Rhodamine B in water at  $0.01 \text{ mol m}^{-3}$  is flow-focused by pure water. The flow velocity in each inlet channel is  $0.004 \text{ m s}^{-1}$ . (A) 2D surface plot of the concentration profile. (B) Cross sections of the outlet channel at  $x = 0 \mu\text{m}$  and  $x = 500 \mu\text{m}$ .

Due to the large surface-to-volume ratio of microchannels, surface properties have a significant impact on the flow resistance and the velocity profile of fluids inside microfluidics devices. An important requirement for simulating the fluid flow in microfluidic devices is thus the definition of suitable boundary conditions. To describe the interaction of a flowing fluid and a solid surface, the Navier boundary condition is generally applied: it is based on the assumption that the flow velocity  $v_x$  tangential to the surface is proportional to the shear stress at the surface,<sup>218,219,220</sup>

$$v_x = \lambda \frac{dv_x}{dy} \quad (1-20)$$

where  $\lambda$  denotes the slip length or Navier length. The slip length can be illustrated as the distance between the surface and an imaginary point inside the solid wall, where the velocity profile extrapolates to zero, as sketched in Figure 13. If  $\lambda = 0$ , no slip is present,

which is widely accepted as suitable boundary condition to describe the interaction of a fluid and a solid wall.

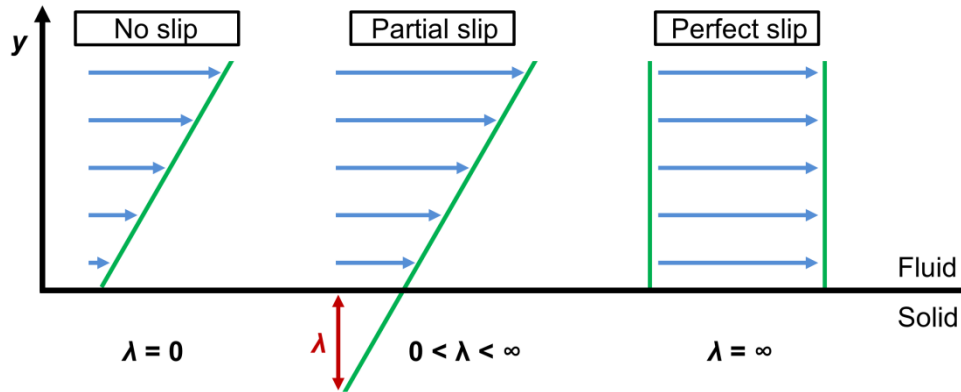


Figure 13: Illustration of the slip length  $\lambda$ . Adapted from <sup>213,218,221</sup>.

It should be noted that the no-slip boundary condition remains an assumption that is rather based on experimental findings than physical principles. The magnitude of fluid slip depends on many parameters, such as the roughness and wettability properties of the surface as well as dissolved gas in the fluid stream. More recently, controlled experiments involving among others SFA (surface force apparatus) and  $\mu$ -PIV (microparticle image velocimetry) demonstrated a violation of the no-slip boundary condition for Newtonian liquids, observing slip lengths in the low-nanometer range.<sup>222,223,224,225</sup> However, as the setup for the flow-focusing experiments merely involves PDMS-based microfluidic devices with untreated surfaces as well as ethanol and aqueous solutions, the no-slip boundary condition is a good approximation. The boundary condition for each line in case of a 2D model and each wall in case of a 3D model are summarized in Figure 14.

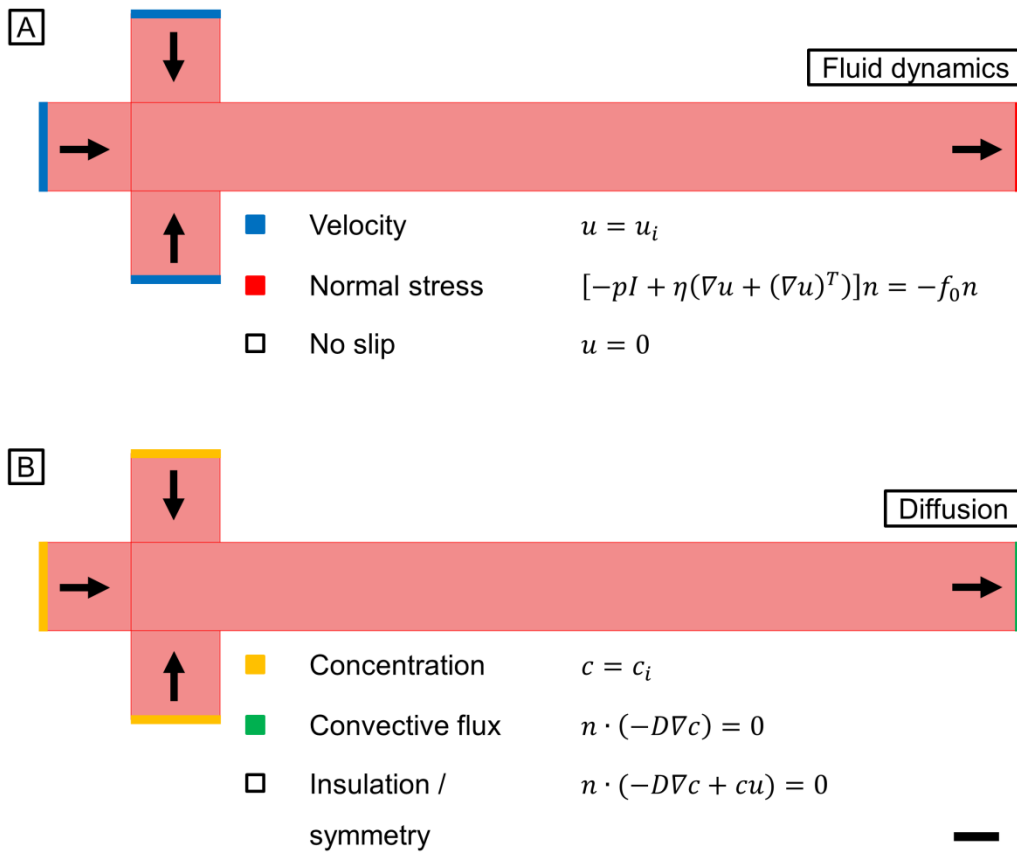


Figure 14: Boundary conditions in a model for simulating flow-focusing experiments in a microfluidic cross junction. To approximate the solution to this fluid dynamics problem by FEM, two sets of PDEs are combined describing (A) the fluid dynamics using the incompressible Navier-Stokes equations and (B) the diffusion of the solvent streams. The inflow velocity is given by  $u_i = -nU_0$ , where  $u_i$  is the velocity vector at each of the three inlets ( $i = 1,2,3$ ) and  $n$  the normal perpendicular to the boundary. Accordingly, the concentration is given by  $c = c_i$ , where  $c_i$  is the initial concentration at each inlet ( $i = 1,2,3$ ). The total stress on the outlet is set equal to a vector  $f_0$ , oriented in negative normal direction, where  $I$  is the identity matrix. In the case of a two-dimensional fluid,  $f_0 \approx p$ . It is assumed that the fluids are transported through the outlet solely by convective flux, thus  $n \cdot (-D\nabla c) = 0$ . As diffusion through the microchannel walls is neglected,  $n \cdot (-D\nabla c + cu) = 0$ .<sup>212</sup> The scale bar for both panels denotes 25  $\mu\text{m}$ .

For generating simulation models, a cluster of eight Intel<sup>®</sup> Xeon<sup>®</sup> processors with a clock speed of 2.83 GHz and 32 GB internal memory was used in the present work. Despite the computational power, another critical issue of FEM simulations is the number of finite elements (FEs) that is applied for discretization of the fluid dynamics problem. To explain this by example, a 3D model of a flow-focusing experiment is discretized applying three different quantities of finite elements at a constant mesh quality, as shown in Figure 15.



The number of FEs as well as the mesh quality is default by COMSOL. The results are compared with a 3D CLSM image of the corresponding experiment.

Although all three models converge to a solution, the discrepancy between simulation and experiment is especially obvious at low FE numbers, as shown in Figure 15A. As the mesh grid merely consists of 4746 FEs, geometric features, such as corners, are not sufficiently resolved. As a result, negative as well as order-of-magnitude higher concentration values than the initial dye concentration are calculated within the confluence of the center stream and the side streams, which leads to a nearly homogeneous distribution of the fluorescent dye in the outlet channel. However, as the number of FEs is increased, such artifacts are largely avoided, and the simulation result is in good agreement with the experiment, as shown in Figure 15C and 15D.

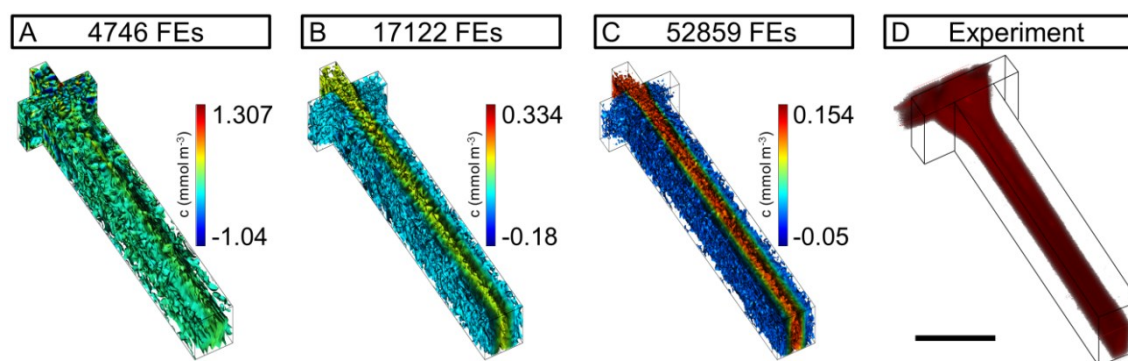


Figure 15: Effect of the number of finite elements (FEs) on the accuracy of CFD simulations. A 3D model of a microfluidic device in which an aqueous solution of Rhodamine B (0.123 M) is flow-focused by water is exemplarily discretized. The flow velocity is  $0.002 \text{ m s}^{-1}$  in each side inlet and  $0.004 \text{ m s}^{-1}$  in the center inlet. The diffusion coefficient  $D$  of the fluorescent dye is estimated to be  $4.2 \cdot 10^{-10} \text{ m}^2 \text{ s}^{-1}$ .<sup>226</sup> Isosurface rendering is used to visualize the dye concentration. (A) The solution predicts a nearly uniform concentration profile in the outlet channel. Artifacts with negative concentration values as well as order-of-magnitude higher values than the initial dye concentration are observed. (B) The formation of a flow-focused jet is simulated, as the number of artifacts is significantly reduced. (C, D) The simulation result is in good agreement with the experiment, represented by a 3D reconstruction of stacks of 2D CLSM images. The scale bar denotes  $100 \mu\text{m}$ .

Although PDMS-based microfluidics offers a rapid turn-around time from experiment design to device fabrication and application, the optimization of complex device

geometries solely based on experimental data is a time-consuming and resource-intensive process, usually requiring screening of a large number of device geometries. This issue can be addressed by incorporating CFD simulations in the device design process. In the following, two examples of microfluidic devices are presented, where simulation-based rapid prototyping (SBRP) was successfully applied to optimize the microchannel geometry by studying the fluid dynamics therein.

As described in chapter 1.2.1, a general geometry for flow focusing a fluid stream, is a channel cross junction with three inlets and one outlet. As the temporal evolution of diffusion between the flow-focused center stream and the two side streams in the outlet channel is separated spatially, the degree of intermixing between a copolymer-loaded solvent injected into the center inlet and water injected into both side channels, for instance, can be controlled by the length of the outlet channel. By allowing for complete diffusion of the copolymer into the water, it can be assumed that the copolymer is entirely consumed in the vesicular self-assembly process and uncontrolled aggregation of remaining copolymer molecules outside the controlled environment of the microfluidic device is prevented. To optimize the flow length  $x_f$  and determine the point of complete diffusion, a series of 2D models of flow-focusing devices were simulated using FITC dextran (10 kDa,  $D = 8 \cdot 10^{-11} \text{ m}^2 \text{ s}^{-1}$ )<sup>227,228</sup> as a model solute, as shown in Figure 16. The optimal flow length  $x_f$  was determined to be 0.411 m taking a flow rate ratio  $f_R$  ranging from 8 to 0.125 into account in the later experiments.

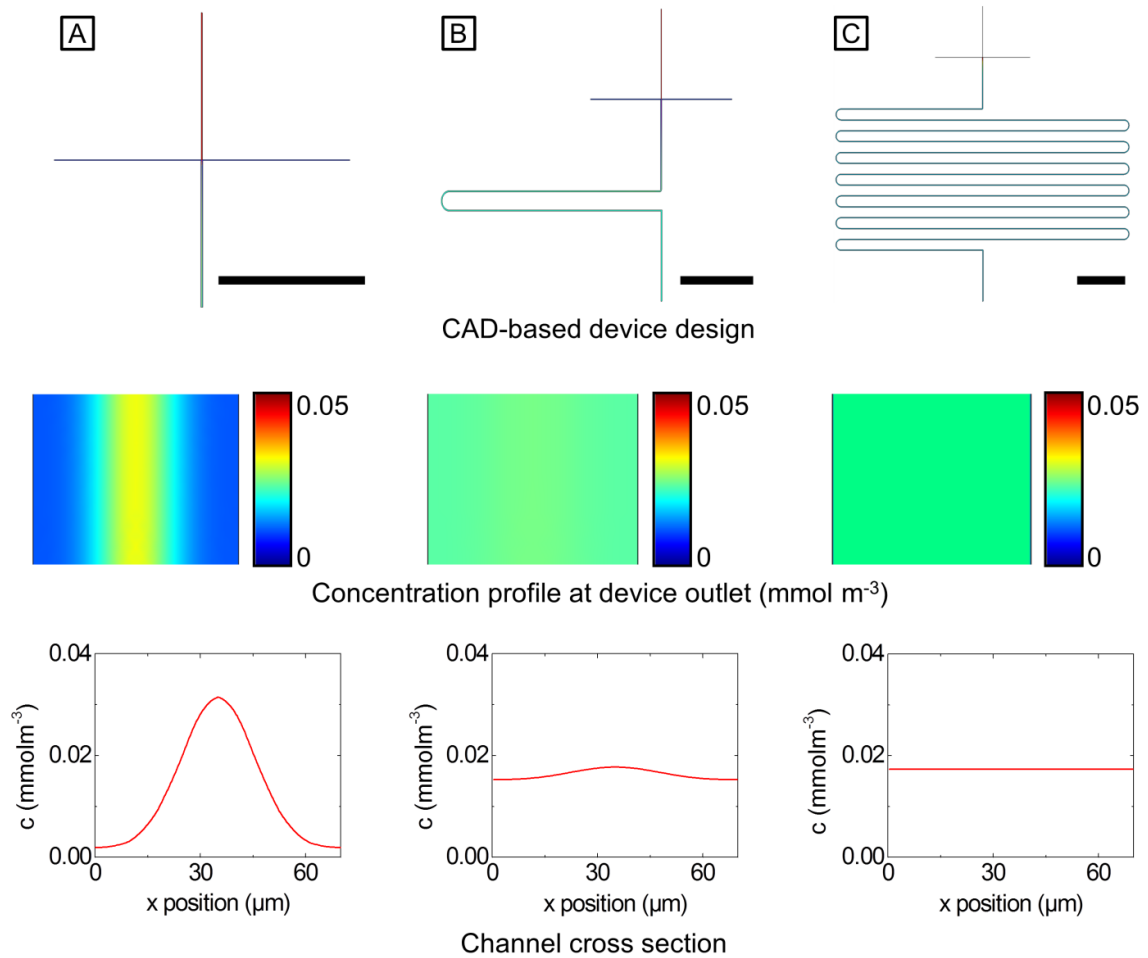


Figure 16: FEM simulation of diffusion-based mixing of water and an aqueous solution of FITC dextran at  $c = 0.05 \text{ mmol m}^{-3}$ . As an example, the flow velocity is equally set to  $0.05 \text{ m s}^{-1}$  for FITC dextran, which is injected into the center channel and water, which is injected into both side channels. By tuning the flow length  $x_f$  inside the microfluidic device, the degree of intermixing of the two fluids can be precisely controlled upon collection at the outlet. Three microchannel geometries are exemplarily shown, and the concentration profile at the outlet of each device is simulated as slide and line plot to determine the degree of intermixing. (A) Single cross junction with a short outlet channel,  $x_f = 0.005 \text{ m}$ ; (B) single cross junction with a single meander turn,  $x_f = 0.028 \text{ m}$ ; (C) single cross junction with a 13-fold meandering outlet channel,  $x_f = 0.411 \text{ m}$ . The scale bars denote  $5 \text{ mm}$ .

In the second example, SBRP was applied to optimize the channel geometry of a microfluidic spray dryer, described in chapter 2.5. To enable processing of hydrophobic drugs and prevent fouling of the PDMS-based device due to the adsorption of precipitates, the surface contact between the hydrophobic drug and the hydrophobic channel walls had to be minimized. This was achieved by optimizing the microchannel's aspect ratio. For this purpose, a series of single, straight microchannels were simulated,

applying 41913 finite elements for each model; danazol was used as a hydrophobic model drug, and its diffusion coefficient in water was estimated to be  $D = 6 \cdot 10^{-10} \text{ m}^2 \text{ s}^{-1}$ .<sup>229</sup> By varying  $h/w$  from 0.5 to 10, the surface contact of the drug-loaded solvent stream with the upper and lower channel wall was reduced significantly, as revealed by line scans of the respective area. The manipulation of the quasi-2D flow pattern is exemplarily demonstrated for  $h/w = 0.5, 1$  and 2 in Figure 17A-C.

Based on these findings using a rather simple model comprised of rigid channel walls, hence ignoring the structural response of the soft PDMS to the internal fluid pressure, a more sophisticated model was developed taking the mechanical properties of the PDMS-based microchannels into account. The simulation results as well as a detailed description of the spray dryer and its application are provided in chapter 2.5 and 7.

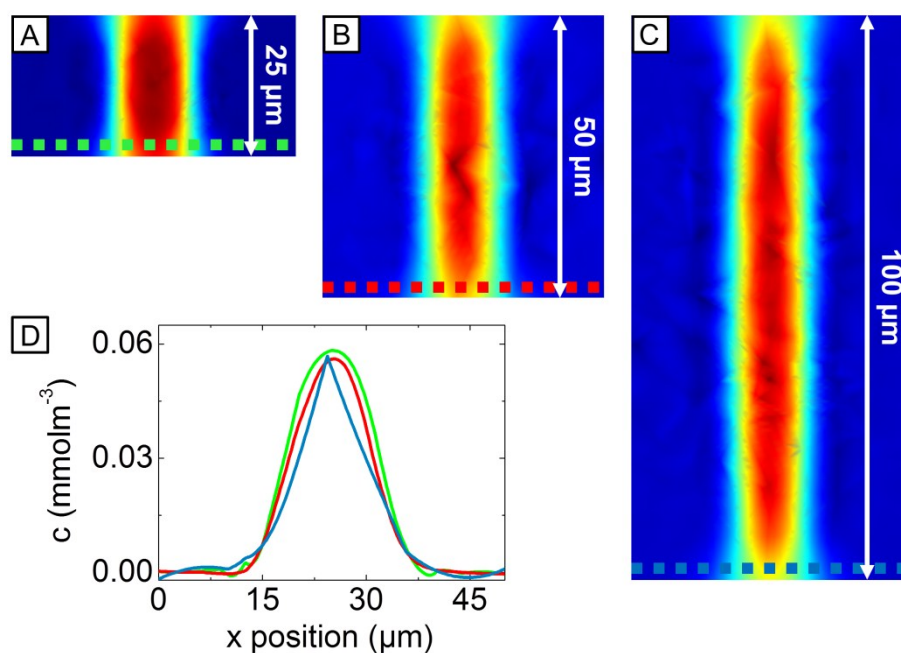


Figure 17: Effect of the device aspect ratio on the surface contact between a flow-focused fluid stream and the upper and lower microchannel walls. The impact of the channel height at a fixed channel width is studied by simulating the concentration profile of a flow-focused solution of Rhodamine B in water in a microchannel, (A) 25 μm, (B) 50 μm, and (C) 100 μm in height, respectively, and 50 μm in width. (d) Line scans of the dye concentration at the lower microchannel wall. With increasing channel height, the width of the concentration profile, and thus the surface of the microchannel in contact with the center stream decreases.

The manipulation and application of emulsions in microfluidic devices as well as elucidating their formation mechanisms is a key element of this thesis. In a first attempt to include CFD simulations in these investigations, the formation of an O/W single emulsion in a microchannel cross was simulated.<sup>177</sup> To model the behavior of the water and the oil phase, the level set method was applied, which describes the transport of a fluid interface separating two phases.<sup>230,231,232,233</sup>

$$\frac{\partial \phi}{\partial t} + u \cdot \nabla \phi = \gamma \nabla \cdot \left[ \varepsilon \nabla \phi - \phi(1 - \phi) \frac{\nabla \phi}{|\nabla \phi|} \right] \quad (1-21)$$

$\phi$  is the level set function describing the volume fraction of a liquid,  $\varepsilon$  is the interface thickness, which is typically half the characteristic mesh size in the area passed by the interface and  $\gamma$  is the reinitialization parameter equal to the maximum flow velocity. The parameter is required as the emulsion formation is simulated stepwise in time. In addition, a modified version of the Navier-Stokes equations considering capillary forces was applied and combined with (1-21).<sup>232</sup> In contrast to the afore discussed CFD models, where no liquid slip was assumed on the microchannel walls throughout the device, wetted walls described by the contact angle  $\theta$  and the slip length  $\beta$  were defined for the outlet channel of the drop maker to mimic a wettability pattern suitable for forming O/W single emulsions. For the fluids, water and the non-toxic hydrofluoroether HFE-7500 were used.<sup>234</sup> The density is  $998.3 \text{ kg m}^{-3}$  for water and  $1614 \text{ kg m}^{-3}$  for the fluorinated oil. The kinematic viscosity is  $1.01 \text{ cSt}$  for water and  $0.77 \text{ cSt}$  for HFE 7500 (all values at  $25 \text{ }^\circ\text{C}$ ). The interfacial tension was estimated to be  $3 \cdot 10^{-3} \text{ N m}^{-1}$ . Due to the complexity of the simulation demanding substantial computational resources, the model of the microchannel junction was merely discretized by 4846 FEs. However, the rather coarse grid allowed for a detailed transient simulation of the drop formation, as shown in Figure 18, with a temporal resolution being comparable to experiments monitored using high speed imaging. In addition, as the properties of each liquid are arbitrary in the simulation, the emulsifiability of other combinations of liquids can be tested without being limited to the library of solvents that is available in a conventional lab.

Future studies will focus on the implementation of CFD simulations for simulating the formation of higher-order emulsions in arrays of quasi-2D and 3D microfluidic junctions. For a detailed *experimental* investigation of drop formation in PDMS-based microfluidic devices, the reader is referred to chapter 2.3 and 5.

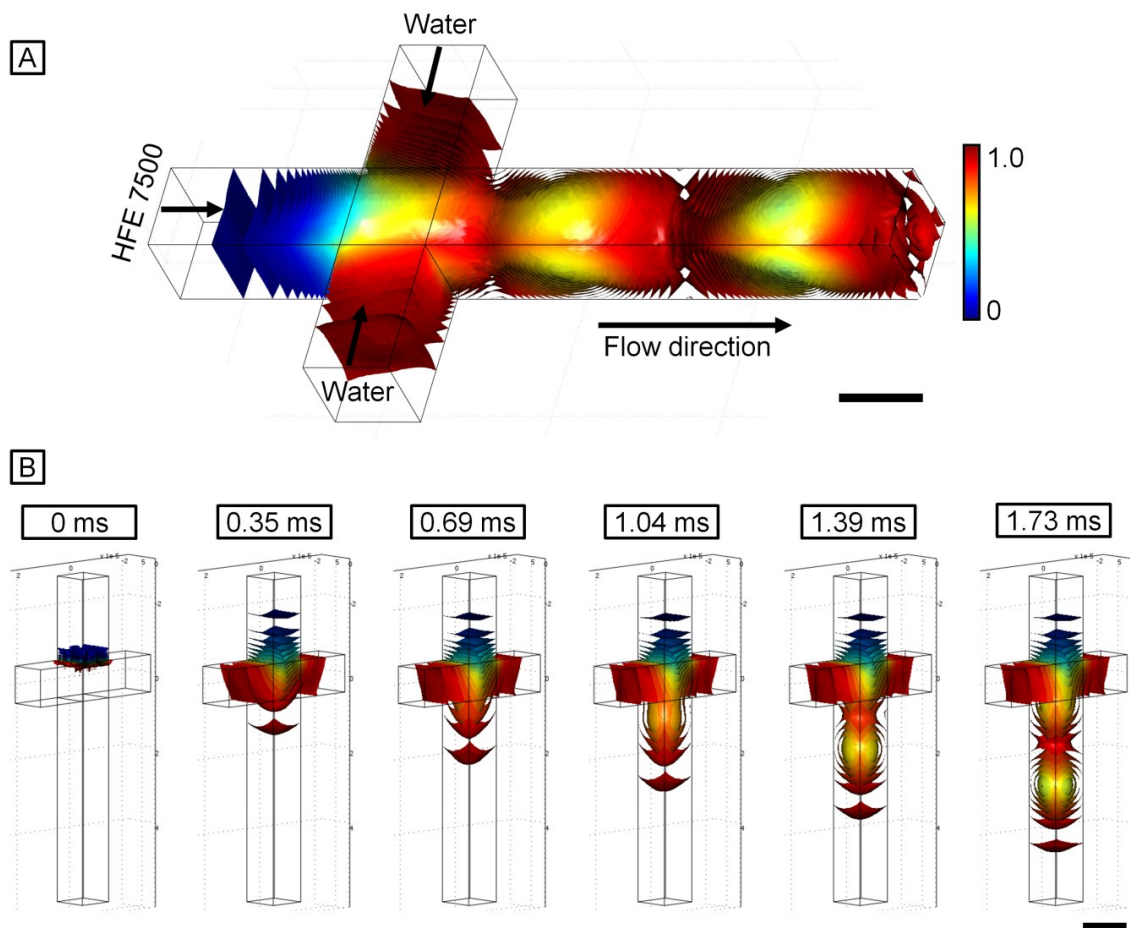


Figure 18: Transient modeling of oil-in-water emulsification applying the LSM for simulating laminar two phase flow.<sup>c</sup> The model consists of 4846 FEs. HFE-7500 and water are injected at equal flow velocities of  $0.05 \text{ m s}^{-1}$ . The device is  $100 \mu\text{m}$  in height and width, the outlet channel is  $550 \mu\text{m}$  in length. (A) Isosurface rendering of the volume fraction of water at  $t = 10$  ms using 100 isosurfaces. (B) To improve the visibility of the encapsulated oil phase, the number of isosurfaces is reduced to 18. The scale bars denote  $100 \mu\text{m}$ .

<sup>c</sup> Original model by courtesy of Prof. Amar S. Basu from Wayne State University.<sup>230</sup>

## 1.4 Motivation, objective and strategy of this thesis

Vesicles formed by the self-assembly of diblock copolymers have gained increasing interest in the last decade, as they provide polymeric containers with controlled biological, chemical and physical properties, which are the basis for a number of applications. This includes the encapsulation, delivery and release of biofunctional compounds such as proteins, enzymes and APIs, and the protective encapsulation of fragrances, flavors and cosmetics. However, while the encapsulation of cosmetics for the uptake through human skin requires polymersomes of several hundreds of microns, targeted drug delivery through cell membranes demands polymersomes of only tens of nanometers. In current research, much effort has thus been devoted to the preparation of polymersomes with controlled size, shell characteristics and polydispersity, as these parameters strongly influence the behavior and functionality of polymersomes for delivery and release applications. Conventional bulk fabrication techniques typically lead to polymersomes with low encapsulation efficiency, broad size distribution and undefined shell characteristics, though, whereas novel microfluidic approaches using glass-capillaries are hard to customize and parallelize for large-scale production. Hence, it would be worthwhile to investigate alternative approaches for forming polymeric vesicles.

The primary objective of this thesis is thus the development of novel techniques for forming polymersomes with controlled size, shell characteristics and narrow polydispersity. This is to be achieved using inexpensive, easy-to-modify and scalable microfluidic devices fabricated by soft lithography in PDMS. Two diblock copolymers, poly(2-vinylpyridine)-*block*-poly(ethylene glycol) and poly(ethylene glycol)-*block*-poly(lactid acid) should be applied as a model system. In the first part of the present work, the undirected vesicular self-assembly of copolymers by HFF is to be explored for fabricating polymersomes in the nanometer range. To elucidate the nucleation and growth of polymersomes and to optimize the device design, simulations of the fluid dynamics in the devices are to be performed. In the second part, the formation of larger, micron-sized polymersomes is in the main focus. The experiments are to be performed employing double-emulsion templates with controlled architecture, which direct the vesicular self-assembly of the copolymer molecules. To investigate the physicochemical properties of

the polymersomes, DLS, CLSM and cryo-TEM should be applied as state-of-the-art characterization methods.

To fabricate polymersomes from double-emulsion templates, fouling of PDMS due to organic solvents has to be prevented, and the surface wettability of the devices needs to be spatially patterned. This is to be achieved by coating the microchannels with a glass-like coating using sol-gel chemistry. However, as this method has only been applied to prevent fouling of simple PDMS-based microchannel geometries so far, initial studies on the controlled distribution of the coating in more complex devices are required. In a subsequent step, the focus is on the surface modification and spatial patterning of coated microchannels. Unfortunately, however, conventional approaches for patterning microfluidic device wettability usually make use of photoinitiators, which do not exhibit long-term stability and that are incorporated into the initial sol-gel coating by a silane-linker, thus narrowing down the number of potential initiators. In addition, those methods require sophisticated optical setups and powerful UV-light sources and do not facilitate fabrication of highly parallelized devices for large scale production of polymersomes. Therefore, a novel method should be derived to simplify the fabrication of patterned microfluidic devices and to allow for parallelization of the device fabrication.

Although, PDMS-based microfluidic devices have extensively been utilized for the formation of single, double and even quintuple emulsions as well as for sorting, manipulating and loading of emulsions, there are no reports on a fundamental and detailed study of multiple emulsion formation in PDMS-based devices. Since double emulsions should be used as templates for the fabrication of polymersomes in the present work, an additional aim of this thesis is thus to provide such fundamental knowledge. For this purpose, the formation of multiple emulsions with water and HFE-7500 as a model system is to be studied, and should be extended to more complex systems such as multiple emulsions formed from viscoelastic polymer solutions and liquids that exhibit a low surface tension with water.

Eventually, the aforementioned different projects converge to the systematic investigation of the fabrication of polymersomes in PDMS-based microfluidic devices as well as the vesicle formation process, the design of microfluidic devices and the fluid dynamics therein. The insights gained from this work should stimulate the exploration of novel applications of microfluidic devices, as described hereinafter.



Over the last decade, the molecular complexity of drugs emerging from drug discovery programs has significantly increased. While molecular complexity generally contributes to biological activity, this trend has also led to poor solubility of potential drug candidates, and, therefore, limited bioavailability and release capability in the human body. As elaborated in chapter 1.2, the encapsulation into polymersomes made from biocompatible building blocks is a promising approach to facilitate the uptake of these drugs. However, despite the many advantages that polymersomes offer, a number of issues related with their design, fabrication and application are still in the focus of ongoing research. In the present work, more interest is thus also devoted to the development of microfluidic processing techniques to increase the bioavailability of drugs by exploring alternative techniques to the polymersome approach. A favorable strategy for this could be decreasing the particle size of the drug by spray drying, which has been demonstrated using conventional spray drying in bulk. On this account, the modification of microfluidic devices, which had been developed and thoroughly investigated for the fabrication of double emulsions in the aforementioned projects, should be used as a basis to implement the spray drying technique in microfluidics.

A comprehensive work schedule summarizing the aims and strategy of this thesis is sketched in Figure 19.

## 1.4 Motivation, objective and strategy of this thesis

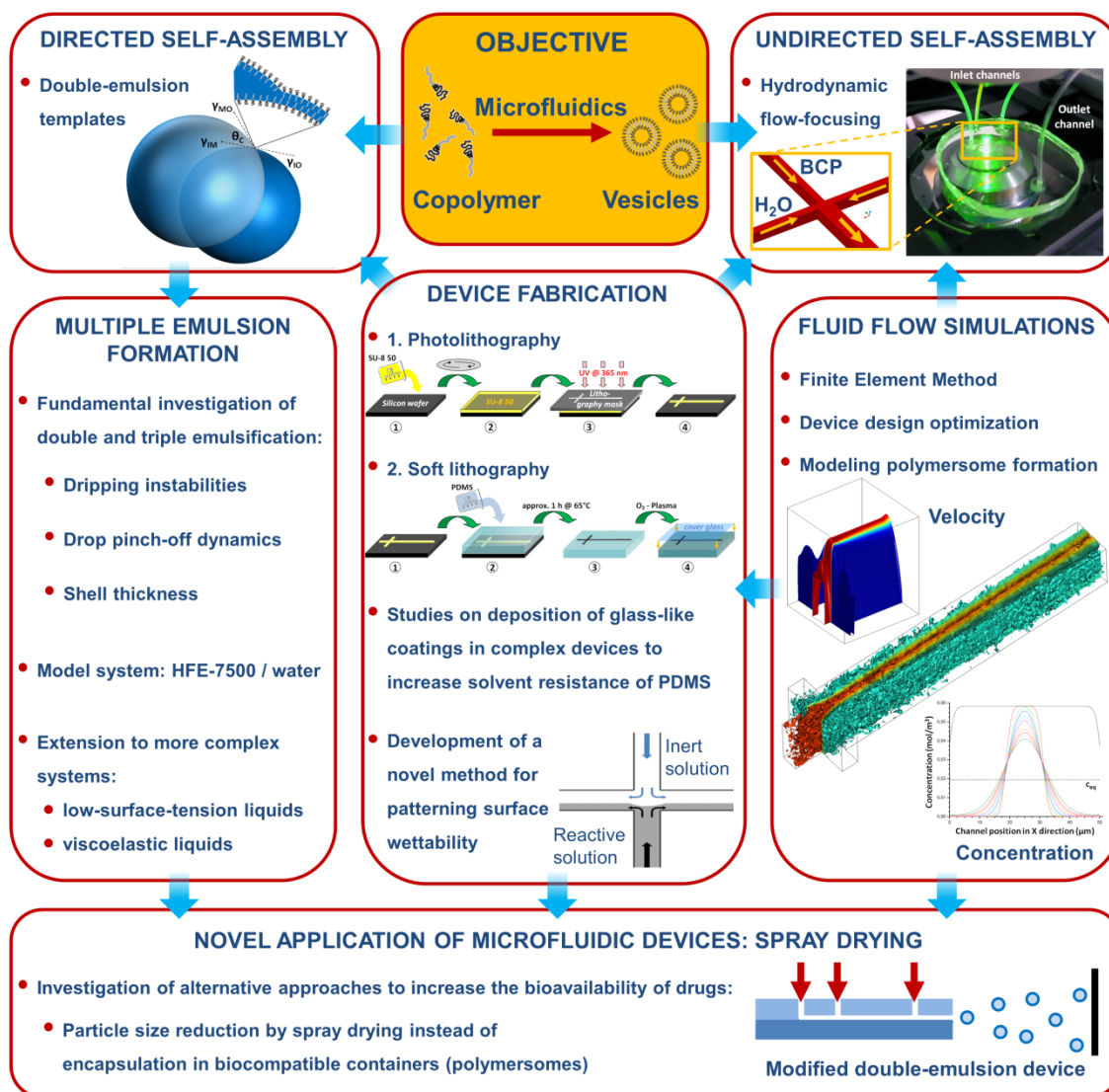


Figure 19: Summarized aim and strategy of this thesis. In order to perform studies on the self-assembly of diblock copolymers by hydrodynamic flow focusing and double-emulsion templates in microfluidic devices, it is necessary to optimize the device design using FEM simulations, and to establish a procedure to increase the resistance of PDMS against organic solvents, as well as to overcome the limitations of conventional methods for patterning surface properties of microfluidic devices by developing a novel, simpler technique. In addition, a deeper understanding of multiple emulsion formation for the controlled fabrication of double-emulsion templates and ultimately polymersomes is required. The knowledge gained from these projects should serve as a basis for novel applications of microfluidic devices, such as spray drying - a promising technique to enhance the bioavailability of hydrophobic drugs and an alternative to the use of polymersomes as biocompatible capsules.

---

## 1.5 References

- (1) Stone, H. A., Stroock, A. D., Ajdari, A. *Annu. Rev. Fluid Mech.* **2004**, *36*, 381-411.
- (2) Groisman, A., Enzelberger, M., Quake, S. R. *Science* **2003**, *300*, 955-958.
- (3) Manz, A., Graber, N., Widmer, H. M. *Sens. Actuators B* **1990**, *1*, 244-248.
- (4) Franke, T., Wixforth, A. *Phys. Unserer Zeit* **2007**, *38(2)*, 88-94.
- (5) Abate, A. R., Agresti, J. J., Weitz, D. A. *Appl. Phys. Lett.* **2010**, *96*, 203509-1-203509-3.
- (6) Abate, A. R., Romanowsky, M. B., Agresti, J. J., Weitz, D. A. *Appl. Phys. Lett.* **2009**, *94*, 023503-1-023503-3.
- (7) Abate, A. R., Hung, T., Mary, P., Agresti, J. J., Weitz, D. A. *Proc. Natl. Acad. Sci. USA* **2011**, *108(5)*, 1821-1826.
- (8) Thorsen, T., Maerkl, S. J., Quake, S. R. *Science* **2002**, *298*, 580-584.
- (9) Tan, Y.-C., Cristini, V., Lee, A. P. *Sens. Actuators B* **2005**, *114(1)*, 350-356.
- (10) Xu, W., Muller, S. J. *Lab Chip* **2011**, *11*, 435-442.
- (11) Pfohl, T. *Analyse, Manipulation und Aggregation von biologischen Makromolekülen im mikrofluidischen Scherfluss*, De Gruyter, **2010**, 331-336.
- (12) Lipman, E. A., Schuler, B., Bakajin, O., Eaton, W. A. *Science* **2003**, *301*, 1233-1235.
- (13) Pihl, J., Sinclair, J., Karlsson, M., Orwar, O. *Mater. Today* **2005**, *8(12)*, 46-51.
- (14) Hany, C., Lebrun, H., Pradere, C., Toutain, J., Batsale, J.-C. *Chem. Eng. J.* **2010**, *160(3)*, 814-822.
- (15) Pennemann, H., Watts, P., Haswell, S. J., Hessel, V., Löwe, H. *Org. Proc. Res. & Dev.* **2004**, *8*, 422-439.
- (16) Song, Y., Hormes, J., Kumar, C. S. S. R. *Small* **2008**, *4(6)*, 698-711.
- (17) Shestopalov, I., Tice, J. D., Ismagilov, R. F. *Lab Chip* **2004**, *4*, 316-321.
- (18) Atencia, J., Beebe, D. J. *Nature* **2005**, *437*, 648-655.
- (19) Squires, T. M., Quake, S. R. *Rev. Mod. Phys.* **2005**, *77(3)*, 977-1026.
- (20) Seiffert, S., Weitz, D. A. *Polymer* **2010**, *51*, 5883-5889.
- (21) Tumarkin, E., Kumacheva, E. *Chem. Soc. Rev.* **2009**, *38*, 2161-2168.
- (22) Priest, C., Quinn, A., Postma, A., Zelikin, A. N., Ralston, J., Caruso, F. *Lab Chip* **2008**, *8*, 2182-2187.
- (23) Kim, C., Chung, S., Kim, Y. E., Lee, K. S., Lee, S. H., Oh, K. W., Kang, J. Y. *Lab Chip* **2011**, *11*, 246-252.
- (24) Morimoto, Y., Tan, W.-H., Tsuda, Y., Takeuchi, S. *Lab Chip* **2009**, *9(15)*, 2217-2223.
- (25) Song, Y., Modrow, H., Henry, L. L., Saw, C. K., Doomes, E. E., Palshin, V., Hormes, J., Kumar, C. S. S. R. *Chem. Mater.* **2006**, *18*, 2817-2827.
- (26) Jahn, A., Reiner, J. E., Vreeland, W. N., DeVoe, D. L., Locascio, L. E., Gaitan, M. J. *Nanopart. Res.* **2008**, *10*, 925-934.
- (27) Kallio, P., Kuncova, J. *Microfluidics – TEKES Technol. Rev.* **2004**, *158*, 1-33.
- (28) Dittrich, P. S., Manz, A. *Nat. Rev. Drug Discovery* **2006**, *5*, 210-218.
- (29) Turgeon, R. T., Bowser, M. T. *Anal. Bioanal. Chem.* **2009**, *394*, 187-198.

## 1.5 References

---

- (30) Zhang, C., Xu, J., Ma, W., Zheng, W. *Biotechnol. Adv.* **2006**, *24*(3), 243-284.
- (31) Dimov, I. K., Basabe-Desmonts, L., Garcia-Cordero, J. L., Ross, B. M., Ricco, A. J., Lee, L. P. *Lab Chip* **2010**, doi: 10.1039/C0LC00403K.
- (32) Trachsel, F., Günther, A., Khan, S., Jensen, K. F. *Chem. Eng. Sci.* **2005**, *60*, 5729-5737.
- (33) Barrett, R., Faucon, M., Lopez, J., Cristobal, G., Destremaut, F., Dodge, A., Guillot, P., Laval, P., Masselon, C., Salmon, J.-B. *Lab Chip* **2006**, *6*, 494-499.
- (34) Chu, L.-Y., Utada, A. S., Shah, R. K., Kim, J.-W., Weitz, D. A. *Angew. Chem. Int. Ed.* **2007**, *46*(47), 8970-8974.
- (35) Shah, R. K., Shum, H. C., Rowat, A. C., Lee, D., Agresti, J. J., Utada, A. S., Chu, L.-Y., Kim, J.-W., Fernandez-Nieves, A., Martinez, C. J., Weitz, D. A. *Mater. Today* **2008**, *11*(4), 18-27.
- (36) Teh, S.-Y., Lin, R., Hung, L.-H., Lee, A. P. *Lab Chip* **2008**, *8*, 198-220.
- (37) Song, H., Chen, D. L., Ismagilov, R. F. *Angew. Chem. Int. Ed.* **2006**, *45*, 7336-7356.
- (38) Huang, C.-J., Lin, H.-I., Shiesh, S.-C., Lee, G.-B. *Biosens. Bioelectron.* **2010**, *25*, 1761-1766.
- (39) Agresti, J. J., Antipov, E., Abate, A. R., Ahn, K., Rowat, A. C., Baret, J.-C., Marquez, M., Klibanov, A. M., Griffiths, A. D., Weitz, D. A. *Proc. Natl. Acad. Sci. U.S.A.* **2010**, *107*(9), 4004-4009.
- (40) Kang, L., Chung, B. G., Langer, R., Khademhosseini, A. *Drug Discovery Today* **2008**, *13*(1,2), 1-13.
- (41) Zheng, B., Tice, J. D., Roach, L. S., Ismagilov, R. F. *Angew. Chem. Int. Ed.* **2004**, *43*(19), 2508-2511.
- (42) Quake, S. R., Scherer, A. *Science* **2000**, *290*, 1536-1540.
- (43) Mata, A., Fleischman, A. J., Roy, S. *Biomed. Microdevices* **2005**, *7*(4), 281-293.
- (44) Zhao, X.-M., Xia, Y., Whitesides, G. M. *J. Mater. Chem.* **1997**, *7*(7), 1069-1074.
- (45) Xia, Y., Whitesides, G. M. *Annu. Rev. Mater. Sci.* **1998**, *28*, 153-184.
- (46) Whitesides, G. M., Ostuni, E., Takayama, S., Jiang, X., Ingber, D. E. *Annu. Rev. Biomed. Eng.* **2001**, *3*, 335-373.
- (47) Priola, A., Bongiovanni, R., Malucelli, G. *Macromol. Chem. Phys.* **1997**, *198*, 1893-1907.
- (48) Rolland, J. P., Van Dam, R. M., Schorzman, D. A., Quake, S. R., DeSimone, J. M. *J. Am. Chem. Soc.* **2004**, *126*, 2322-2323.
- (49) Hoang, P. H., Nguyen, C. T., Perumal, J., Kim, D.-P. *Lab Chip* **2011**, *11*, 329-335.
- (50) Begolo, S., Colas, G., Viovy, J.-L., Malaquin, L. *Lab Chip* **2011**, *11*, 508-512.
- (51) Metz, S., Holzer, R., Renaud, P. *Lab Chip* **2001**, *1*, 29-34.
- (52) Metz, S., Trautmann, C., Bertsch, A., Renaud, P. *J. Micromech. Microeng.* **2004**, *14*, 324-331.
- (53) Nie, Z., Seo, M.-S., Xu, S., Lewis, P. C., Mok, M., Kumacheva, E., Whitesides, G. M., Garstecki, P., Stone, H. A. *Microfluid. Nanofluid.* **2008**, *5*, 585-594.
- (54) Galloway, M., Stryjewski, W., Henry, A., Ford, S. M., Llopis, S., McCarley, R. L., Soper, S. A. *Anal. Chem.* **2002**, *74*, 2407-2415.
- (55) Soper, S. A., Henry, A. C., Vaidya, B., Galloway, M., Wabuyele, M., McCarley, R. L. *Anal. Chim. Acta* **2002**, *470*, 87-99.

- 
- (56) Martinez, A. W., Phillips, S. T., Whitesides, G. M. *Proc. Natl. Acad. Sci. U.S.A.* **2008**, *105*(50), 19606-19611.
- (57) Martinez, A. W., Phillips, S. T., Nie, Z., Cheng, C.-M., Carrilho, E., Wiley, B. J., Whitesides, G. M. *Lab Chip* **2010**, *10*, 2499-2504.
- (58) Whitesides, G. M. *Nature* **2006**, *442*, 368-373.
- (59) Wootton, R. C. R., deMello, A. J. *Nature* **2010**, *464*, 839-840.
- (60) Tetradis-Meris, G., Rossetti, D., Pulido de Torres, C., Cao, R., Lian, G., Janes, R. *Ind. Eng. Chem. Res.* **2009**, *48*, 8881-8889.
- (61) Nisisako, T., Torii, T. *Lab Chip* **2008**, *8*, 287-293.
- (62) Ng, J. M. K., Gitlin, I., Stroock, A. D., Whitesides, G. M. *Electrophoresis* **2002**, *23*, 3461-3473.
- (63) Kim, S. H., Cui, Y., Lee, M. J., Nam, S.-W., Oh, D., Kang, S. H., Kim, Y. S., Park, S. *Lab Chip* **2011**, *11*, 348-353.
- (64) Abdelgawad, M., Wu, C., Chien, W.-Y., Geddie, W. R., Jewett, M. A. S., Sun, Y. *Lab Chip* **2011**, *11*, 545-551.
- (65) Sasoglu, F. M. Bohl, A. J., Layton, B. E. *J. Micromech. Microeng.* **2007**, *17*, 623-632.
- (66) McDonald, J. C., Whitesides, G. M. *Acc. Chem. Res.* **2002**, *35*(7), 491-499.
- (67) Friend, J., Yeo, L. *Biomicrofluidics* **2010**, *4*, 026502-1-026502-5.
- (68) Mukhopadhyay, R. *Anal. Chem.* **2007**, *79*(9), 3248-3253.
- (69) Johnson, M., Liddiard, G., Eddings, M., Gale, B. *J. Micromech. Microeng.* **2009**, *19*, 095011-1-095011-9.
- (70) Zhang, J., Tan, K. L., Hong, G. D., Yang, L. J., Gong, H. Q. *J. Micromech. Microeng.* **2001**, *11*, 20-26.
- (71) Zhang, J., Tan, K. L., Gong, H. Q. *Polym. Test.* **2001**, *20*, 693-701.
- (72) Stegmann, H. *Low voltage SEM imaging of photoresist line arrays using GEMINI<sup>®</sup> technology*, Carl Zeiss SMT, **2007**, 1-4.
- (73) Samsonov, G. V. *Handbook of the PHYSICOCHEMICAL PROPERTIES of the ELEMENTS*, IFI/Plenum **1968**, 383-385.
- (74) Bhattacharya, S., Datta, A., Berg, J. M., Gangopadhyay, S. *J. Microelectromech. Syst.* **2005**, *14*(3), 590-597.
- (75) Dootz, R., Evans, H., Köster, S., Pfohl, T. *Small* **2007**, *3*(1), 96-100.
- (76) Thiele, J., Trebbin, M., Perlich, J., Steinhauser, D., Förster, S. *Perpendicular orientation of cylinder micelles in microchannels*, in preparation.
- (77) Lee, J. N., Park, C., Whitesides, G. M. *Anal. Chem.* **2003**, *75*, 6544-6554.
- (78) Wu, L. Y. L., Tan, G. H., Zeng, X. T., Li, T. H., Chen, Z. *J. Sol-Gel Sci. Technol.* **2006**, *38*(1), 85-89.
- (79) Zhang, X., Lu, H., Qian, M., Zeng, X. *J. Sol-Gel Sci. Technol.* **2008**, *48*(1,2), 143-147.
- (80) Kim, B.-Y., Hong, L.-Y., Chung, Y.-M., Kim, D.-P., Lee, C.-S. *Adv. Funct. Mater.* **2009**, *19*(23), 3796-3803.
- (81) Shin, Y. S., Cho, K., Lim, S. H., Chung, S., Park, S.-J., Chung, C., Han, D.-C., Chang, J. K. *J. Micromech. Microeng.* **2003**, *13*(5), 768-774.

## 1.5 References

---

- (82) Sasaki, H., Onoe, H., Osaki, T., Kawano, R., Takeuchi, S. *Sens. Actuators B* **2010**, *150(1)*, 478-482.
- (83) Lei, Y., Liu, Y., Wang, W., Wu, W., Li, Z. *Lab Chip* **2011**, doi: 10.1039/c0lc00486c.
- (84) Hench, L. L., West, J. K. *Chem. Rev.* **1990**, *90(1)*, 33-72.
- (85) MacCraith, B. D., McDonagh, C. *J. Fluoresc.* **2002**, *12(3,4)*, 333-342.
- (86) Dreyfus, R., Tabeling, P., Willaime, H. *Phys. Rev. Lett.* **2003**, *90(14)*, 144505-1-144505-4.
- (87) Ebara, M., Hoffman, J. M., Stayton, P. S., Hoffman, A. S. *Radiat. Phys. Chem.* **2007**, *76(8-9)*, 1409-1413.
- (88) Wu, D., Zhao, B., Dai, Z., Qin, J., Lin, B. *Lab Chip* **2006**, *6*, 942-947.
- (89) Bauer, W.-A. C., Fischlechner, M., Abell, C., Huck, W. T. S. *Lab Chip* **2010**, *10*, 1814-1819.
- (90) Romanowsky, M. B., Heymann, M., Abate, A. R., Krummel, A. T., Fraden, S., Weitz, D. A. *Lab Chip* **2010**, *10*, 1521-1524.
- (91) Schneider, M. H., Willaime, H., Tran, Y., Rezgui, F., Tabeling, P. *Anal. Chem.* **2010**, *82(21)*, 8848-8855.
- (92) Priest, C. *Biomicrofluidics* **2010**, *4*, 032206-1-032206-13.
- (93) Lipowsky, R., Sackmann, E. *Structure and Dynamics of Membranes – From Cells to Vesicles*, Elsevier B. V., 1st edn., **1995**.
- (94) LoPresti, C., Lomas, H., Massignani, M., Smart, T., Battaglia, G. *J. Mater. Chem.* **2009**, *19*, 3576-3590.
- (95) Zhang, L., Eisenberg, A. *Science* **1995**, *268*, 1728-1731.
- (96) Onaca, O., Enea, R., Hughes, D. W., Meier, W. *Macromol. Biosci.* **2009**, *9*, 129-139.
- (97) Förster, S., Plantenberg, T. *Angew. Chem.* **2002**, *114*, 712-739.
- (98) Hayward, R. C., Pochan, D. J. *Macromolecules* **2010**, *43*, 3577-3584.
- (99) Kita-Tokarczyk, K., Grumelard, J., Haefele, T., Meier, W. *Polymer* **2005**, *46*, 3540-3563.
- (100) Lee, J. C.-M., Bermudez, H., Discher, B. M., Sheehan, M. A., Won, Y.-Y., Bates, F. S., Discher, D. E. *Biotechnol. Bioeng.* **2001**, *73(2)*, 135-145.
- (101) Bermudez, H., Brannan, A. K., Hammer, D. A., Bates, F. S., Discher, D. E. *Macromolecules* **2002**, *35*, 8203-8208.
- (102) Won, Y.-Y., Davis, H. T., Bates, F. S. *Science* **1999**, *283*, 960-963.
- (103) Longo, M. L., Waring, A. J., Hammer, D. A. *Biophys. J.* **1997**, *73*, 1430-1439.
- (104) Meng, F., Zhong, Z., Feijen, J. *Biomacromol.* **2009**, *10(2)*, 197-209.
- (105) Photos, P. J., Bacakova, L., Discher, B., Bates, F. S., Discher, D. E. *J. Controlled Release* **2003**, *90(3)*, 323-334.
- (106) Christian, D. A., Cai, S., Bowen, D. M., Kim, Y., Pajerowski, J. D., Discher, D. E. *Eur. J. Pharm. Biopharm.* **2009**, *71(3)*, 463-474.
- (107) Massignani, M., LoPresti, C., Blanazs, A., Madsen, J., Armes, S. P., Lewis, A. L., Battaglia, G. *Small* **2009**, *5(21)*, 2424-2432.
- (108) Lomas, H., Massignani, M., Abdullah, K. A., Canton I., LoPresti, C., MacNeil, S., Du, J., Blanazs, A., Madsen, J., Armes, S. P., Lewis, A. L., Battaglia, G. *Faraday Discuss.* **2008**, *139*, 143-159.

- 
- (109) Massignani, M., Canton, I., Patikarnmonthon, N., Warren, N., Armes, S. P., Lewis, A. L., Battaglia, G. *Nature Precedings* **2010**, <http://hdl.handle.net/10101/npre.2010.4427.1>.
- (110) van Dongen, S. F. M., Verdurmen, W. P. R., Peters, R. J. R. W., Nolte, R. J. M., Brock, R., van Hest, J. C. M. *Angew. Chem. Int. Ed.* **2010**, *49*, 7213-7216.
- (111) Pang, Z., Feng, L., Hua, R., Chen, J., Gao, H., Pan, S., Jiang, X., Zhang, P. *Mol. Pharmaceutics* **2010**, *7(6)*, 1995-2005.
- (112) Sanson, C., Schatz, C., Le Meins, J.-F., Soum, A., Thévenot, J., Garanger, E., Lecommandoux, S. *J. Controlled Release* **2010**, *147(3)*, 428-435.
- (113) Tong, R., Christian, D. A., Tang, L., Cabral, H., Baker, Jr., J. R., Kataoka, K., Discher, D. E., Cheng, J. *MRS Bull.* **2009**, *34*, 422-431.
- (114) Ahmed, F., Pakunlu, R. I., Brannan, A., Bates, F. S., Minko, T., Discher, D. E. *J. Controlled Release* **2006**, *116(2)*, 150-158.
- (115) Li, S., Garreau, H., Pauvert, B., McGrath, J., Toniolo, A., Vert, M. *Biomacromol.* **2002**, *3(3)*, 525-530.
- (116) Batycky, R. P., Hanes, J., Langer, R., Edwards, D. A. *J. Pharm. Sci.* **1997**, *86*, 1464-1477.
- (117) Napoli, A., Boerakker, M. J., Tirelli, N., Nolte, R. J. M., Sommerdijk, N. A. J. M., Hubbell, J. A. *Langmuir* **2004**, *20(9)*, 3487-3491.
- (118) Brown, L., McArthur, S. L., Wright, P. C., Lewis, A., Battaglia, G. *Lab Chip* **2010**, *10*, 1922-1928.
- (119) Agut, W., Brûlet, A., Schatz, C., Taton, D., Lecommandoux, S. *Langmuir* **2010**, *26(13)*, 10546-10554.
- (120) Discher, D. E., Ahmed, F. *Annu. Rev. Biomed. Eng.* **2006**, *8*, 323-341.
- (121) Antonietti, M., Förster, S. *Adv. Mater.* **2003**, *15(16)*, 1323-1333.
- (122) Lasic, D. D. *Biochem. J.* **1988**, *256*, 1-11.
- (123) Wang, Z.-G. *Macromolecules* **1992**, *25(14)*, 3702-3705.
- (124) Du, J., O'Reilly, R. K. *Soft Matter* **2009**, *5*, 3544-3561.
- (125) He, X., Schmid, F. *Macromolecules* **2006**, *39*, 2654-2662.
- (126) Marrink, S. J., Mark, A. E. *J. Am. Chem. Soc.* **2003**, *125*, 15233-15242.
- (127) Uneyama, T. *J. Chem. Phys. C* **2007**, *126*, 114902-1-114902-17.
- (128) Yamamoto, S., Maruyama, Y., Hyodo, S. *J. Chem. Phys.* **2002**, *116(13)*, 5842-5849.
- (129) Noguchi, H., Takasu, M. *Phys. Rev. E: Stat. Nonlinear Soft Matter Phys.* **2001**, *64*, 041913-1-041913-7.
- (130) Rank, A., Hauschild, S., Förster, S., Schubert, R. *Langmuir* **2009**, *25(3)*, 1337-1344.
- (131) Israelachvili, J. N., Mitchell, D. J., Ninham, B. W. *J. Chem. Soc., Faraday Trans. 2* **1976**, *72*, 1525-1568.
- (132) Won, Y.-Y., Brannan, A. K., Davis, H. T., Bates, F. S. *J. Phys. Chem. B* **2002**, *106(13)*, 3354-3364.
- (133) Hyde, S. T. *J. Phys. Colloques* **1990**, *51(C7)*, 209-228.
- (134) Storm, G., Crommelin, D. J. A. *PSTT* **1998**, *1(1)*, 19-31.
- (135) Mui, B. L.-S., Döbereiner, H.-G., Madden, T. D., Cullis, P. R. *Biophys. J.* **1995**, *69(3)*, 930-941.

## 1.5 References

---

- (136) Döbereiner, H.-G., Evans, E., Kraus, M., Seifert, U., Wortis, M. *Phys. Rev. E: Stat. Nonlinear Soft Matter Phys.* **1997**, *55*(4), 4458-4474.
- (137) Angelova, M. I., Dimitrov, D. S. *Faraday Discuss. Chem. Soc.* **1986**, *81*, 303-311.
- (138) Angelova, M. I., Soléau, S., Méléard, P., Faucon, F., Bothorel, P. *Prog. Colloid Polym. Sci., Trends Coll. Interface Sci. VI* **1992**, *89*, 127-131.
- (139) Olson, F., Hunt, C. A., Szoka, F. C., Vail, W. J., Papahadjopoulos, D. *Biochim. Biophys. Acta* **1979**, *557*, 9-23.
- (140) Schneider, T., Sachse, A., Rössling, G., Brandl, M. *Drug Dev. Ind. Pharm.* **1994**, *20*, 2787-2807.
- (141) Rameez, S., Bamba, I., Palmer, A. F. *Langmuir* **2010**, *26*(7), 5279-5285.
- (142) Hauschild, S., Lipprandt, U., Rumpelcker, A., Borchert, U., Rank, A., Schubert, R., Förster, S. *Small* **2005**, *1*(12), 1177-1180.
- (143) Stachowiak, J. C., Richmond, D. L., Li, T. H., Brochard-Wyart, F., Fletcher, D. A. *Lab Chip* **2009**, *9*, 2003-2009.
- (144) Li, T. H., Stachowiak, J. C., Fletcher, D. A. *Methods Enzymol.* **2009**, *465*, 75-94.
- (145) Howse, J. R., Jones, R. A. L., Battaglia, G., Ducker, R. E., Leggett, G. J., Ryan, A. J. *Nat. Mater.* **2009**, *8*, 507-511.
- (146) Discher, D. E., Eisenberg, A. *Science* **2002**, *297*, 967-973.
- (147) Bangham, A. D., Standish, M. M., Watkins, J. C. *J. Mol. Biol.* **1965**, *13*, 238-252.
- (148) Rajagopal, K., Christian, D. A., Harada, T., Tian, A., Discher, D. E. *Int. J. Polym. Sci.* **2010** *ID379286*, 1-10.
- (149) Thiele, J., Steinhauser, D., Pfohl, T., Förster, S. *Langmuir* **2010**, *26*(9), 6860-6863.
- (150) Thiele, J., Abate, A. R., Shum, H. C., Bachtler, S., Förster, S., Weitz, D. A. *Small* **2010**, *6*(16), 1723-1727.
- (151) Rosen, B. M., Wilson, C. J., Wilson, D. A., Peterca, M., Imam, M. R., Percec, V. *Chem. Rev.* **2009**, *109*, 6275-6540.
- (152) Percec, V., Wilson, D. A., Leowanawat, P., Wilson, C. J., Hughes, A. D., Kaucher, M. S., Hammer, D. A., Levine, D. H., Kim, A. J., Bates, F. S., Davis, K. P., Lodge, T. P., Klein, M. L., DeVane, R. H., Aqad, E., Rosen, B. M., Argintaru, A. O., Sienkowska, M. J., Rissanen, K., Nummelin, S., Ropponen, J. *Science*, **2010**, *328*, 1009-1014.
- (153) Knight, J. B., Vishwanath, A., Brody, J. P., Austin, R. H. *Phys. Rev. Lett.* **1998**, *80*(17), 3863-3866.
- (154) Redford, G. I., Majumdar, Z. K., Sutin, J. D. B., Clegg, R. M. *J. Chem. Phys.* **2005**, *123*, 224504-1-224504-6.
- (155) Pollack, L., Tate, M. W., Darnton, N. C., Knight, J. B., Gruner, S. M., Eaton, W. A., Austin, R. H. *Proc. Natl. Acad. Sci. USA* **1999**, *96*, 10115-10117.
- (156) Hoffmann, M., Schlüter, M., Rübiger, N. *Chem. Ing. Tech.* **2007**, *79*(7), 1067-1075.
- (157) DeMello, A. J. *Nature* **2006**, *442*, 394-402.
- (158) Karnik, R., Gu, F., Basto, P., Cannizzaro, C., Dean, L., Kyei-Manu, W., Langer, R., Farokhzad, O. C. *Nano Lett.* **2008**, *8*(9), 2906-2912.



- (159) Kolishetti, N., Dhar, S., Valencia, P. M., Lin, L. Q., Karnik, R., Lippard, S. J., Langer, R., Farokhzad, O. C. *Proc. Natl. Acad. Sci. U.S.A.* **2010**, doi: 10.1073/pnas.1011368107.
- (160) Wagner, J., Köhler, J. M. *Nano Lett.* **2005**, *5*(4), 685-691.
- (161) Yun, J., Zhang, S., Shen, S., Chen, Z., Yao, K., Chen, J. *Chem. Eng. Sci.* **2009**, *64*, 4115-4122.
- (162) Abou-Hassan, A., Sandre, O., Cabuil, V. *Angew. Chem. Int. Ed.* **2010**, *49*, 6268-6286.
- (163) Schneider, T., Zhao, H., Jackson, J. K., Chapman, G. H., Dykes, J., Häfeli, U. O. *J. Pharm. Sci.* **2008**, *97*(11), 4943-4954.
- (164) Köster, S., Steinhauser, D., Pfohl, T. *J. Phys.: Condens. Matter* **2005**, *17*(49), S4091-S4104.
- (165) Köster, S., Leach, J. B., Struth, B., Pfohl, T., Wong, J. Y. *Langmuir* **2007**, *23*, 357-359.
- (166) Köster, S., Evans, H. M., Wong, J. Y., Pfohl, T. *Biomacromol.* **2008**, *9*, 199-207.
- (167) Jahn, A., Vreeland, W. N., Gaitan, M., Locascio L. E. *J. Am. Chem. Soc.* **2004**, *126*, 2674-2675.
- (168) Jahn, A., Vreeland, W. N., DeVoe, D. L., Locascio, L. E., Gaitan, M. *Langmuir* **2007**, *23*, 6289-6293.
- (169) Jahn, A., Stavis, S. M., Hong, J. S., Vreeland, W. N., DeVoe, D. L., Gaitan, M. *ACS Nano* **2010**, *4*(4), 2077-2087.
- (170) Hong, J. S., Stavis, S. M., DePaoli Lacerda, S. H., Locascio, L. E., Raghavan, S. R., Gaitan, M. *Langmuir* **2010**, *26*(13), 11581-11588.
- (171) Campanhã, M. T. N., Mamizuka, E. M., Carmona-Ribeiro, A. M. *J. Lipid Res.* **1999**, *40*, 1495-1500.
- (172) Joscelyne, S. M., Trägårdh, G. *J. Membr. Sci.* **2000**, *169*, 107-117.
- (173) Aichele, C. P., Chapman, W. G., Rhyne, L. D., Subramani, H. J., House, W. V. *Energy Fuels* **2009**, *23*, 3674-3680.
- (174) Ahn, K., Agresti, J. J., Chong, H., Marquez, M., Weitz, D. A. *Appl. Phys. Lett.* **2006**, *88*, 264105-1-264105-3.
- (175) Tan, Y.-C., Ho, Y. L., Lee, A. P. *Microfluid. Nanofluid.* **2007**, *3*, 495-499.
- (176) Chabert, M., Viovy, J.-L. *Proc. Natl. Acad. Sci. USA* **2008**, *105*(9), 3191-3196.
- (177) Zhou, C., Yue, P., Feng, J. J. *Phys. Fluids* **2006**, *18*, 092105-1-092105-14.
- (178) Ward, T., Faivre, M., Abkarian, M., Stone, H. A. *Electrophoresis* **2005**, *26*, 3716-3724.
- (179) Nisisako, T., Torii, T., Higuchi, T. *Lab Chip* **2002**, *2*, 24-26.
- (180) Garstecki, P., Fuerstman, M. J., Stone, H. A., Whitesides, G. M. *Lab Chip* **2006**, *6*, 437-446.
- (181) Xu, J. H., Li, S. W., Tan, J., Wang, Y. J., Luo, G. S. *AIChE J.* **2006**, *52*(9), 3005-3010.
- (182) Zhao, C.-X., Middelberg, A. P. J. *Chem. Eng. Sci.* **2010**, doi:10.1016/j.ces.2010.08.038.
- (183) Hong, Y., Wang, F. *Microfluid. Nanofluid.* **2007**, *3*, 341-346.
- (184) Garstecki, P., Stone, H. A., Whitesides, G. M. *Phys. Rev. Lett.* **2005**, *94*, 164501-1-164501-4.
- (185) Abate, A. R., Weitz, D. A. *Small* **2009**, *5*, 2030-2032.
- (186) de Cindio, B., Grasso, G., Cacace, D. *Food Hydrocolloids* **1991**, *4*(5), 339-353.
- (187) Abate, A. R., Thiele, J., Weitz, D. A. *Lab Chip* **2011**, *11*, 253-258.
- (188) Yoo, H. S. *Colloids Surf., B* **2006**, *52*, 47-51.
- (189) Senatra, D., Gabrielli, G., Guarini, G. G. T. *Europhys. Lett.* **1986**, *2*(6), 455-463.
- (190) Tobio, M., Gref, R., Sánchez, A., Langer, R., Alonso, M. J. *Pharm. Res.* **1998**, *15*(2), 270-275.

## 1.5 References

---

- (191) Liu, J., Qiu, Z., Wang, S., Zhou, L., Zhang, S. *Biomed. Mater.* **2010**, *5*, 065002-1-065002-10.
- (192) Chen, C.-H., Abate, A. R., Lee, D., Terentjev, E. M., Weitz, D. A. *Adv. Mater.* **2009**, *21*, 1-4.
- (193) Hennequin, Y., Pannacci, N., de Torres, C. P., Tetradis-Meris, G., Chapuliot, S., Bouchaud, E., Tabeling, P. *Langmuir* **2009**, *25(14)*, 7857-7861.
- (194) Mikado, S., Yanagie, H., Yasuda, N., Higashi, S., Ikushima, I., Mizumachi, R., Murata, Y., Morishita, Y., Nishimura, R., Shinohara, A., Ogura, K., Sugiyama, H., Iikura, H., Ando, H., Ishimoto, M., Takamoto, S., Eriguchi, M., Takahashi, H., Kimura, M. **2009**, *605*, 171-174.
- (195) Dickinson, E. *Food Biophys.* **2010**, doi: 10.1007/s11483-010-9188-6.
- (196) Fabiilli, M. L., Lee, J. A., Kripfgans, O. D., Carson, P. L., Fowlkes, J. B. *Pharm. Res.* **2010**, *27*, 2753-2765.
- (197) Fechner, A., Knoth, A., Scherze, I., Muschiolik, G. *Food Hydrocolloids* **2007**, *21(5-6)*, 943-952.
- (198) Shum, H. C., Lee, D., Yoon, I., Kodger, T., Weitz, D. A. *Langmuir* **2008**, *24*, 7651-7653.
- (199) Lorenceau, E., Utada, A. S., Link, D. R., Cristobal, G., Joanicot, M., Weitz, D. A., *Langmuir* **2005**, *21*, 9183-9186.
- (200) Perro, A., Nicolet, C., Angly, J., Lecommandoux, S., Le Meins, J.-F., Colin, A. *Langmuir* **2011**, doi: 10.1021/la1037102.
- (201) Shum, H. C., Kim, J.-W., Weitz, D. A. *J. Am. Chem. Soc.* **2008**, *130*, 9543-9549.
- (202) Nikova, A. T., Gordon, V. D., Cristobal, G., Talingting, M. R., Bell, D. C., Evans, C., Joanicot, M., Zasadzinski, J. A., Weitz, D. A. *Macromolecules* **2004**, *37*, 2215-2218.
- (203) Vrij, A. *Physica A* **1997**, *235*, 120-128.
- (204) Hayward, R. C., Utada, A. S., Dan, N., Weitz, D. A. *Langmuir* **2006**, *22(10)*, 4457-4461.
- (205) Schrader, M. E. *Langmuir* **1995**, *11(9)*, 3585-3589.
- (206) Brannon-Peppas, L. *Int. J. Pharm.* **1995**, *116*, 1-9,
- (207) Holland, S. J., Tighe, B. J., Gould, P. L. *J. Controlled Release* **1986**, *4*, 155-180.
- (208) Chung, T. J. *Computational Fluid Dynamics*, Cambridge University Press, 1st edn., **2002**, 6-16, 243-260.
- (209) Kämmer, G., Franek, H., Recke, H.-G. *Einführung in die Methode der finiten Elemente*, Carl Hanser Verlag, 2nd revised edn., **1990**.
- (210) Wesseling, P. *Principles of Computational Fluid Dynamics*, Springer, **2000**, 12-20, 227-229.
- (211) Zienkiewicz, O. C., Taylor, R. L. *The Finite Element Method, Vol. 3: Fluid Dynamics*, Butterworth Heinemann, 5th edn., **2000**, 13-63.
- (212) COMSOL AB *Modeling Guide*, COMSOL AB, Version 3.5a, **2008**, 133-166.
- (213) Neto, C., Evans, D. R., Bonaccorso, E., Butt, H.-J., Craig, V. S. J. *Rep. Prog. Phys.* **2005**, *68*, 2859-2897.
- (214) Brody, J. P., Yager, P., Goldstein, R. E., Austin, R. H. *Biophys. J.* **1996**, *71*, 3430-3441.
- (215) Guyon, E., Hulin, J.-P., Petit, L., Mitescu, C. D. *Physical Hydrodynamics*, Oxford University Press, **2001**, 311-324.
- (216) Groisman, A., Quake, S. R. *Phys. Rev. Lett.* **2004**, *92(9)*, 094501-1-094501-4.
- (217) Was, G. S. *Fundamentals of Radiation Materials Science – Metals and Alloys*, Springer, **2007**, 167-180.

- 
- (218) Cottin-Bizonne, C., Barrat, J.-L., Bocquet, L., Charlaix, E. *Nat. Mater.* **2003**, 3, 237-240.
- (219) Navier, C. L. M. H. *Mem. Acad. R. Sci. Inst. France* **1823**, 6, 389-440.
- (220) Tretheway, D. C., Meinhart, C. D. *Phys. Fluids* **2002**, 14(3), 9-12.
- (221) Lauga, E., Brenner, M. P., Stone, H. A. *Microfluidics: The No-Slip Boundary Condition*, in *Handbook of Experimental Fluid Dynamics*, Springer, **2005**, 1-27.
- (222) Walther, J. H., Jaffe, R. L., Werder, T., Halicioglu, T., Koumoutsakos, P. *Center for Turbul. Res. - Proc. Sum. Prog.* **2002**, 317-329.
- (223) Baudry, J., Charlaix, E., Tonck, A., Mazuyer, D. *Langmuir* **2001**, 17, 5232-5236.
- (224) Cottin-Bizonne, C., Jurine, S., Baudry, J., Crassous, J., Restagno, F., Charlaix, É. *Eur. Phys. J.* **2002**, 9, 47-53.
- (225) Santiago, J. G., Wereley, S. T., Meinhart, C. D., Beebe, D. J., Adrian, R. J. *Exp. Fluids* **1998**, 25, 316-319.
- (226) Gendron, P.-O., Avaltroni, F., Wilkinson, K. J. *J. Fluoresc.* **2008**, 18, 1093-1101.
- (227) Jayaraman, S., Joo, N. S., Reitz, B., Wine, J. J., Verkman, A. S. *Proc. Natl. Acad. Sci. USA* **2001**, 98(14), 8119-8123.
- (228) Walker, G. M., Sai, J., Richmond, A., Stremmer, M., Chung, C. Y., Wikswo, J. P. *Lab Chip* **2005**, 5, 611-618.
- (229) Zentner, G. M., Cardinal, J. R., Feijen, J., Song, S.-Z. *J. Pharm. Sci.* **1979**, 68(8), 970-975.
- (230) Trivedi, V., Doshi, A., Kurup, G. K., Ereifej, E., Vandevord, P. J., Basu, A. S. *Lab Chip* **2010**, 10, 2433-2442.
- (231) Osher, S., Sethian, J. A. *J. Comput. Phys.* **1988**, 79, 12-49.
- (232) COMSOL AB *MEMS Module*, COMSOL AB, Version 3.5a, **2008**, 390-410.
- (233) Cubaud, T., Tatineni, M., Zhong, X., Ho, C.-M. *Phys. Rev. E: Stat. Nonlinear Soft Matter Phys.* **2005**, 72, 037302-1-037302-4.
- (234) Tsai, W.-T. *J. Hazard. Mater.* **2005**, 119(1-3), 69-78.
- (235) Abate, A. R., Thiele, J., Weinhart, M., Weitz, D. A. *Lab Chip* **2010**, 10, 1774-1776.
- (236) Abate, A. R., Chen, C.-H., Agresti, J. J., Weitz, D. A. *Lab Chip* **2009**, 9, 2628-2631.
- (237) Gallardo, J., Galliano, P., Durán, A. *J. Sol-gel Sci. Technol.* **2000**, 19, 393-397.

## 2 Thesis overview

This thesis addresses the tailor-made fabrication of PDMS-based microfluidic devices and their application for the preparation of polymersomes with controlled size, shell characteristics and narrow polydispersity. The dissertation comprises four publications and one submitted manuscript, which are presented in the chapter three to seven. The chapters can basically be divided into three parts.

The first part, presented in chapter three, deals with the formation of nanometer-sized vesicles from P2VP-*b*-PEG. The polymersomes are grown at the interface of an ethanolic copolymer solution and water in a flow focusing cross junction geometry. The microfluidic device is applied without additional modification of the microchannels' surface properties. Based on experimental findings and supported by fluid flow simulations, a vesicle nucleation and growth model is developed.

To extend the vesicle size range achievable by means of PDMS-based microfluidics, and thus the field of application, a second approach for forming polymersomes employing double-emulsion templates is explored in the second part of the thesis as well as issues related therewith, comprising chapters four to six. As the formation of double emulsions in PDMS devices requires microchannels with spatially patterned surfaces, chapter four focuses on the development of a novel, scalable and easy-to-apply patterning technique which overcomes the limitations of current patterning techniques. In addition to that, multiple emulsion formation in PDMS devices is illuminated by investigating double and triple emulsification of a water/perfluorinated oil system as well as liquids, that are hitherto difficult to be controllably emulsified. The results of this study are presented in chapter five. Finally, the formation of micrometer-sized vesicles from PEG-*b*-PLA using double-emulsion templates in solvent-resistant PDMS devices is described in chapter six.

The third part of this thesis concerns the development of a novel microfluidic spray dryer, presented in chapter seven. The fabrication of drug nanoparticles from a hydrophobic model drug, danazol, is demonstrated.

In the following, a brief summary of the key results of each publication is presented. For a more detailed discussion, the reader is referred to the respective chapter.

## 2.1 Fabrication of polymersomes using flow focusing

A novel method to form unilamellar polymersomes with controlled size and narrow PDI by means of microfluidics was developed. Special attention was drawn to the fabrication of polymersomes in the size range of 50-150 nm with respect to future applications as degradable containers for drug delivery into cells without affecting the cell viability. For this purpose, PDMS-based microfluidic devices were employed as a fabrication platform. Their operation requires only basic equipment, but allows for manipulation of reaction conditions with unprecedented accuracy. P2VP-*b*-PEG was chosen as a model copolymer due to its easily triggerable pH-dependent release mechanism. As P2VP-*b*-PEG is soluble in ethanol - a polar solvent, which does not swell PDMS - a modification of the microchannel surface to increase the chemical resistance of the device prior to use was not required.

In common bulk fabrication techniques the vesicular self-assembly is induced by mixing a solvent-antisolvent system. To achieve this in PDMS-based microfluidic devices, a flow-focusing cross junction with a meander-shaped outlet channel was designed. To optimize the microchannel geometry, FEM-based simulations of fluid dynamics were performed in two and three dimensions by coupling the Navier-Stokes equations to describe the fluid flow of the solvent and antisolvent with the PDEs to describe diffusion and convection at their interface.<sup>f</sup> In a typical set of experiments, a solution of P2VP-*b*-PEG in ethanol was injected into the device and flow-focused between two water streams in the cross junction. Diffusion-based mixing at the interface of water and ethanol resulted in the spontaneous vesicular self-assembly of the copolymer molecules in the meandering outlet channel. The outlet stream was directly collected in micro cuvettes without further purification, and DLS measurements were conducted to determine size and PDI of the polymersomes as prepared. In another set of experiments, Rhodamine B was added as a fluorescent dye to the copolymer solution to visualize the vesicle formation and diffusion at the ethanol-water interface by CLSM. To investigate the shell characteristics of the polymersomes, and their lamellarity in particular, cryo-TEM imaging was conducted.

---

<sup>f</sup> For a discussion in depth, the reader is referred to chapter 1.3.

## 2.1 Fabrication of polymersomes using flow focusing

To elucidate the influence of the flow conditions on the polymersome formation process, the hydrodynamic radius  $R_H$  of the vesicles was monitored as a function of the flow rate ratio  $f_R$ . By changing  $f_R$  and, therefore, the width of the focused copolymer stream, the vesicle size could be tuned over several orders of magnitude from 40 nm to 2  $\mu\text{m}$  with narrow PDI and exceptional reproducibility. Similar to other studies on liposomes, it could be found that small polymersomes are generated at low flow rate ratios, whereas large polymersomes are yielded at high flow rate ratios, as illustrated in Figure 20.

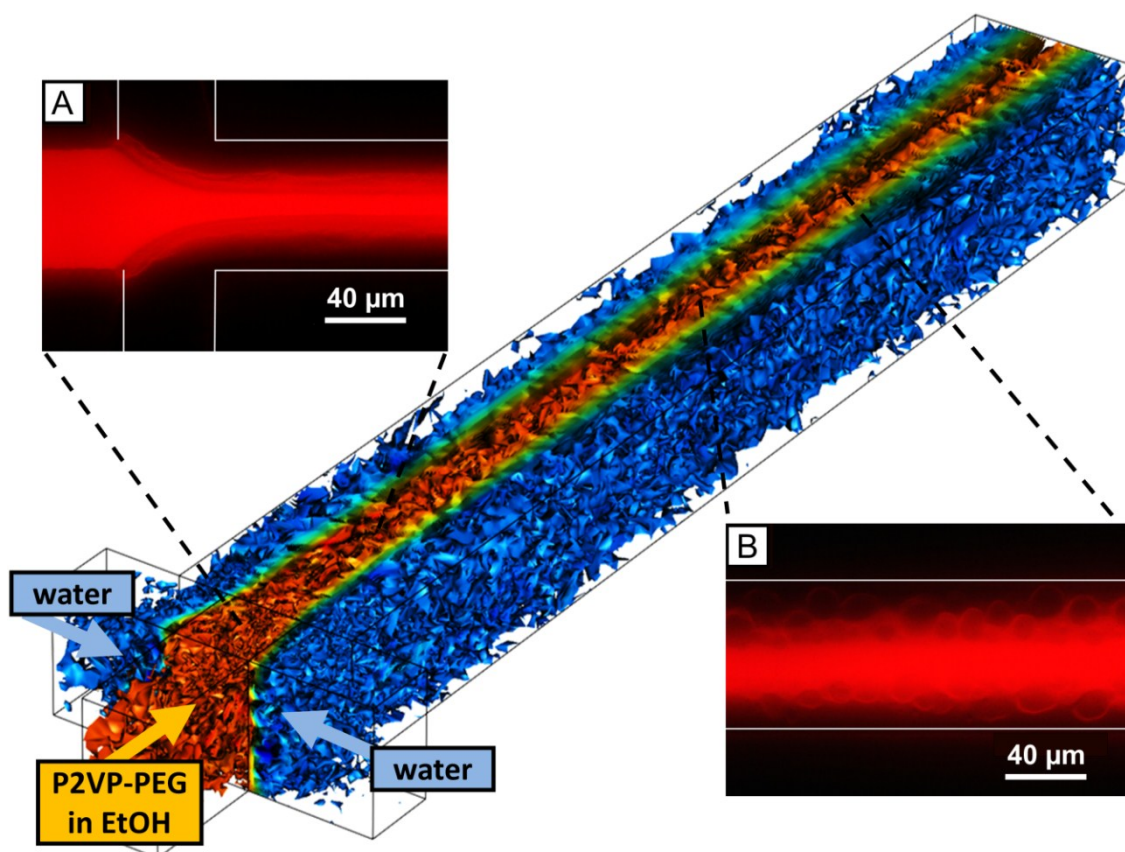


Figure 20: FEM-based isosurface rendering of the Rhodamine B concentration in a copolymer-loaded flow-focused solvent stream. The concentration profile inside the cross junction is calculated applying 41913 finite elements. By controlling  $f_R$  of the copolymer solution and water, the polymersome size can be precisely controlled. (A) Dense layer of small polymersomes on the periphery of the hydrodynamically focused copolymer solution at low  $f_R$ , (B) accumulated giant polymersomes at the interface of the copolymer solution between center and water at high  $f_R$ . Adapted and reproduced from <sup>149</sup>. Copyright 2010 American Chemical Society.

Based on these results, a nucleation and growth model was proposed. As the polymersome nuclei at the ethanol-water interface grow by the uptake of copolymer

molecules from the ethanol stream, it is anticipated that the width of the focused stream governs the number of copolymer molecules available at the interface and, therefore, the size of the polymersomes. Consequently, larger polymersomes grow from focused streams with larger width at high  $f_R$ , and smaller polymersomes from focused streams with smaller width at low  $f_R$ .

## 2.2 Patterning microfluidic device wettability

An innovative technique to spatially pattern the surface properties of PDMS-based microfluidic devices was presented. The experiments were performed in a microchannel geometry with two flow focusing junctions designed for the fabrication of double emulsions. Inert fluids were used to physically confine the grafting of hydrophilic polymers to selected regions of the microchannel network to pattern the wettability, therefore circumventing the need for sophisticated optical setups and powerful UV sources to form a spatially controlled light pattern that imparts a wettability pattern to the microchannels as is the case with conventional patterning techniques.

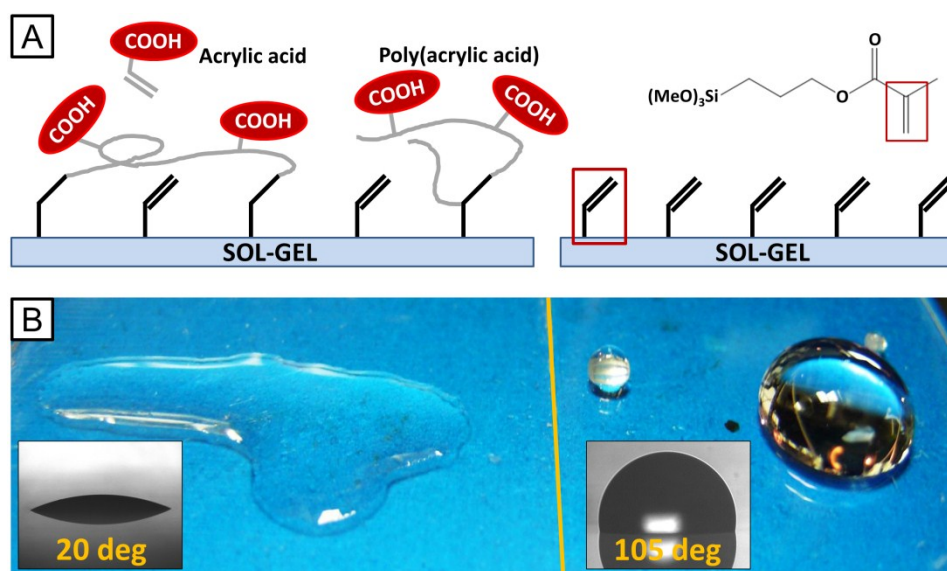


Figure 21: Surface wettability control using sol-gel approach. (A) The sol-gel is intrinsically hydrophobic due to incorporation of the fluorinated silane (heptadecafluoro-1,1,2,2-tetrahydrodecyl)triethoxysilane, but can be converted to hydrophilic. This is achieved by incorporating 3-(trimethoxysilyl)propyl methacrylate into the sol-gel, providing binding sites for a thermal or UV-induced grafting of PAA onto the surface. (B) Contact angle measurement of water drops in air on a sol-gel coated glass slide using the drop shape method. The left side is converted to hydrophilic by attaching PAA to the surface, as shown by the hydrophilic contact angle of 20°; the right side remains hydrophobic, as confirmed by the hydrophobic contact angle of 105°.



To achieve this, the microfluidic devices were coated with a sol-gel, which was intrinsically hydrophobic due to the incorporation of a fluorinated silane. However, by also incorporating 3-(trimethoxysilyl)propyl methacrylate, binding sites for the grafting of hydrophilic PAA to the sol-gel coated microchannel surface were provided. To confirm the wettability control using the functionalized sol-gel, contact angle measurements were performed on sol-gel coated glass-slides. A distinct decrease in the contact angle from  $\sim 105^\circ$  to  $\sim 20^\circ$  confirmed that the surface was made hydrophilic by the grafting process, as shown in Figure 21. Exposure of the patterned surface to standard organic solvents as well as ultrasonication treatment did not affect the quality of the hydrophilic coating.

To control the shape of the wettability pattern inside the microfluidic device, the AA monomer solution was injected into one part of the device, and the inert blocker phase, water or glycerol, was injected into another part. Where the two fluids met, a stable interface was formed. To describe the ratio of advective to diffusive transport at the interface, and thus the grade of confinement of the reaction, the Péclet number  $Pe$  was used, which is derived from the product of Reynolds number and Schmidt number:

$$Pe = Re \cdot Sc = \frac{vd}{\kappa} \cdot \frac{\kappa}{D} = \frac{vd}{D} \quad (2-1)$$

$D$  is the diffusion coefficient of the monomer,  $1.3 \cdot 10^{-9} \text{ m}^2 \text{ s}^{-1}$ ,  $v$  is the flow velocity of the monomer solution,  $\kappa$  the kinematic viscosity, and  $d$  the length of the liquid-liquid interface in the drop formation region. Consequently, a sharp interface with negligible interdiffusion could be achieved by choosing the appropriate set of flow rates via the syringe pumps.

Two distinct approaches to initiate the polymerization of the AA monomer solution inside the device were studied: a photolytically induced polymerization using Darocur<sup>®</sup> 1173 and a thermally induced polymerization using ammonium persulfate (APS) with tetramethylethylenediamine (TEMED) as the accelerant. In contrast to conventional microfluidic patterning techniques using a photoinitiator that is incorporated into the sol-gel coating thus requiring a silane linker group, the initiator was directly added to the monomer solution allowing for a large variety of initiators to be used. After a stable interface of the flowing reactive and inert phases had been formed, the device was either

## 2.2 Patterning microfluidic device wettability

---

irradiated with an UV light, without the need of spatial control, or simply placed on a hot plate, depending on the trigger of the polymerization reaction.

To demonstrate the versatility of the flow-confinement technique, the wettability of PDMS-based microfluidic devices was spatially patterned to form double emulsions from HFE-7500 and water. The required configuration of the inlet flows to pattern a device is exemplarily sketched for W/O/W double emulsions in Figure 22.

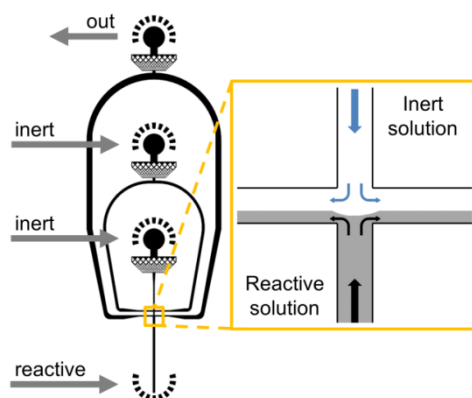


Figure 22: AutoCAD design of a microfluidic device for fabricating double emulsions. To form W/O/W double emulsions requires the outlet channel to be hydrophilic. To accomplish this, the AA monomer solution is injected into the outlet of the device, and the blocker solution into the inner and middle-phase inlets; the outer-phase inlet is left open and acts as outlet for both solutions. Due to laminar flow conditions in the device, a sharp interface is formed in the second cross junction where the two fluids meet.<sup>235</sup> Adapted and reproduced by permission of The Royal Society of Chemistry.

The surface pattern was either visualized using a dye that electrostatically binds to PAA, as shown in Figure 23A, or by locating the meniscus between oil and water at the confluence of inert blocker phase and reactive monomer solution under static conditions. However, if the grafting process proceeded for an adequate time, the surface pattern could be directly observed, as shown in Figure 23B.

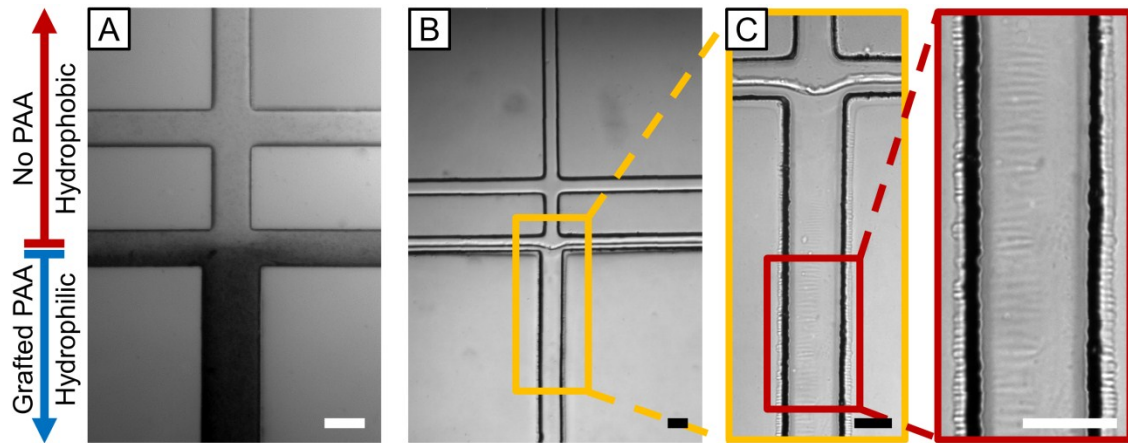


Figure 23: Visualization of the wettability pattern for forming W/O/W double emulsions. The first drop maker remains untreated, while the second drop maker is made hydrophilic. (A) Staining of grafted PAA with Toluidine blue confirms that the hydrophilic surface treatment is confined to the outlet channel of the device. (B) A thick layer of PAA is observed on the microchannel surface after 10 minutes into the grafting process. (C) Typically, PAA starts to penetrate the PDMS walls, and a wrinkling of the polymer layer is observed on the microchannel surface perpendicular to the flow direction. Scale bars denote 100  $\mu\text{m}$ .

## 2.3 One-step formation of multiple emulsions

A fundamental investigation of multiple emulsion formation in PDMS-based microfluidic devices was conducted to broaden the knowledge of emulsion formation mechanisms in quasi two dimensional microfluidic devices as well as the field of application of multiple emulsions. In a first set of experiments, O/W/O double emulsions were fabricated from HFE-7500 and water in a series of two flow-focus junctions and the drop formation dynamics were visualized recording movies with a high-speed camera. To create a device with the appropriate wettability pattern, the flow-confinement technique was applied, which was introduced earlier in chapter 2.2. To quantify the drop formation and flow conditions inside the microfluidic device, two dimensionless numbers were introduced: the Weber number of the inner phase

$$We_{in} = \frac{\rho \cdot v_{in}^2 \cdot l}{\gamma_{in}}, \quad (2-2)$$

which relates the magnitude of inertial forces to the surface tension of the inner phase, and the Capillary number of the outer phase

$$Ca_{out} = \frac{\mu \cdot v_{out}}{\gamma_{out}}, \quad (2-3)$$

which relates the magnitude of shear on the inner phase, induced by the surrounding outer phase, to its surface tension;  $v_{in}$ ,  $v_{out}$  and  $\gamma_{in}$ ,  $\gamma_{out}$  are the flow velocity and surface tension of the inner and outer phase,  $\rho$  the density of the inner phase,  $l$  the diameter of the channel, and  $\mu$  the viscosity of the outer phase. By varying the inner phase flow while keeping the middle and outer phase flow at a constant rate, the number of dripping instabilities in the device could be precisely controlled. The study revealed two regimes of double emulsification. At low inner phase flow rates, and  $\{We_{in}, Ca_{out}\} < 1$  in both microfluidic junctions, one dripping instability was observed in each junction, causing the emulsions to be formed in a two-step process. However, as the inner flow rate was increased such that  $We_{in} > 1$ , the formation of a coaxial jet of inner and middle phase was observed in the first junction. As  $\{We_{in}, Ca_{out}\} < 1$  for the second junction, the coaxial jet was broken into a double emulsion by the remaining dripping instability, emulsifying

inner and middle phase at the same time, and, therefore, forming the double emulsion in a one-step process.

The transition between one-step and two-step process was further quantified by measuring the pinch-off locations of the drops in the device as well as the shell-thickness  $T$  of the double emulsions as a function of  $We_{in}$ . As the shell-thickness of a double emulsion depends on the ratio of inner-to-middle phase, shell-thicknesses lower than approximately  $7 \mu\text{m}$  were not accessible using the conventional two-step process, due to the limitation to certain flow rates to enable dripping in both junctions. In contrast, by using the one-step process, double emulsions with much thinner shells could be prepared. To relate  $T$  with the inner phase flow velocity, and thus  $We_{in}$ , the shell volume was equated to the middle phase volume supplied over a single drop cycle. In detail, the middle phase volume  $V_{shell}$ , which could be described as the difference of double-emulsion and inner drop volume, was set equal to the volumetric flow rate of the middle phase  $U_{mid}$  supplied over one drop formation cycle with the time interval  $t$ :

$$V_{double} - V_{in} = U_{mid} \cdot t \quad (2-4)$$

As the drop formation in the second microchannel junction is triggered by the drop formation in the first junction,<sup>236</sup>  $t$  can be described by the inner drop volume and the inner phase volumetric flow rate  $U_{in}$ .

$$t = \frac{V_{in}}{U_{in}} \quad (2-5)$$

Insertion of (2-5) into (2-4) gives:

$$V_{double} - V_{in} = \frac{U_{mid} \cdot V_{in}}{U_{in}} \quad (2-6)$$

Assuming, the double emulsion is a sphere with a volume  $V = \frac{4}{3}\pi r^3$ , (2-6) can be written as:

$$\frac{4}{3}\pi r_{double}^3 - \frac{4}{3}\pi r_{in}^3 = \frac{U_{mid} \cdot \frac{4}{3}\pi r_{in}^3}{U_{in}} \quad (2-7)$$

### 2.3 One-step formation of multiple emulsions

---

$$r_{double}^3 = \frac{U_{mid} \cdot r_{in}^3}{U_{in}} + r_{in}^3 \quad (2-8)$$

With  $U_{in} = v_{in} \cdot l^2$ , the volumetric flow rate of the inner phase can be written in terms of the Weber number  $We_{in} = \frac{\rho \cdot v_{in}^2 \cdot l}{\gamma_{in}} \leftrightarrow v_{in} = \left( \frac{We_{in} \cdot \gamma_{in}}{\rho l} \right)^{\frac{1}{2}}$ .

$$r_{double}^3 = U_{mid} \cdot r_{in}^3 \left( \frac{We_{in} \cdot \gamma_{in} \cdot l^3}{\rho} \right)^{-\frac{1}{2}} + r_{in}^3 \quad (2-9)$$

Taking the third root gives:

$$r_{double} = \left( U_{mid} \cdot r_{in}^3 \left( \frac{We_{in} \cdot \gamma_{in} \cdot l^3}{\rho} \right)^{-\frac{1}{2}} + r_{in}^3 \right)^{\frac{1}{3}} \quad (2-10)$$

The radius of the middle phase layer, referred to as the shell thickness  $T$  hereafter, can be expressed as the difference between the radius of the double emulsion and the radius of the inner drop:

$$T = r_{double} - r_{in} \quad (2-11)$$

$$T = \left( U_{mid} \cdot r_{in}^3 \left( \frac{We_{in} \cdot \gamma_{in} \cdot l^3}{\rho} \right)^{-\frac{1}{2}} + r_{in}^3 \right)^{\frac{1}{3}} - r_{in} \quad (2-12)$$

Placing  $r_{in}$  outside the brackets gives:

$$T = r_{in} \left[ \left( 1 + U_{mid} \cdot \left( \frac{We_{in} \cdot \gamma_{in} \cdot l^3}{\rho} \right)^{-\frac{1}{2}} \right)^{\frac{1}{3}} - 1 \right] \quad (2-13)$$

By defining the parameter  $a$ , which is the product of known constants,

$$a = U_{mid} \left( \frac{\rho}{\gamma_{in} \cdot l^3} \right)^{\frac{1}{2}}, \quad (2-14)$$

equation (2-13) is simplified to

$$T = r_{in} \left[ \left( 1 + aWe_{in}^{-\frac{1}{2}} \right)^{\frac{1}{3}} - 1 \right]. \quad (2-15)$$

The shell thickness thus only depends on  $We_{in}$ , the known constants and the inner drop radius, which can be obtained from images of the collected double emulsions.

To verify that the one-step process was not only applicable to the fabrication of double emulsions from easily emulsifiable liquids such as water and HFE-7500, the studies were subsequently extended to higher-order emulsions as well as to liquids that cannot be controllably emulsified in conventional microfluidic drop makers, as shown in Figure 24.

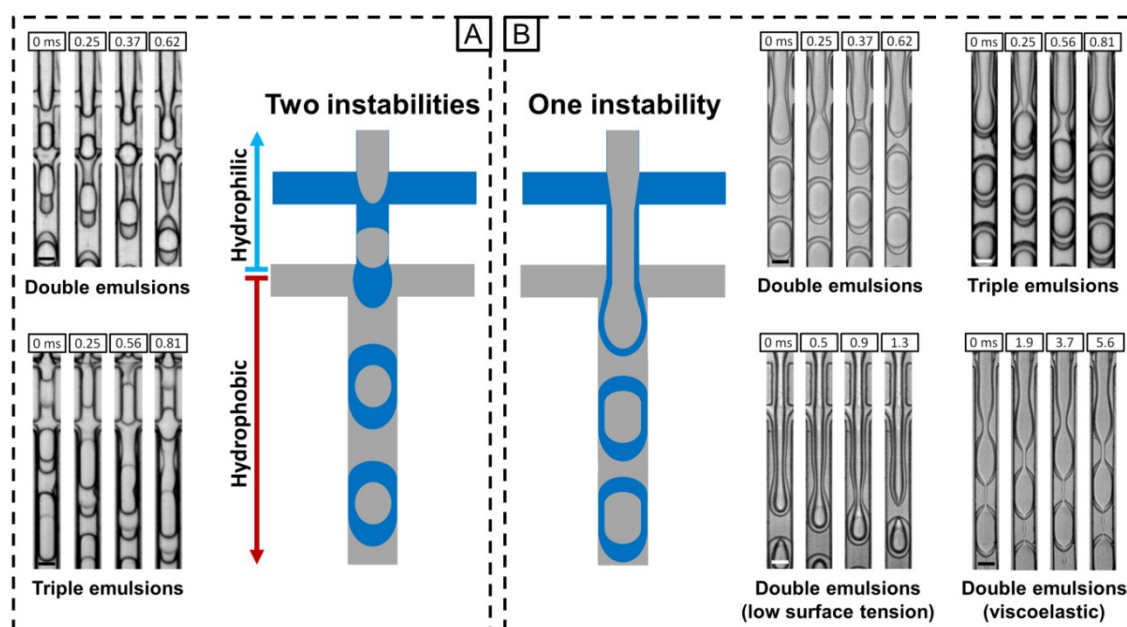


Figure 24: Formation of multiple emulsions controlling the number of dripping instabilities. (A) When forming double emulsions in a series of two flow focusing cross junctions, dripping instabilities are normally present in both junctions, forming the emulsion in a two-step process: The inner drop is formed in the first junction and encapsulated in the outer drop in the second junction, as shown in the upper row. In the same manner, triple emulsions are formed by using a series of three cross junctions, as shown in the lower row. (B) By removing all dripping instabilities but the last, multiple emulsions are formed in a one-step process. This method is not only applicable to form multiple emulsions from a rather simple system such as water and HFE-7500, as shown in the upper row. It also facilitates the formation of emulsions from fluids, which are otherwise difficult to be controllably emulsified such as octanol, which exhibits a low surface tension, or a viscoelastic polymer solution (PEG, 10 wt% in water,  $M_w = 600000 \text{ g mol}^{-1}$ ), as shown in the lower row. The scale bars denote  $50 \mu\text{m}$  for the double-emulsion devices and  $80 \mu\text{m}$  for the triple-emulsion devices.<sup>187</sup> Reproduced by permission of The Royal Society of Chemistry.

### 2.3 One-step formation of multiple emulsions

---

To demonstrate the scalability of one-step emulsification, W/O/W/O triple emulsions were prepared in a series of three flow-focus junctions setting the flow rates such that  $\{We_{in}, Ca_{out}\} < 1$  only at the third junction. This created a W/O/W triple jet, which was eventually broken into a W/O/W/O triple emulsion by a dripping instability at the third junction. By using high-speed imaging, it was revealed that the jet break-up always occurred from the inside to the outside of the coaxial jets independent of the emulsion order, as shown in Figure 24B, upper row. However, when forming double emulsions from a viscoelastic polymer solution or a liquid with a low surface tension, the inner jet was more stable than the outer jet.<sup>195</sup> In that case, the inner jet was squeezed into a drop by the pinch-off of the surrounding middle jet, as shown in Figure 24B, lower row.

To quantify the different dynamics of jet break-up, the width of the jets was measured as a function of time, and the functional form of the jet collapse fitted to power laws. The results suggest that the jet breakup of double and triple emulsions, where the inner jet is less stable than the outer jet, is similar to the breakup of a single jet due to Rayleigh-Plateau instability. However, when the inner jet is more stable than the outer one, the pinching dynamics are more complex involving interactions between the coaxial jets and depending on the fluid properties.



## 2.4 Fabrication of polymersomes from double-emulsion templates

As elaborated in previous chapters, microfluidic glass capillaries can be used to form monodisperse polymersomes in the micrometer range with narrow size distribution and almost quantitative encapsulation efficiency from copolymer-stabilized water/organic solvent/water double emulsions. However, as the design of glass capillary devices is not easily customized, this technique can neither be easily scaled-up to fabricate polymersomes in larger quantities for industrial application, nor does it allow for injecting and in-situ mixing of several organic solvents to form a tailored solvent system that prevents copolymers from precipitating inside the microfluidic device - a crucial aspect of this technique. To overcome these limitations and to extend the vesicle size range achievable by means of PDMS-based microfluidics into the micrometer range, a novel method to fabricate PEG-*b*-PLA polymersomes from double-emulsion templates in PDMS-based microfluidic devices was developed.

Since PDMS is fouled by most organic solvents, initial studies focused on the modification of the microchannel surface to prevent swelling and degradation of the PDMS building material and to spatially control the surface wettability, which would eventually enable the formation of double emulsions with a shell of organic solvents. To achieve this, the devices were coated with a functionalized sol-gel that was intrinsically hydrophobic due to the incorporation of a fluorosilane, but could be rendered hydrophilic by a subsequent surface treatment. Although the sol-gel coating approach had previously only been applied to PDMS devices with a simple microchannel design, it could be demonstrated in this work that this method is also applicable to devices with complex microchannel geometry. By optimizing the composition of the sol-gel as well as the process parameters of the sol-gel pre-conversion and deposition, an even distribution of the coating throughout the device with an average thickness of 2-5  $\mu\text{m}$  was achieved, as revealed by SEM analysis of vertical slices of coated PDMS microchannels. While the nanoporous structure of the sol-gel allowed small organic solvent molecules to penetrate the coating into the PDMS,<sup>237</sup> the rigid sol-gel network prevented a collapse of the microchannels during operation of the microfluidic device. Further investigations of the

swelling behavior of coated and uncoated PDMS devices confirmed that the swelling could be significantly reduced by 40%.

To form copolymer-stabilized double emulsions, a device with two cross junctions of alternating wettability was chosen in the initial experiments to mimic the typical design of a glass-capillary device for forming double emulsions, as illustrated in Figure 25, left half. As in previous studies, the dynamics of drop formation in the device were monitored by high-speed imaging. For the inner and outer phase, an aqueous solution of glucose and PVA, respectively, with matched osmolarity was injected into the device. For the shell phase, PEG-*b*-PLA and a hydrophobic fluorescent dye, Nile Red, were dissolved in chloroform, and toluene was added to lower the density of the shell phase thus preventing the double emulsions from sedimenting on the bottom of the collection vial and destabilizing upon dewetting transition. However, as the device geometry did not allow for manipulation of the composition of the solvent mixture inside the device, the different tendencies in diffusion of chloroform and toluene into the PDMS replica could not be balanced. Therefore, the initial solvent ratio could not be maintained, and the copolymer instantaneously precipitated on the channel walls, fouling them, and preventing the formation of stable double-emulsion templates. Due to the observed limitations using two junctions to form copolymer-stabilized double emulsions, a novel device design was developed, enabling independent injection and in-situ mixing of two organic solvents to form the double-emulsion shell, as sketched in Figure 25, right half. The microchannel geometry facilitated independent control over the flow rate of each solvent and the optimization of the solvent composition by direct observation of the drop formation inside the device. Thus the uncontrolled loss of chloroform and toluene due to evaporation into the PDMS replica could be compensated for and prevented the copolymer concentration to drop below its solubility limit as well as the formation of precipitates in the device.

To study the emulsion-to-polymersome transition, single samples of the outlet stream of the microfluidic device were directly collected between glass slides. By sealing the sample with a silicone isolator, the evaporation rate of the organic phase was slowed down to a rate that could be monitored by CLSM, as shown in Figure 25D. With the device applied in this work, polymersomes of approximately 50 to 100  $\mu\text{m}$  in diameter were obtained depending on the size of the inner drop of the double emulsion template and the smallest feature size of the double emulsion maker.

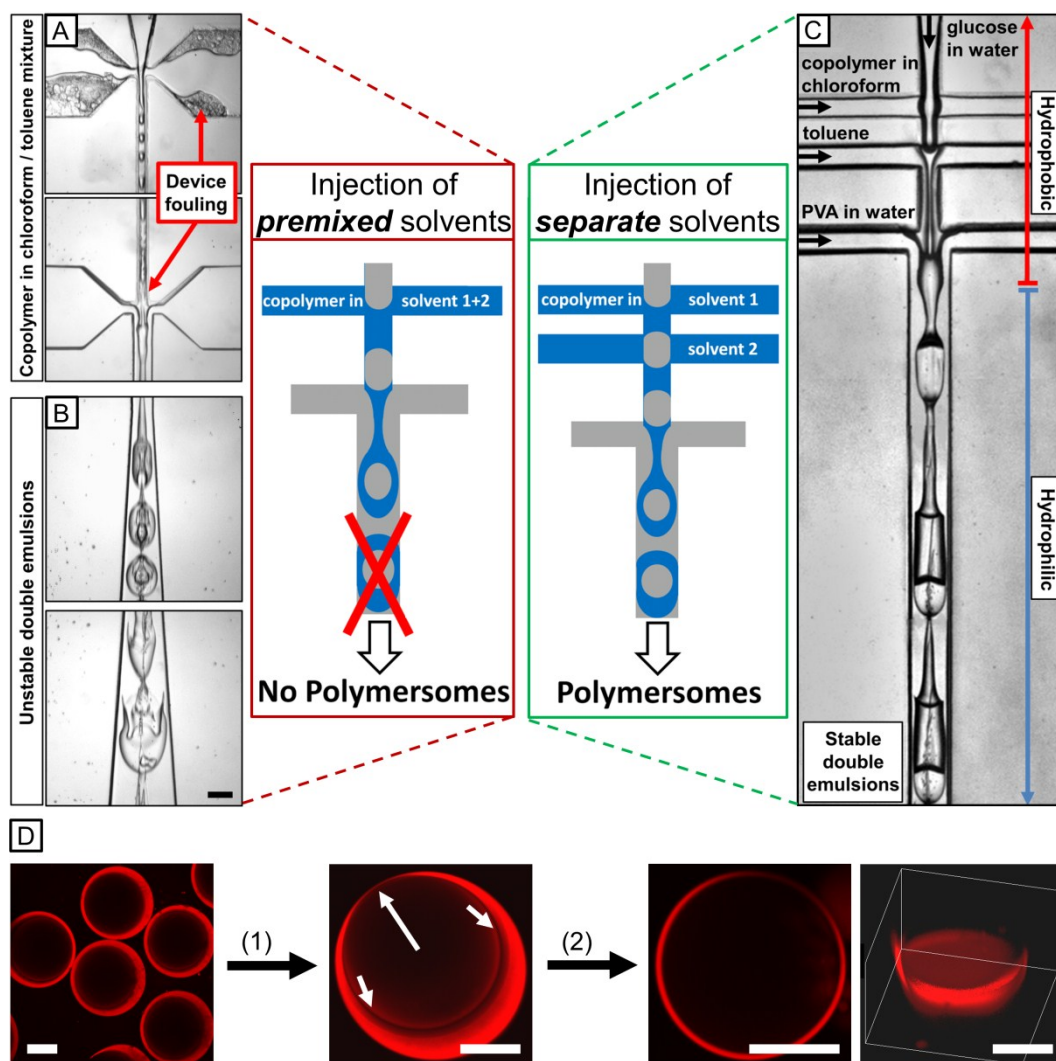


Figure 25: Formation of PEG-*b*-PLA-stabilized W/O/W double emulsions using a conventional double emulsion device with two junctions for injecting premixed mixtures of toluene and chloroform (left), and a microfluidic device allowing separate injection of organic solvents (right). Both microfluidic devices are sol-gel coated to increase their chemical resistance. The coating in the upper half is untreated and remains hydrophobic, while the coating in the lower part is rendered hydrophilic by grafting PAA to the microchannel surface. (A) Most of the copolymer precipitates after the more volatile chloroform starts to evaporate in the device. The precipitates adhere to the microchannel surface and build up a thick layer. (B) Some of the precipitates are observed in the shell phase of the double-emulsion drops. Since the organic solvent phase is depleted of the copolymer before double emulsions are formed, the two interfaces of the shell inside the double emulsions are not sufficiently stabilized. Thus the double-emulsion droplets burst downstream. (C) Novel device geometry enabling formation of stable copolymer-stabilized double emulsions. Scale bar for all panels denotes 100  $\mu\text{m}$ . (D) Dewetting transition of PEG-*b*-PLA-stabilized double emulsions to form polymersomes. (1) The organic solvent mixture, which is labeled with Nile Red, homogeneously wets the inner drop at first, but dewets during solvent evaporation causing the double emulsion to adopt an acorn-like structure. (2) From this state of partial wetting, copolymer molecules at the inner/middle and middle/outer interphase self-assemble into a vesicular bilayer. The scale bars denote 20  $\mu\text{m}$ . Adapted and reproduced from <sup>150</sup>. Copyright 2010 Wiley-VCH Verlag GmbH & Co. KGaA.

## **2.5 Appendix: Development and application of a microfluidic spray dryer**

Despite the promising results in the fabrication of polymersomes by means of stamped microfluidics that are presented in this thesis, some impairments were considered as a motivation for further studies. Specifically, although the microfluidics-based approach to form vesicles is most promising for solubilization, encapsulation, delivery and release of drugs, a quantitative encapsulation efficiency is required for a commercial use to be economically reasonable. However, this is only achieved by a few polymersome fabrication techniques. Moreover, polymersomes are made from tailored copolymers, whose synthesis is potentially cost-intensive. In addition, the proof of applicability of stamped microfluidics for the large-scale production and industrial application of systems, which are substantially less sophisticated than polymersomes, double emulsions for instance, is still pending. Finally, as many APIs, which currently emerge from drug discovery programs, are poorly soluble in water due to their complex molecular structure, an increased need exists to also explore alternative routes to a polymersome based approach for the delivery and release of drugs. Thus, the knowledge gained from the investigation, development and fabrication of stamped microfluidics in this thesis was used to come up with a novel method.

A major approach to improve the bioavailability of hydrophobic drugs is increasing their interfacial surface through the reduction of their particle size, for instance by processing the drug in a spray dryer. Although spray drying is a powerful and versatile tool enabling the fabrication of fine powders with a large surface from emulsions, suspensions or solutions, the method suffers from certain limitations, such as complex experimental setups or the minimum particle size, that is achievable. To overcome these limitations, the spray drying technique was implemented by means of PDMS-based microfluidics. The concept to form nanoparticles from hydrophobic APIs using a stamped microfluidic spray dryer was demonstrated using danazol as a model drug.

The microfluidic spray dryer consisted of two cross junctions. In contrast to conventionally fabricated devices using a glass slide to seal the microchannels, a flat sheet of cured PDMS was bonded to the PDMS replica. As the spray dryer was thus

entirely fabricated from PDMS, the preparation of the spray nozzle by vertically slicing through the outlet channel of the device was significantly facilitated.

As hydrophobic compounds tend to adsorb onto PDMS and foul its surface, special attention was drawn to reduce the attraction between the hydrophobic drug and the hydrophobic PDMS surface. This was achieved by optimizing the device design and manipulating the surface wettability. The microchannel structure was designed to have a high aspect ratio. As suggested by CFD simulations, which were discussed earlier in chapter 1.3, this reduced the contact surface between the drug-loaded solvent stream and the microchannel walls. In addition, the device was treated using oxygen plasma, thus rendering the microchannel surface hydrophilic. However, grafting of PAA to the microchannel surface failed to minimize fouling, as the rough PAA layer facilitated the nucleation of danazol crystals.

In initial experiments, the range of operating parameters of the spray dryer was determined. For this purpose, the drop size and spray pattern was monitored as a function of the air pressure using high-speed imaging. As characteristic for this kind of spray nozzle, the spray formed a full cone pattern. The minimal drop size was determined to be approximately 4  $\mu\text{m}$  at an air pressure of 2.1 bar, which was the upper pressure limit the device could resist without delamination of the PDMS sheets.

To study the effect of the solvent system on the particle formation process, a solution of danazol in IPA was directly mixed with pure IPA as the solvent or water as the antisolvent in the first junction of the spray dryer. By injecting compressed air into the second junction, the spray was formed at the spray nozzle. The size of the drug nanoparticles as prepared was examined by SEM and atomic force microscopy (AFM), as shown in Figure 26. To elucidate the composition of the particles, further characterization was performed using energy dispersive X-ray analysis (EDX). Independent of the solvent system, the formation of danazol nanoparticles of identical size and composition was observed. This indicates that the particle formation was primarily driven by evaporative precipitation of the spray and not by the formation of particle nuclei due to supersaturation of the drug solution in the presence of the antisolvent.

A crucial aspect of the spray drying process was the collection distance of the spray and the time of flight of the drug-loaded drops, respectively. XRD (X-ray diffraction) analysis

of spatially sampled danazol revealed that insufficient drying of the spray at low collection distances led to particle/drop fusion in the collection area and to the formation of unfavorable crystalline structures. As opposed to this, nanoparticles with amorphous structure, and thus significantly higher bioavailability compared to the crystalline modification, were obtained at a large collection distance.

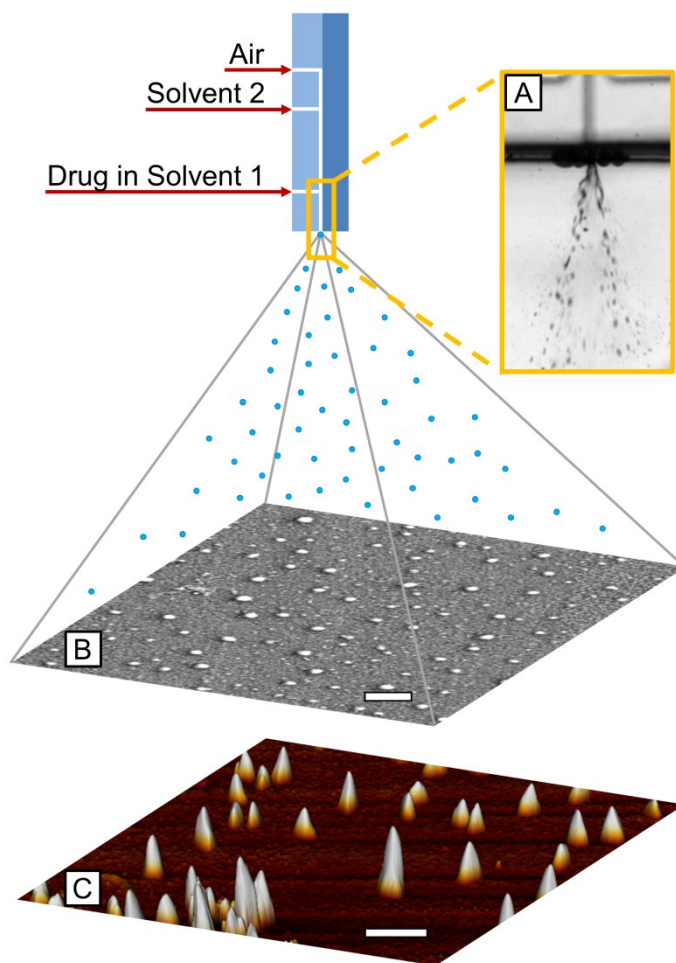


Figure 26: Formation of drug nanoparticles in a microfluidic spray dryer (schematic side view). (A) A saturated solution of danazol in IPA is ejected from the spray nozzle at 1.72 bar air pressure and adopts a typical full cone spray pattern. (B, C) SEM and AFM characterization of processed danazol, collected at a distance of 30 cm from the spray nozzle.<sup>§</sup> The particles are 20-60 nm in diameter and exhibit a narrow particle size distribution (PSD). The scale bars denote 100 nm.

<sup>§</sup> AFM measurements were performed by Dipl. Chem. Isabell Mattern and Dr. Andreas Meyer at the Institute of Physical Chemistry, University of Hamburg.

In addition to the aforementioned set of experiments, the co-spray drying of danazol and a crystallization inhibitor, poly(vinylpyrrolidone) (PVP), was performed to also inhibit the crystallization of danazol at low collection distances and to provide an alternative route for the fabrication of amorphous hydrophobic drugs. Finally, spray drying experiments with the same formulations as described above were performed in a conventional laboratory-scale spray dryer and the results compared by SEM and XRD analysis of the product, emphasizing the advantages of the microfluidic spray dryer, as shown in Figure 27.

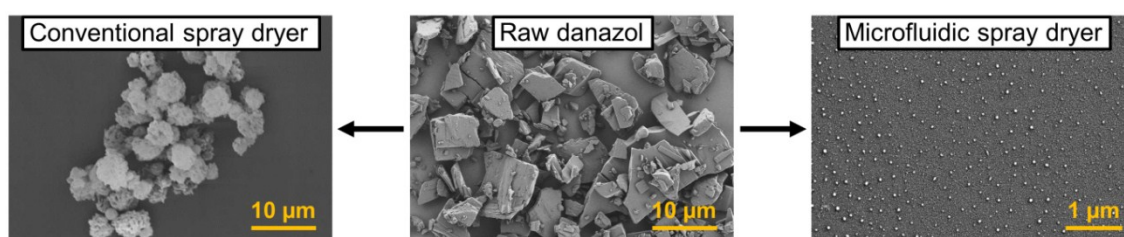


Figure 27: Comparison of the ability to reduce the particle size of hydrophobic drugs using a conventional and the microfluidic spray dryer. Raw danazol is processed in a Mini Spray Dryer B 191, Buechi, Germany, yielding particles approximately 4 µm in diameter. In contrast, by using the significantly less complex microfluidic device, danazol particles with an average size of less than 40 nm are formed, greatly improving the bioavailability of the hydrophobic drug.

## 2.6 Individual contribution to joint publications

The results presented in this thesis were obtained in collaboration with others, and have been published or submitted for publication. The contribution of all co-authors to each publication is specified below; the asterisk denotes the corresponding author.

### Chapter 3

This work is published in *Langmuir* **2010**, *26*, 6860-6863, entitled:

**"Preparation of Monodisperse Block Copolymer Vesicles via Flow Focusing in Microfluidics"**, by Julian Thiele, Dagmar Steinhauser, Thomas Pfohl, and Stephan Förster\*<sup>h</sup>

I wrote the manuscript and performed all experiments. Dagmar Steinhauser helped in the fabrication of microfluidic devices and was involved in scientific discussions. Thomas Pfohl corrected the manuscript. Stephan Förster supervised the project and corrected the manuscript.

### Chapter 4

This work is published in *Lab Chip* **2010**, *10*, 1774-1776, entitled:

**"Patterning microfluidic device wettability using flow confinement"**, by Adam R. Abate, Julian Thiele, Marie Weinhart, and David A. Weitz\*<sup>i</sup>

Adam Abate and I wrote the manuscript (shared co-authorship). While Adam Abate developed the UV-initiated surface treatment of the microfluidic devices, I developed the thermal-initiated reaction, conducted the contact angle measurements, and performed all further experiments. Marie Weinhart was involved in scientific discussions. David Weitz supervised the project and corrected the manuscript.

---

<sup>h</sup> Reproduced from <sup>149</sup>. Copyright 2010 American Chemical Society.  
<sup>i</sup> <sup>235</sup> Reproduced by permission of The Royal Society of Chemistry.



## Chapter 5

This work is published in *Lab Chip* **2011**, *11*, 253-258, entitled:

**"One-step formation of multiple emulsions in microfluidics"**, by Adam R. Abate, Julian Thiele, and David A. Weitz\*<sup>j</sup>

Adam Abate and I wrote the manuscript (shared co-authorship). Adam Abate performed the data analysis and overviewed the experiments to form multiple emulsions from fluids exhibiting viscoelasticity or low surface tension; I performed all further experiments and data acquisition. David Weitz supervised the project and corrected the manuscript. Parts of this work have been submitted for patenting.

## Chapter 6

This work is published in *Small* **2010**, *6*, 1723-1727, and featured in *Materials Views* on 08/09/10 entitled:

**"Fabrication of Polymersomes using Double-Emulsion Templates in Glass-Coated Stamped Microfluidic Devices"**, by Julian Thiele, Adam R. Abate, Ho Cheung Shum, Simone Bachtler, Stephan Förster, David A. Weitz\*<sup>k</sup>

I performed all experiments and wrote the manuscript. Adam Abate and Ho Cheung Shum corrected the manuscript and were involved in scientific discussions. Simone Bachtler helped in the fabrication of microfluidic devices. Stephan Förster and David Weitz supervised the project and corrected the manuscript.

---

<sup>j</sup> <sup>187</sup> Reproduced with permission of The Royal Society of Chemistry.

<sup>k</sup> Reproduced from <sup>150</sup>. Copyright 2010 Wiley-VCH Verlag GmbH & Co. KGaA.

### Chapter 7: Appendix

This work is published in *Lab on a Chip* **2011**, *11*, 2362-2368, and featured in *Chemistry World* on 05/26/11 entitled:

**"Early development drug formulation on a chip: Fabrication of nanoparticles using a microfluidic spray dryer"**, by Julian Thiele, Maike Windbergs, Adam R. Abate, Martin Trebbin, Ho Cheung Shum, Stephan Förster, and David A. Weitz\*

I performed most of the experiments and wrote the manuscript. Adam Abate was involved in scientific discussions. Maike Windbergs performed the spray experiments in bulk and was involved in scientific discussions. Ho Cheung Shum conducted the SEM analysis of the drug. Martin Trebbin developed the FEM-based simulation model. Stephan Förster corrected the manuscript. David Weitz supervised the project. Parts of this work have been submitted for patenting.

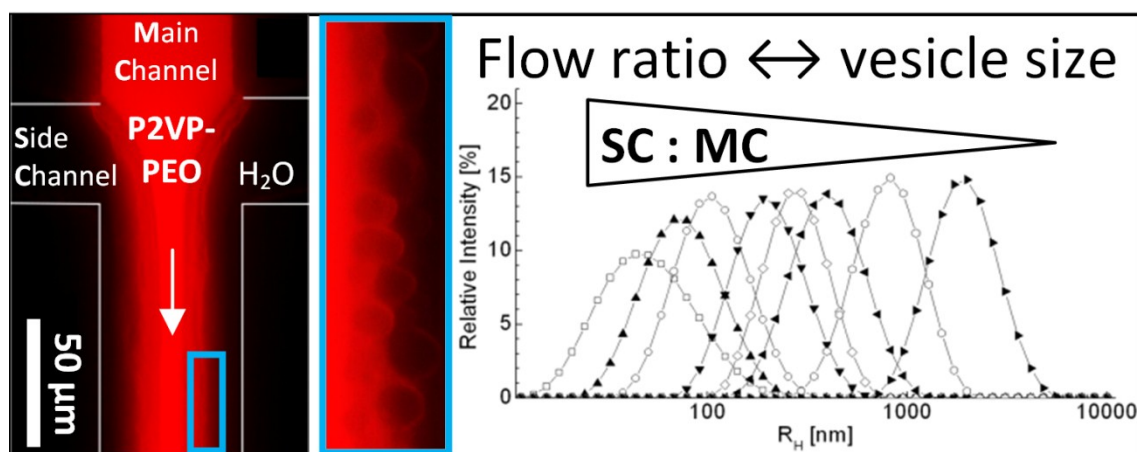
## Preparation of Monodisperse Block Copolymer Vesicles via Flow Focusing in Microfluidics

Julian Thiele,<sup>†</sup> Dagmar Steinhauser,<sup>‡</sup> Thomas Pfohl,<sup>‡,§</sup> Stephan Förster<sup>\*,†</sup>

<sup>†</sup> Institute of Physical Chemistry, University of Hamburg, D-20146 Hamburg, Germany

<sup>‡</sup> Max-Planck-Institute for Dynamics and Self-Organization, D-37073 Göttingen, Germany

<sup>§</sup> Chemistry Department, University of Basel, CH-4056 Basel, Switzerland



Published in *Langmuir* 2010, 26(9), 6860-6863.

## Abstract

We demonstrate that microfluidic flow devices enable a rapid, continuous, well-reproducible and size-controlled preparation of unilamellar block copolymer vesicles. The PDMS-based microfluidic device consists of perpendicularly crossed channels allowing hydrodynamic flow focusing of an ethanolic block copolymer solution in a stream of water. By altering the flow rate ratio in the water and ethanol inlet channels, the vesicle size can be tuned over a large size range from 40 nm to 2  $\mu\text{m}$  without subsequent processing steps manipulating size and shell characteristics. The ability of tuning the vesicle mean size over a range of several orders of magnitude with the possibility of *in situ* encapsulation of active ingredients creates new opportunities for the preparation of tailored drug delivery systems in science, medicine and industry.

## Introduction

Amphiphilic molecules such as lipids and surfactants are able to self-assemble and form vesicles.<sup>1</sup> Applications of lipid vesicles or “liposomes” as model systems for biomembranes as well as in the area of cosmetics and pharmaceuticals have been limited due to their insufficient stability and occasionally unregulated release of encapsulated active agents.<sup>2</sup> On this account, block copolymer vesicles or “polymersomes” have attracted increasing interest based on their excellent stability and the potential to control biological, chemical and physical properties by tailoring block lengths, block chemistry and functionalization.<sup>3-6</sup>

Experiments have shown that for drug delivery applications the diameter of polymersomes should range from 50-150 nm to ensure an optimal intake in cells and preserve the cell viability.<sup>7</sup> However, none of the classical vesicle-formation techniques such as film rehydration, electroformation, homogenization, phase transfer, or ultrasonication<sup>8</sup> enables vesicle formation and encapsulation with predefined vesicle diameters in this size range with the possibility of simultaneous *in situ* encapsulation.

Recently, it has been demonstrated that modified inkjet printers allow the preparation and *in situ* loading of lipid vesicles in the size-range of 50-200 nm.<sup>9,10</sup> However, the capability

for modification of inkjet devices is limited, and their usage is restricted to certain solvent systems.

A promising alternative approach for the preparation of polymersomes providing a high degree of flexibility are microfluidic devices fabricated by poly(dimethylsiloxane) (PDMS) based soft lithography. PDMS based soft lithography has developed to the most significant fabrication method for microfluidic flow devices in recent years.<sup>11-16</sup> It allows the fabrication of high quality devices in short time entailing only small manufacturing costs. Moreover, PDMS based channel dimensions in microfluidic devices are adjustable in a wide range from less than 10 nm to several hundred micrometers, providing an environment where reproducible self-assembly processes and nanometer-scale synthesis are well controllable.<sup>17</sup> The combination of diffusion-based mixing and the capability to load vesicles during the formation process in situ with active agents has led to very innovative applications of microfluidic devices. This includes the preparation, surface modification and efficient filling of lipid vesicles with active agents<sup>18-22</sup> or the usage of double emulsions as templates to direct vesicular assembly and allowing in situ encapsulation in giant polymersomes.<sup>23-25</sup>

Herein, we report the capability of hydrodynamic flow focusing in microfluidics to exert size control over the spontaneous self-assembly of unilamellar poly-2-vinylpyridine-*b*-poly(ethylene oxide), P2VP-PEO, vesicles. P2VP-PEO is an extensively studied vesicle-forming amphiphile. While the polybase poly-2-vinylpyridine exhibits a pH-dependent solubility, the PEO blocks solubility is temperature dependent.<sup>9,26</sup> The amphiphile has been chosen because of its good solubility in ethanol, in which PDMS exhibits a low swelling ratio  $S$ .<sup>27</sup>

## Experimental Section

### Materials

Poly-2-vinylpyridine-*b*-poly(ethylene oxide) (P2VP<sub>47</sub>-PEO<sub>29</sub>, mean  $M_w = 6400$ , 21 wt% PEO) was synthesized by sequential living anionic polymerization, yielding a block copolymer with narrow polydispersity in molecular weight of  $M_w/M_N = 1.06$ , where  $M_w$  and  $M_N$  are the weight- and number-averaged molecular masses. The synthesis and

characterization of P2VP-PEO is described in detail elsewhere.<sup>26,28</sup> The dry polymer is stored in the freezer at -32 °C before use.

#### **Fabrication of Microfluidic Devices**

The device consists of two perpendicular crossed channels which have a depth of 50  $\mu\text{m}$ . The side channels as well as the main channel section leading to the intersection have a width of 30  $\mu\text{m}$  (cf. Figure 1). Not shown is the meander-shaped channel leading away from the intersection which has a width of 70  $\mu\text{m}$ . As pumps, three Nemesys units from CETONI GmbH, Korbussen, Germany, were used.

#### **Vesicle Preparation**

Depending on the experimental requirements, P2VP<sub>47</sub>-PEO<sub>29</sub> is dissolved in ethanol (0.05-0.1 wt%), filtered through a 0.2  $\mu\text{m}$  PTFE filter, and injected into the main channel. Millipore-quality water is injected into the side channels and hydrodynamically focuses the polymer stream. The vesicle solution is directly collected in microcuvettes with a minimum volume of 40  $\mu\text{L}$ .

#### **Vesicle Characterization**

Dynamic light scattering (DLS) is performed on a Zetasizer Nano ZS from Malvern Instruments Ltd., U.K., at  $\lambda = 632 \text{ nm}$  with a scattering angle of 173° (noninvasive back scatter technology). Cryo-transmission electron microscopy (cryo-TEM) is carried out on a TEM LEO912 electron microscope from Zeiss, Oberkochen. Confocal laser scanning microscopy (CLSM) was performed on an Olympus FluoView 1000.

#### **FEM Simulations**

In order to adapt the AutoCAD based channel structure to experimental parameters, simulations based on the finite element method (FEM) were performed, which are well-

suiting for the understanding of the hydrodynamics present during the polymersome formation process as well as to quantify the influence of viscosity effects (simulation-based rapid prototyping).<sup>29</sup> We utilize COMSOL 3.5 applying 20346 finite elements for 3D simulations and 117146 for 2D simulations.

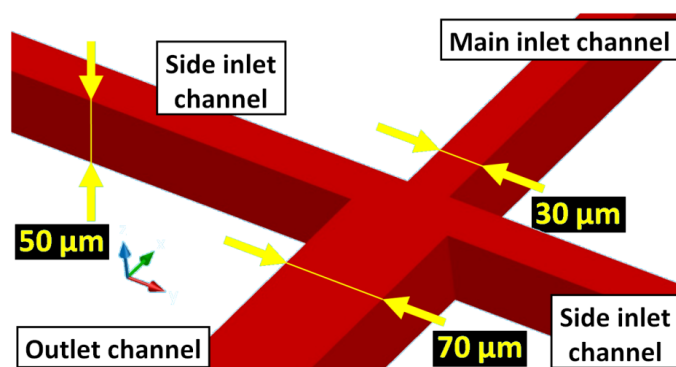


Figure 1: Cross section of the AutoCAD-based microchannel design used for the preparation of block copolymer vesicles via flow focusing.

## Results and Discussion

In a typical experiment (see scheme in Figure 1), ethanol containing the dissolved block copolymer (0.05-0.1 wt%) flows through the main inlet channel, and demineralized water (Milli-Q, Millipore) flows through the two side inlet channels. The volumetric flow rate for each channel ranges between 5 and 40  $\text{nL s}^{-1}$ , which corresponds to an outlet flow velocity of 4.28-34.3  $\text{mm s}^{-1}$ . The flow rates in the main channel (MC) and the two side channels (SC) are adjusted to control the degree of hydrodynamic focusing. The width of the ethanol stream in the outlet channel depends on the ratio of the volumetric flow rates of the main channel (MC) to the two side channels ( $\text{SC}_1, \text{SC}_2$ ), where the flow rates of the side channels are kept equal. With volumetric flow ratios ( $\text{MC}:\text{SC}_{1,2}$ ) ranging from 4 to 0.13, the width of the central ethanol stream in the outlet channel can be adjusted in the range 8-42  $\mu\text{m}$ .

For high volumetric flow ratios the formation of vesicles can directly be observed by fluorescence microscopy. To facilitate the visualization of the polymersomes, Rhodamine-B was added to the ethanol stream. The fluorescent dye readily solubilizes

into the polymersome bilayer thereby labeling the bilayer. Figure 2A shows that the polymersomes are all located along the phase boundary between the focused polymer solution and the aqueous phase. For smaller volumetric flow ratios the obtained polymersomes are smaller (Figure 2B). Their size cannot be determined by fluorescence microscopy any more.

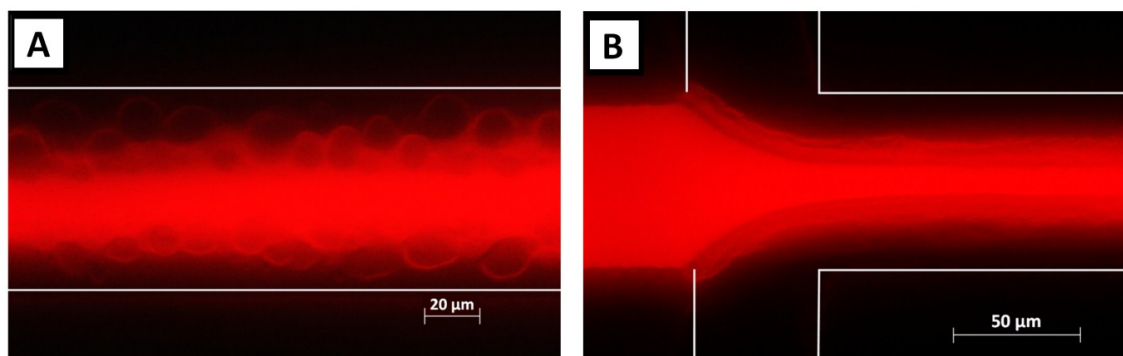


Figure 2: Fluorescence images of a Rhodamine B labeled P2VPPEO stream, hydrodynamically focused with Millipore-quality water: (A) accumulated giant polymersomes on the periphery of the focused stream at high volumetric flow ratio; (B) dense layer of small accumulated polymersomes at the periphery of the focused stream at small volumetric flow ratio.

For determination of their size distribution and structure, the collected polymersome solutions are directly characterized by dynamic light scattering (DLS) and cryo-transmission electron microscopy (cryo-TEM), without subsequent processing steps such as purification and manipulation of the polymersome size distribution. Figure 3 shows a typical cryo-TEM image of polymersomes prepared from a 0.1 wt % ethanolic polymer solution at low flow ratios. We observe unilamellar polymersomes with a unimodal, well-defined size distribution.



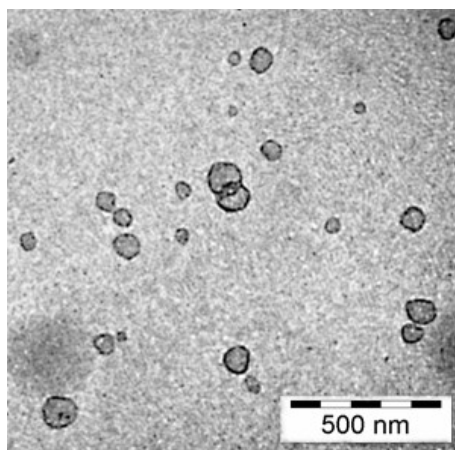


Figure 3: Cryo-TEM images of P2VP-PEO vesicles, prepared from a 0.1 wt % ethanolic solution, which was hydrodynamic focused with Millipore-quality water at a flow velocity of  $30 \text{ nL s}^{-1}$  in each channel. All vesicles are unilamellar.

Figure 4 shows that the size of the polymersomes can be easily adjusted over a wide range of 40 nm to 2  $\mu\text{m}$  by altering the flow rate ratio between the main inlet channel (MC) and the side channels ( $\text{SC}_{1,2}$ ). This is possible for both concentrations investigated in this study, (A) 0.05 and (B) 0.1 wt%. We would like to point out that the size distributions of all P2VP-PEO polymersome solutions prepared in our microfluidic device are more monodisperse compared to P2VP-*b*-PEO polymersomes prepared by us by any of the above-mentioned conventional methods. The relative standard deviation of the vesicle size as determined by dynamic light scattering is in the range 0.05-0.2.

### 3 Fabrication of polymersomes using flow focusing

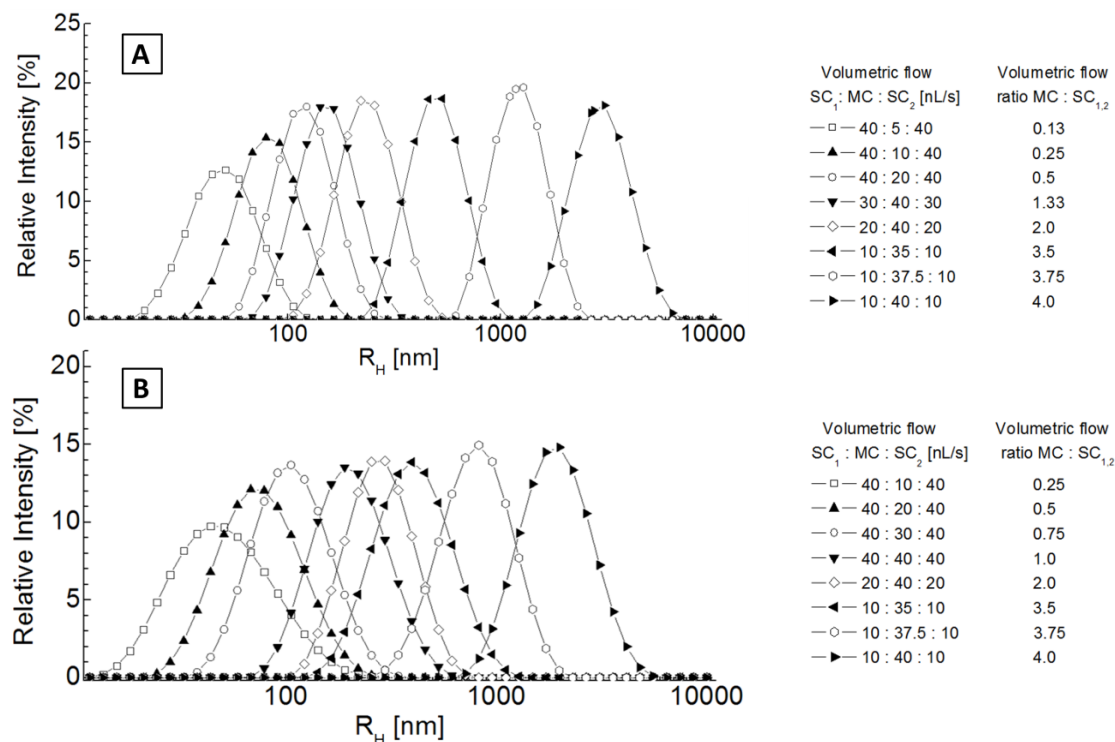


Figure 4: Size distributions of P2VP-PEO polymersomes determined by dynamic light scattering, prepared from P2VP-PEO in ethanol, (A) 0.05 wt% and (B) 0.1 wt%. The polymersome size is adjusted by altering the flow rate ratio between main and side inlet channel with a high degree of control.

In Figure 5, the mean hydrodynamic radii as determined by dynamic light scattering are plotted as a function of the flow rate ratio. Similar to a previous study on lipid vesicles,<sup>30</sup> we observe that the polymersome size increases with increasing flow rate ratio.

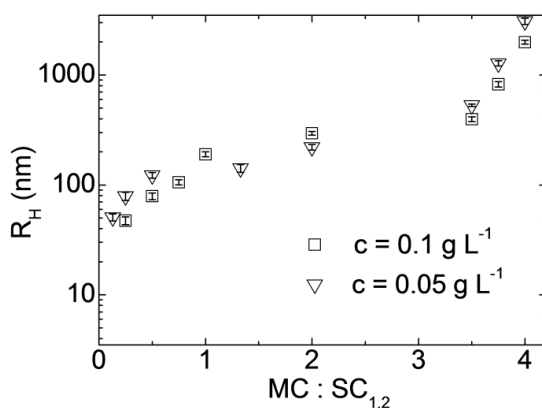


Figure 5: Flow ratio dependence of the mean hydrodynamic radii ( $R_H$ ) of P2VP-PEO vesicles prepared using different polymer concentrations for three repeated experiments (blue, 0.1 wt %; red, 0.05 wt %).

Our results suggest that a hydrodynamically well-controlled nucleation and growth process leads to the observed dependence of vesicle size on the flow rate ratio. The flow rate ratio directly determines the width of the focused stream. This is shown in Figure 6 where the simulated concentration profiles for Rhodamine B dissolved in the focused stream are shown for a flow rate ratio of 0.5 at different positions down the outlet channel. Directly after the cross junction at the entrance to the outlet channel ( $x = 0 \mu\text{m}$ ) there is a sharp drop of the Rhodamine B concentration at the periphery of the focused stream. Further down the outlet channel ( $x = 600, 1200, 1800 \mu\text{m}$ ), the concentration profile broadens, developing into a Gaussian distribution. With decreasing flow rate ratio, the width of the focused stream becomes smaller.

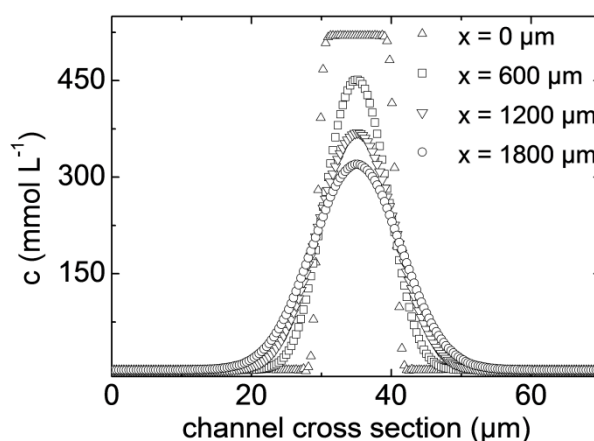


Figure 6: FEM-simulated concentration profiles for Rhodamine B dissolved in the central stream are shown for a flow rate ratio of 0.5 at different positions down the outlet channel ( $x=600, 1200, 1800 \mu\text{m}$ ). With increasing distance from the channel cross the concentration profile broadens, developing into a Gaussian distribution.

In our experiments the focused stream contains the ethanolic block copolymer polymer solution. With decreasing ethanol concentration, the solvent quality for the polymer decreases. At the periphery of the focused ethanol/polymer stream, the ethanol concentration decreases to a level, below which the P2VP-block becomes insoluble. Polymersomes are then nucleated at the periphery of the focused stream in agreement with our experimental observations (Figure 2A).

The polymersome nuclei formed at the periphery of the focused stream will then grow by uptake of polymers from the central part of the focused stream. Since the number of such

polymers is proportional to the width of the focused stream, larger polymersomes are grown from focused streams with larger widths. This is in agreement with the results in Figure 5 where the width is controlled via the flow rate ratio. Whereas at lower flow rate ratios the size of the polymersomes is roughly proportional to the flow rate ratio, allowing good control of the size distribution, at the highest ratio the polymersome size is more strongly increasing. This indicates that a different polymersome growth mechanisms exists, which is the topic of ongoing studies. Yet, for both mechanisms, by tuning the flow rates at the confluence of the main inlet channel and the side channels, the self-assembly process as well as the size of the vesicles can be well controlled and is well reproducible.

## Conclusions

Summarizing, we have shown that hydrodynamic flow focusing microfluidic devices can be used to control the size of polymersomes over a wide range of sizes from 40 nm to 2  $\mu\text{m}$  with narrow size distributions with excellent reproducibility. The polymersomes are formed at the ethanol/water boundary interface. A simple nucleation and growth model is proposed to explain the observed relation between polymersome size and focused stream width. This example shows the versatile use of current PDMS-based microfluidics for the formation of polymersomes, whose diameter can be well controlled for an optimal intake in cells for applications in drug delivery systems.

## Acknowledgements

The authors would like to thank Kim König from the Lower Saxony Water Management, Coastal Defense and Nature Conservation Agency, Germany, for the adaptation of the AutoCAD files as well as Sabine Barnert from the Department of Pharmaceutical Technology and Biopharmacy, University of Freiburg, Germany, for the cryo-TEM characterization. J.T. was supported by the Interdisciplinary Graduate School 611 “Design and Characterization of Functional Materials” of the German Research Foundation (DFG). D.S. and T.P. were supported by the SPP 1164 “Micro- and Nanofluidics” of the DFG (PF 375/4).

## References

- (1) Förster, S., Plantenberg, T. *Angew. Chem. Int. Ed.* **2002**, *41*, 688-714.
- (2) Antonietti, M., Förster, S. *Adv. Mater.* **2003**, *15*, 1323-1333.
- (3) Gan, Z., Jim, T., Li, M., Yuer, Z., Wang, S.; Wu, C. *Macromolecules* **1999**, *32*, 590-594.
- (4) Meier, M., Aerts, S., Staal, B., Rasa, M., Schubert, U. *Macromol. Rapid Commun.* **2005**, *26*, 1918-1924.
- (5) Oh, K., Lee, E., Kim, D., Bae, Y. *Int. J. Pharm.* **2008**, *358*, 177-183.
- (6) Pang, Z., Lu, W., Gao, H., Hu, K., Chen, J., Zhang, C., Gao, X., Jiang, X., Zhu, C. *J. Controlled Release* **2008**, *128*, 120-127.
- (7) Campanhã, M., Mamizuka, E., Carmona-Ribeiro, A. *J. Lipid Res.* **1999**, *40*, 1495-1500.
- (8) Kita-Tokarczyk, K., Grumelard, J., Haefele, T., Meier, W. *Polymer* **2005**, *46*, 3540-3563.
- (9) Hauschild, S., Lipprandt, U., Rumplecker, A., Borchert, U., Rank, A., Schubert, R., Förster, S. *Small* **2005**, *(1)12*, 1177-1180.
- (10) Stachowiak, J. C., Richmond, D., Li, T. H., Brochard-Wyart, F., Fletcher, D. A. *Lab Chip* **2009**, *9*, 2003-2009.
- (11) Sasoglu, F., Bohl, A., Layton, B. *J. Micromech. Microeng.* **2007**, *17*, 623-632.
- (12) McDonald, J., Whitesides, G. M. *Acc. Chem. Res.* **2002**, *35*, 491-499.
- (13) Whitesides, G. M. *Nat. Biotechnol.* **2003**, *21*, 1161-1165.
- (14) Xia, Y., Whitesides, G. M. *Angew. Chem. Int. Ed.* **1998**, *37*, 550-575.
- (15) Duffy, D., McDonald, J., Schueller, O., Whitesides, G. M. *Anal. Chem.* **1998**, *70*, 4974-4984.
- (16) Sandison, M., Morgan, H. *J. Micromech. Microeng.* **2005**, *15*, S139-S144.
- (17) Jahn, A., Vreeland, W., Gaitan, M., Locascio, E. *J. Am. Chem. Soc.* **2004**, *126*, 2674-2675.
- (18) Skalko, N., Bouwstra, J., Spies, F., Gregoriadis, G. *Biochim. et. Biophys. Acta* **1996**, 249-254.
- (19) Dittrich, P., Heule, M., Renaud, P., Manz, A. *Lab Chip* **2006**, *6*, 488-493.
- (20) Tresset, G., Iliescu, C. *Appl. Phys. Lett.* **2007**, *90*, 173901-1-173901-3.
- (21) Wagner, A., Vorauer-Uhl, K., Kreismayr, G., Katinger, H. *J. Liposome Res.* **2002**, *12(3)*, 271-283.

- (22) Tresset, G., Takeuchi, S. *Biomed. Microdevices* **2004**, 6:3, 213-218.
- (23) Shum, H. C., Kim, J.-W., Weitz, D. A. *J. Am. Chem. Soc.* **2008**, 130, 9543-9549.
- (24) Hayward, R. C., Utada, A. S., Dan, N., Weitz, D. A. *Langmuir* **2006**, 22(10), 4457-4461.
- (25) Lorenceau, E., Utada, A. S., Link, D. R., Christobal, G., Joanicot, M., Weitz, D. A. *Langmuir* **2005**, 21, 9183-9186.
- (26) Borchert, U., Lipprandt, U., Bilanz, M., Kimpfler, A., Rank, A., Peschka-Süss, R., Schubert, R., Lindner, P., Förster, S. *Langmuir* **2006**, 22, 5843-5847.
- (27) Lee, J., Park, C., Whitesides, G. M. *Anal. Chem.* **2003**, 75, 6544-6554.
- (28) Martin, T. J., Prochazka, K., Munk, P., Webber, S. E. *Macromolecules* **1996**, 29, 6071-6073.
- (29) Köster, S., Evans, H., Wong, J., Pfohl, T. *Biomacromol.* **2008**, 9, 199-207.
- (30) Jahn, A., Vreeland, W. N., DeVoe, D. L., Locascio, L. E., Gaitan, M. *Langmuir* **2007**, 23, 6289-6293.

## Patterning Microfluidic Device Wettability using Flow Confinement

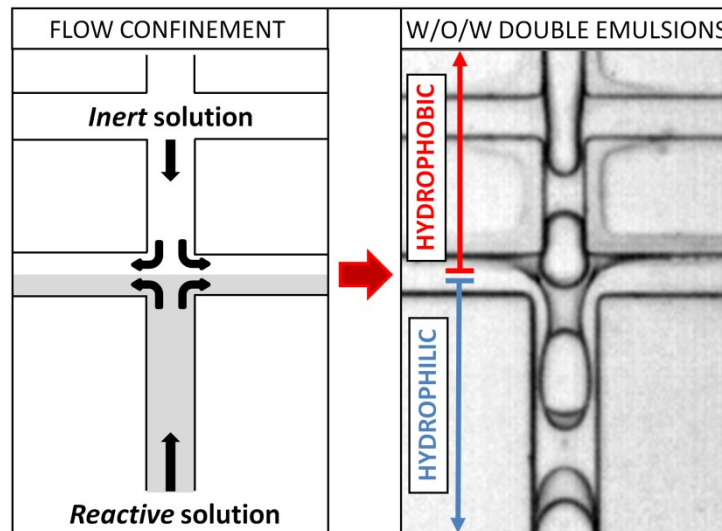
Adam R. Abate,<sup>‡a</sup> Julian Thiele,<sup>‡a,b</sup> Marie Weinhart,<sup>c</sup> David A. Weitz\*<sup>a</sup>

<sup>a</sup> School of Engineering and Applied Sciences/Department of Physics, Harvard University, Cambridge, Massachusetts, USA

<sup>b</sup> Institute of Physical Chemistry, University of Hamburg, Germany

<sup>c</sup> Institute of Chemistry and Biochemistry-Organic Chemistry, Freie Universität Berlin, Germany

<sup>‡</sup> Both authors contributed equally to this work.



Published in *Lab on a Chip* **2010**, *10*, 1774-1776.

### **Abstract**

We present a simple method to spatially pattern the surface properties of microfluidic devices using flow confinement. Our technique allows surface patterning with micron-scale resolution. To demonstrate its effectiveness, we use it to pattern wettability to form W/O/W and O/W/O double emulsions.

### **Introduction**

Many applications of microfluidic devices require channels with patterned surface properties.<sup>1</sup> One such application is the formation of multiple emulsions which consist of large drops with smaller drops inside.<sup>2-4</sup> To make these structures requires microfluidic devices with spatially patterned wettability; this allows the inner drops to be formed in one part of the device and the outer drops in another part.<sup>5-7</sup> However, current methods to spatially pattern the wettability of microfluidic devices are difficult to use and of limited versatility. The best approach for patterning wettability uses a polymerization reaction that is initiated by exposure to ultraviolet (UV) light.<sup>8-11</sup> To spatially control wettability, the microfluidic device is exposed to a spatially controlled light pattern, imparting a wettability pattern of the same shape. However, since micron-scale resolution is required, sophisticated optics and a powerful UV-light source are needed. Moreover, this method is difficult to use to fabricate many devices with the same pattern, since this requires precise alignment of the optical pattern with all devices simultaneously, a technically challenging procedure. A superior wettability patterning approach would combine simplicity with high-resolution patterning, and would allow fabrication of large numbers of devices with identical properties.

In this paper, we present a versatile method for patterning surface wettability. We use an inert fluid to physically confine a chemical treatment that alters wettability in selected regions of the device; this requires only basic equipment and allows high-resolution wettability patterning. Moreover, since spatial control is achieved by physical confinement of the reaction, this approach is versatile, allowing many different surface treatments to be used.<sup>12,13</sup> To illustrate this, we use photo-initiated and thermal-initiated surface treatments with our method. To demonstrate the effectiveness of our approach, we



use it to pattern the wettability of microfluidic devices to form both W/O/W and O/W/O double emulsions.

## Results and Discussion

We fabricate our microfluidic devices using soft-lithography in polydimethylsiloxane (PDMS).<sup>14,15</sup> Our devices consist of microchannels 100  $\mu\text{m}$  in height. To control the wettability of our devices, we use a sol-gel coating approach.<sup>9,16</sup> We design a sol-gel coating that is intrinsically hydrophobic, but can be converted to hydrophilic after a chemical treatment. To accomplish this, we incorporate fluorosilanes and methacrylate-silanes into the sol-gel. To prepare the sol-gel solution we combine 1 mL tetraethylorthosilicate (TEOS), 1 mL methyltriethoxysilane (MTES), 0.5 mL (heptadecafluoro-1,1,2,2-tetrahydrodecyl) triethoxysilane, 2 mL trifluoroethanol and 1 mL 3-(trimethoxysilyl)propylmethacrylate. Before the coating can be applied the sol-gel must be preconverted by adding an acid catalyst. We combine 0.5 mL of the sol-gel solution, 0.9 mL methanol, 0.9 mL trifluoroethanol, and 0.1 mL aqueous HCl, pH 2. After the catalyst is added the solution may turn cloudy; it is vigorously shaken for several seconds and placed on a hot plate set to 85  $^{\circ}\text{C}$  for 30 s. This is repeated until the mixture clears, which takes approximately 2 minutes. To coat the channels, we fill them with the sol-gel mixture immediately after plasma bonding. We then heat the device on a hot plate set to 180  $^{\circ}\text{C}$ ; this vaporizes the mixture, depositing a uniform sol-gel coating on the channel walls. The coating thickness can be reduced by diluting the sol-gel mixture several times in methanol, without adversely affecting wettability control. Due to the fluorosilanes in the sol-gel, the coated channels are very hydrophobic.

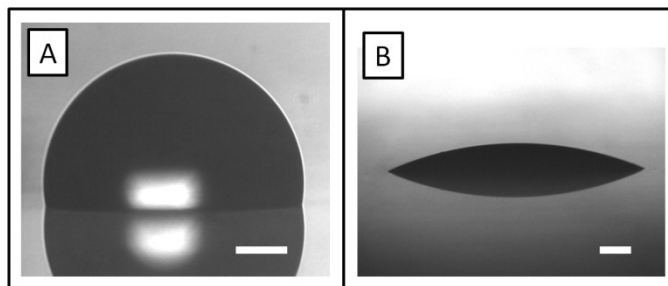


Figure 1: The sol-gel coating allows us to control the wettability of microfluidic channels. To confirm this, we perform contact angle measurements of sol-gel-coated glass slides with water drops in air. The sol-gel is intrinsically hydrophobic due to the incorporation of fluorosilanes, as confirmed by the hydrophobic contact angle of  $105^\circ$  (A). It is converted to hydrophilic by attaching PAA to the surface using a polymerization reaction, as shown by the hydrophilic contact angle after treatment of  $20^\circ$  (B). The scale bars denote  $50\ \mu\text{m}$ .

To confirm this wettability, we perform contact angle measurements of sol-gel coated glass slides with water drops in air. On a sol-gel coated glass slide the water drop beads up, achieving a hydrophobic contact angle of  $\sim 105^\circ$ , as shown in Fig. 1A. To switch the wettability to hydrophilic, we use the methacrylate-silanes in the sol-gel. These silanes contain double bonds, which can be used to graft hydrophilic polymers to the surface, to make it hydrophilic. For the polymers we use poly(acrylic acid) (PAA) because it has high electrical polarity and is thus very hydrophilic. To graft the PAA, we fill the channels with acrylic acid (AA) monomer solution and initiate polymerization; this creates AA polymers, some of which react with the double bonds on the sol-gel, grafting them to the surface. This switches the wettability to hydrophilic, as confirmed by the hydrophilic contact angle of  $\sim 20^\circ$  on a glass slide treated the same way, as shown in Fig. 1B. With the sol-gel, we can thus control the wettability of our microfluidic devices.<sup>17</sup>

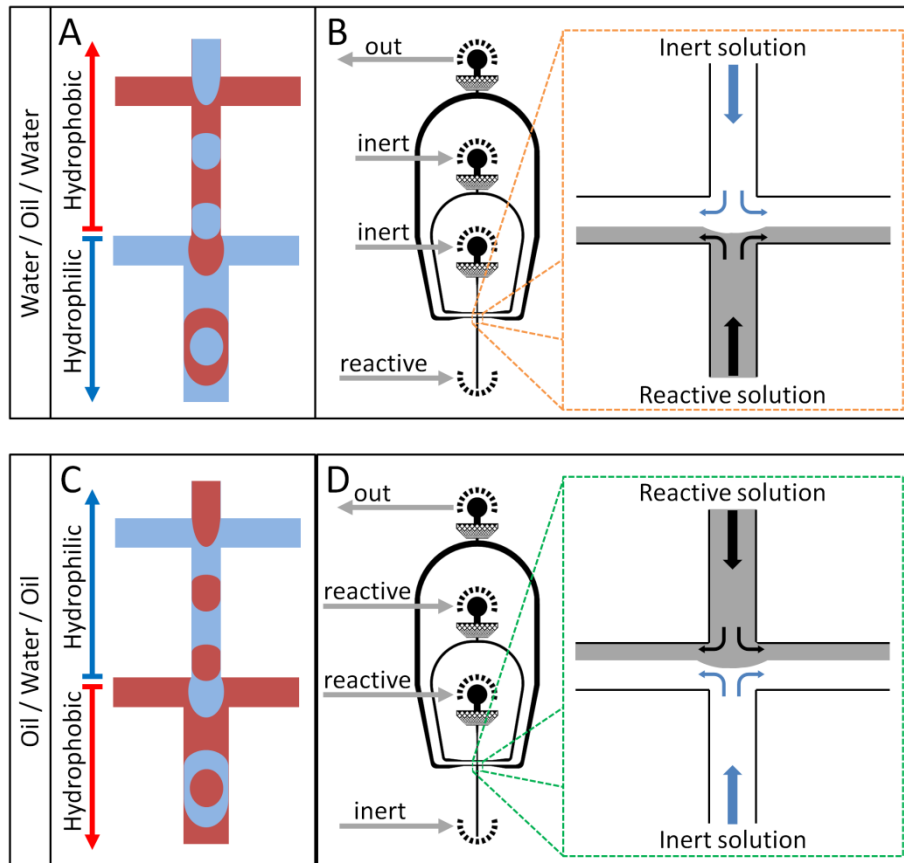


Figure 2: To form W/O/W double emulsions requires a device in which the upper portion is hydrophobic and the lower portion hydrophilic (A). To create this wettability pattern, we inject a reactive surface treatment solution into the device outlet and an inert blocker solution into the inner and middle-phase inlets (B). Where the two solutions meet a sharp interface forms, due to laminar flow conditions; this sets the cross-over between the treated and un-treated regions. To form O/W/O double emulsions, we invert the pattern (C); this is achieved by switching the inlets into which the reactive and inert solutions are injected (D).

Channel wettability is the most important parameter when forming emulsions in microfluidics, and spatially controlled wettability is essential when forming multiple emulsions. This is because channel wettability determines the type of drops that a microfluidic device forms: if the channels are hydrophobic, water drops in oil are formed, whereas if the channels are hydrophilic, oil drops in water are formed. Thus, a microfluidic device that creates multiple emulsions is a stringent demonstration of the coating technology presented here.

To make double emulsions requires a microfluidic device consisting of two dropmakers in series; the outlet of the first drop maker feeds into the inlet of the second drop maker, as depicted in Fig. 2A. To make W/O/W double emulsions, the first drop maker is made

hydrophobic and the second hydrophilic; this allows the first to make water drops which are encapsulated in oil drops in the second drop maker, as depicted in Fig. 2A. To make a device with this wettability pattern, we use our flow-confinement technique to make the second drop maker hydrophilic. To accomplish this, we inject the reactive monomer solution into the outlet of the device at  $200 \text{ mL h}^{-1}$  and the inert fluid into the inner-phase and middle-phase inlets at  $2000 \text{ mL h}^{-1}$ ; the continuous phase inlet is left open, to act as the outlet for both solutions, as indicated in Fig. 2B. This causes the reactive and inert fluids to meet in the second drop maker, so that a stable interface forms between them. The interface is sharp or fuzzy depending on the magnitude of diffusive to advective transport. If diffusion across the interface is small compared to the flow velocity, the reaction is confined to the lower part of the device. This is achieved by controlling the fluid flow rates; this allows us to adjust the Péclet number, which is the ratio of advective to diffusive transport at a fluid–fluid interface. The Péclet number is defined as  $Pe = vd/D$ , where  $v$  is the flow velocity controlled by syringe pumps,  $d = 100 \text{ mm}$  the length of the liquid–liquid interface in the drop formation region, and  $D$  the diffusion coefficient of the monomer,  $1.3 \times 10^{-9} \text{ m}^2 \text{ s}^{-1}$ . We calculate  $Pe$  to be  $\sim 300$ ; thus, diffusion is negligible in our system, yielding a sharp interface that confines the reaction. This interface sets the location at which the wettability transitions from hydrophobic to hydrophilic. Our technique can also create the inverse wettability pattern, to form O/W/O double emulsions. In this case, we switch the inlets into which we inject the reactive and inert fluids, as shown in Fig. 2C; this makes the first drop maker hydrophilic and the second hydrophobic, as illustrated in Fig. 2D. Other injection strategies can also be used to pattern more complex devices, as discussed in the ESI.<sup>†</sup>

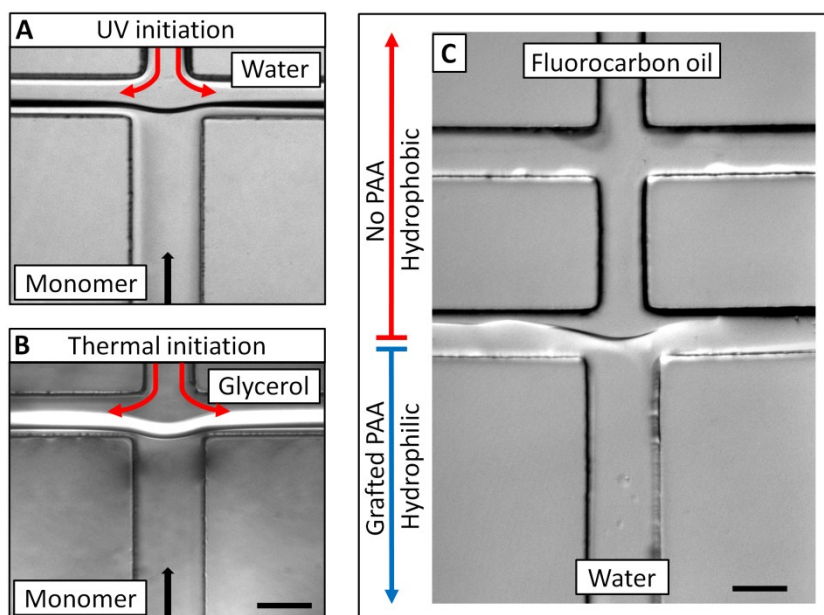


Figure 3: Since confinement of the surface treatment is achieved by physical means, our approach is general with respect to the surface chemistries that can be used to control wettability, which we demonstrate by using (A) a UV-initiated reaction and (B) a thermal-initiated reaction. Because the same flow pattern is used for both reactions, the resulting wettability patterns are the same. To confirm these patterns, we image the meniscus between HFE-7500 fluorocarbon oil and deionized water under static conditions in the channel. Due to the different wettability properties in the upper and lower junctions, a meniscus forms between them at the wettability crossover; this allows us to image the shape of the crossover, as shown in (C). The scale bars denote 100  $\mu\text{m}$ .

Since spatial control of the hydrophilic treatment is achieved by physically confining the reaction, our approach is very general with respect to the surface reactions that can be used. To demonstrate this, we use photo-initiated and thermal-initiated polymerization reactions, though many other reactions are possible.<sup>12,13,18</sup> For the photo-initiated reaction, we use a monomer solution consisting of 5.8 mol L<sup>-1</sup> AA in ethanol. To initiate the reaction, we incorporate 2-hydroxy-2-methylpropiophenone (Darocur® 1173) as a photo-initiator at 22.6 mol%, relative to the amount of AA. Under exposure to UV light, these molecules release radicals that initiate polymerization of the AA. The monomers covalently bond, forming polymers; some of these polymers attach to the double bonds on the surface, attaching them to the surface. The device is exposed to light everywhere, but attachment of the polymers occurs only in the lower portion, because the other regions are blocked by the inert fluid, as shown in Fig. 3A. For the thermal-initiated reaction, we use AA in water at 5.8 mol L<sup>-1</sup> concentration; however, rather than a photo-initiator we use a

thermal initiator. We use APS at 1.50 mol% with TEMED at 3.7 mol% as an accelerant, both in relation to the amount of AA. We inject the solutions as before, but this time initiate the reaction by placing the device on a hot plate set to 80 °C. Again, even though the device is heated everywhere, the reaction is confined to the lower portion of the device by the inert fluid, as shown in Fig. 3B. To verify that this allows us to spatially control grafting of PAA, we image the meniscus between HFE-7500 fluorocarbon oil and deionized water under static conditions in the channel. Due to the different wettability properties in the upper and lower junctions, a meniscus forms between them at the wettability crossover; this allows us to image the shape of the crossover, as shown in Fig. 3C. This confirms that we can spatially control where PAA is grafted.

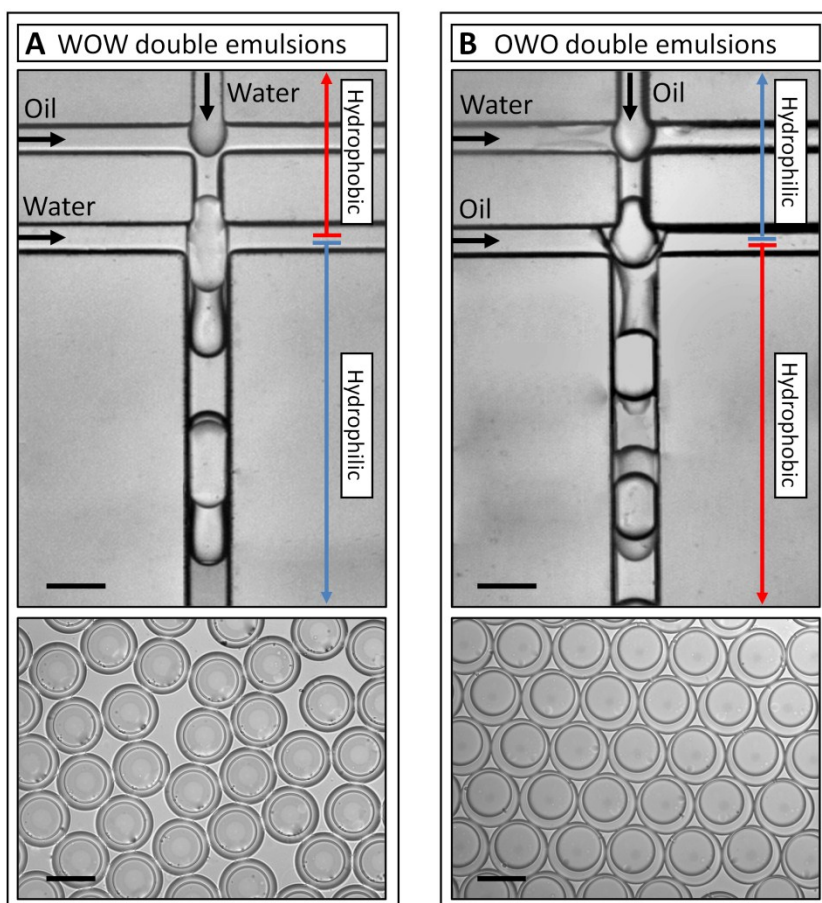


Figure 4: To form W/O/W double emulsions we use flow confinement to pattern the wettability of a double emulsion device. We make the first drop maker hydrophobic and the second hydrophilic (A). To form O/W/O double emulsions, we invert the pattern (B). To confirm that the double emulsions are formed properly, we image samples collected from both devices, lower panels. The scale bars denote 100  $\mu\text{m}$ .

To demonstrate that flow patterning provides the control needed to form double emulsions, we use it to pattern devices to form both W/O/W and O/W/O double emulsions. As fluids for the double emulsions, we use HFE-7500 fluorocarbon oil with the ammonium salt of Krytox® 157 FSL at 1.8% by weight as the surfactant; for the drops we use deionized water with Pluronic® F127 at 1.0% by weight as the surfactant. To form W/O/W double emulsions, we use flow confinement to make the first drop maker hydrophobic and the second hydrophilic. We inject the fluids into the first, second, and third inlets at 1000, 900 and 1500 mL h<sup>-1</sup>, respectively; this allows the first drop maker to produce water drops in oil and the second to encapsulate the water drops in larger oil drops, forming W/O/W double emulsions, as shown in Fig. 4A. To produce O/W/O double emulsions, we simply invert the wettability pattern, as shown in Fig. 4B.

## Conclusions

Spatial control of wettability is necessary for a variety of applications of microfluidic devices. In contrast to other wettability patterning methods which require precise alignment of an optical pattern with the microfluidic device, our method requires only that fluids are injected in the correct configuration; this makes our approach simple and very scalable. This should be useful for applications that require fabrication of large numbers of devices with identical properties, as needed in scale-up. It should also be useful for patterning the functional properties of devices for biological applications, as in cancer-cell screening applications in which cells must pass through certain regions of the device but be captured by others.<sup>19</sup>

## Acknowledgements

This work was supported by the NSF (DMR-0602684), the Harvard MRSEC (DMR-0820484), and the Massachusetts Life Sciences Center. JT received funding from the Fund of the Chemical Industry (Germany) which is gratefully acknowledged.

## References

- (1) Kane, R. S., Takayama, S., Ostuni, E., Ingber, D. E., Whitesides, G. M. *Biomaterials* **1999**, *20*, 2363-2376.
- (2) Chu, L.-Y., Utada, A. S., Shah, R. K., Kim, J.-W., Weitz, D. A. *Angew. Chem.* **2007**, *119(47)*, 9128-9132.
- (3) Utada, A. S., Lorenceau, E., Link, D. R., Kaplan, P. D., Stone, H. A., Weitz, D. A. *Science*, **2005**, *308*, 537-541.
- (4) Aserin, A. *Multiple Emulsion: Technology and Applications*, Wiley-VCH, **2007**.
- (5) Abate, A. R., Weitz, D. A. *Small* **2009**, *5*, 2030-2032.
- (6) Nisisako, T. *Chem. Eng. Technol.* **2008**, *31*, 1091-1098.
- (7) Okushima, S., Nisisako, T., Torii, T., Higushi, T. *Langmuir* **2004**, *20*, 9905-9908.
- (8) Seo, M., Paquet, C., Nie, Z., Xu, S., Kumacheva, E. *Soft Matter* **2007**, *3*, 986-992.
- (9) Abate, A. R., Krummel, A. T., Lee, D., Marquez, M., Holtze, C., Weitz, D. A. *Lab Chip* **2008**, *8*, 2157-2160.
- (10) Hu, S., Ren, X., Bachman, M., Sims, C. E., Li, G. P., Allbritton, N. L. *Anal. Chem.* **2004**, *76*, 1865-1870.
- (11) Fidalgo, L. M., Abell, C., Huck, W. T. S. *Lab Chip* **2007**, *7*, 984-986
- (12) Zhao, B., Moore, J. S., Beebe, D. J. *Science* **2001**, *291*, 1023-1026.
- (13) Kenis, P. J. A., Ismagilov, R. F., Whitesides, G. M. *Science* **1999**, *285*, 83-85.
- (14) Duffy, D. C., McDonald, J. C., Schueller, O. J. A., Whitesides, G. M. *Anal. Chem.* **1998**, *70*, 4974-4984.
- (15) McDonald, J. C., Duffy, D. C., Anderson, J. R., Chiu, D. T., Wu, H., Schueller, O. J. A., Whitesides, G. M. *Electrophoresis* **2000**, *21*, 27-40.
- (16) Sakka, S. *J. Sol-Gel Sci. Technol.* **1994**, *2*, 451-455.
- (17) A detailed discussion of the sol-gel coating process, as well as the grafting process, can be found in the supplemental information for this communication.
- (18) Evans, C. E., Lovell, P. A. *Chem. Commun.* **2009**, *17*, 2305-2307.
- (19) Vanapalli, S. A., Duits, M. H. G., Mugele, F. *Biomechanics* **2006**, *3*, 012006-1-012006-15.



## Supplemental information

This supplemental information contains details for fabricating microfluidic devices to make double emulsions. It is organized into three sections: device design, fabrication, and wettability patterning. In the wettability patterning section, we provide two surface modification reactions, UV-initiated and thermal-initiated reactions. Both methods are simple and robust, and we hope that by providing two options, more people will try the method out.

### Device design

We fabricate our devices using photolithography. An essential part of this process is a photomask containing a picture of the device to be fabricated. To make the photomask, we draw a to-scale schematic of the device in AutoCAD, and send it to Cad Art Services, Inc., Bandon, OR, USA for printing. Cad art prints the picture on transparency plastic in UV absorbent ink. An inverse image of the device is shown in Fig. S1. To inject fluids into the device, we require inlet ports that can be interfaced with tubing. We punch holes in the device (Harris Unicore 0.75 mm biopsy punch) that intersect with the microchannels. The holes must be punched accurately, or they will miss the microchannels; to ensure accurate punching, we use an optical guide to make the punch location easier to see. We surround the punch location with polygons that scatter light, making it easy to see. We also provide a large target for the punch by creating a wide basin channel at the punch location. This ensures that even if the punch is slightly misaligned, there will still be an intersection with the channel. Below the punch basin is a filter consisting of an array of rhombic posts, as shown in Fig. S1. The gaps between the posts are made narrower than the narrowest constriction on the device, allowing it to filter debris that could lead to clogging.

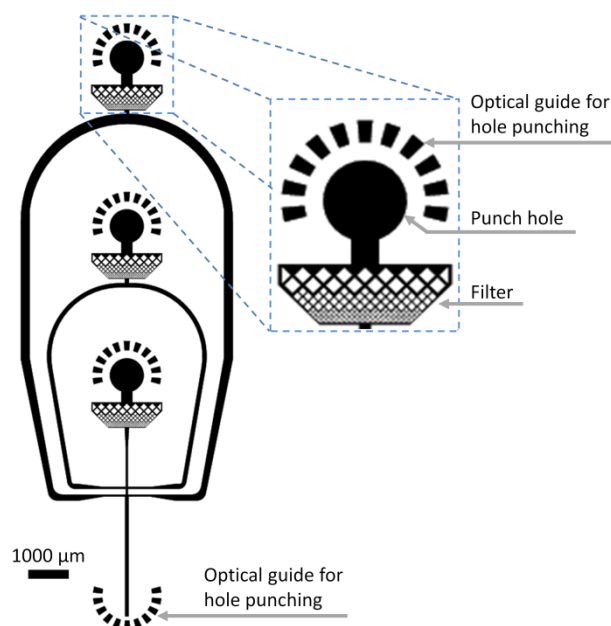


Figure S1: Inverse grayscale image of AutoCAD drawing of the microfluidic device used to create double emulsions. Depending on how the wettability of the device is patterned, it can form O/W/O or W/O/W double emulsions. The device has three inlets and an outlet, which must be punched manually to interface with fluids. The punch locations are surrounded by rectangular posts that scatter light, making it easier to see where to punch. Below each punch is a filter that prevents debris from entering the device.

## Coating PDMS devices with sol-gel

To control the wettability of our devices we coat them with sol-gel. To prepare the sol-gel solution we combine 1 mL tetraethylorthosilicate (TEOS), 1 mL methyltriethoxysilane (MTES), 0.5 mL (heptadecafluoro-1,1,2,2-tetrahydrodecyl)-triethoxysilane, 2 mL trifluoroethanol and 1 mL 3-(trimethoxysilyl)-propylmethacrylate; the solution should be yellow and clear, and can be stored for up to a week at 2-8 °C. Before the coating can be applied the sol-gel must be preconverted by adding an acid catalyst. To preconvert, we combine 0.5 mL of the sol-gel solution, 0.9 mL methanol, 0.9 mL trifluoroethanol, and 0.1 mL HCl aqueous pH 2. After the catalyst is added the solution may turn cloudy; it is vigorously shaken for several seconds and placed on a hot plate set to 85 °C for 30 s; this is repeated until the reaction mixture clears, which takes approximately 2 minutes. The solution is loaded into a 1 mL plastic syringe with a 27 G needle. The amount of trifluoroethanol and methanol added can be varied, to control the coating thickness; by adding more of these solvents, thinner coatings are produced because the sol-gel is more dilute. The dilution should be chosen to match the dimensions

of the channels: the smaller the channels, the thinner the coating must be and, thus, the higher the dilution. The dilution we describe is appropriate for channels about 100  $\mu\text{m}$  in diameter, the dimensions of our device. We have found that the sol-gel can be diluted by as much ten times, without adversely affecting wettability control.

The device must be coated immediately after plasma bonding. A 1 cm piece of poly(ethylene) (PE) tubing is inserted into the outlet of the device. The device is then filled with the pre-converted sol-gel mixture via the tubing. The device is then placed on a hotplate set to 180  $^{\circ}\text{C}$ , and held down with tweezers to ensure good thermal contact. After a few seconds a popping sound can be heard as the sol-gel mixture vaporizes and the channels are blown clear. At this point, the PE tubing is removed so that it does not melt, but the device is left on the hotplate for additional 60 s to allow the coating to fully cure. The device is then removed from the hotplate and allowed to cool. The coated device can be stored for several months wrapped in aluminum foil, before patterning wettability. This process describes coating a single drop maker; however, normally our devices consist of between 5-10 drop makers, all on the same chip. The coating process is the same, except that many devices are coated in parallel.

## **Patterning microfluidic device wettability**

Flow confinement can be used to pattern wettability using a variety of surface modifying reactions. Here, we describe two reactions, both polymerization reactions, but one initiated by UV light and the other by heat.

### **UV initiation**

For the UV-initiated reaction we require a bright UV light source. We use a homebuilt microscope outfitted with Koehler illumination as the light source. The lamp of the Koehler illumination can be switched between a fiber-coupled halogen lamp (Thorlabs) and a fiber-coupled 300 W UV-arc lamp (Exfo). With the Koehler focusing optics this setup produces a UV beam on the sample with an optical power 150  $\text{mW cm}^{-2}$  at a wavelength of 365 nm. This setup also allows us to see the sample during the exposure.

We set the device up and start the flows using the halogen lamp, and then, when everything is aligned and flowing steadily, start the exposure by switching to the UV lamp. We continue to watch the sample during the exposure, to monitor polymerization and adjust flow rates as needed. This, admittedly, is a somewhat specialized piece of equipment, although it only cost approximately \$ 5000 to build: \$ 3000 for the UV lamp and \$ 2000 for the halogen lamp, objectives (Mitutoyo), and optics (Thorlabs). Alternatively, the exposure could also be done using a standard fluorescence microscope with a UV source. In this case, an appropriate filter set must be inserted into the filter cube of the microscope, to expose the sample to UV light. Another option would be to use a flood UV system or black light with the correct wavelengths; however, a drawback to this approach is that, without a microscope, it will not be possible to see the polymerization as it is progressing. Another drawback is that it is unlikely that such a system will provide high light intensity, so that longer polymerization times will be needed to achieve sufficient grafting.

To prepare the monomer solutions we combine 0.5 mL ethanol, 0.2 mL acrylic acid and 0.1 mL 2 hydroxy-2-methylpropiophenone (Darocur® 1173). The solution is loaded into a 1 mL syringe (Hamilton Gas Tight). A 3 mL plastic syringe is filled with deionized water for the blocker phase. The water syringe is connected to the microfluidic device and used to flush trapped air from the channels. The monomer solution is then connected to the device, along with an additional piece of PE tubing to the continuous phase inlet, which serves as the outlet during the patterning process. The remaining fourth inlet is plugged with a melted small piece of PE tubing. Using bright field illumination, the device is aligned with the light source and the syringe pumps are started at  $200 \mu\text{L h}^{-1}$  for the monomer solution and  $2000 \mu\text{L h}^{-1}$  for the inert solution. Once the flows are stable, the light source is switched to the UV lamp to initiate polymerization. As polymerization proceeds, the viscosity of the monomer solution increases; to maintain the interface at the correct location, we increase the flow rate of the water phase in  $300 \mu\text{L h}^{-1}$  steps and reduce the flow rate of the monomer in  $10 \mu\text{L h}^{-1}$  steps approximately every 30 seconds. After 6 minutes the UV light is switched off. With the inert phase still running, the monomer tubing is pulled out of the device; this flushes the device with the inert phase, removing unreacted monomer.

There are two benefits to using bulk initiators rather than surface-immobilized initiators for the polymerization. Unlike with an immobilized strategy in which there are a finite number of initiators on the surface, in a bulk strategy there are essentially a limitless number of initiators; as the reaction progresses and initiators are consumed, new initiators are introduced by the flow. This enables the reaction to run as short or as long as desired, to control the amount of polymer grafted. Another advantage is that there are a larger variety of bulk initiators available for purchase than initiators that can be bonded to the surface; this affords greater flexibility when choosing the initiators and the linkage chemistry, which may be important for certain applications.

### **Thermal initiation**

To pattern wettability using a thermal-initiated polymerization reaction, all which is required is a hotplate; we also use a reflection microscope, so that we can visualize the polymerization. We prepare the monomer solution for this reaction by combining 500  $\mu\text{L}$  deionized water, 200  $\mu\text{L}$  acrylic acid, 100  $\mu\text{L}$  of a freshly prepared solution of APS in water (10 wt%) and 16  $\mu\text{L}$  tetramethylethylenediamine (TEMED). The monomer solution is loaded into a 1 mL syringe (Hamilton Gas Tight) and cooled with an ice package. A 3 mL plastic syringe is filled with glycerol, which will act as the blocker phase. The glycerol syringe is connected to the device, and the device is flushed to remove trapped air. After connecting the monomer solution, an additional piece of PE tubing is connected to the continuous phase, to serve as the outlet during the patterning process. Again, the remaining fourth inlet is plugged with a melted small piece of PE tubing. Using the reflection microscope, the device is aligned on the hotplate and the syringe pumps are started at 200  $\mu\text{L h}^{-1}$  for the monomer solution and 2000  $\mu\text{L h}^{-1}$  for the inert solution. Once the flows are stable and a sharp interface has formed in the junction, the hotplate is set to 80  $^{\circ}\text{C}$ . As the temperature rises above 75  $^{\circ}\text{C}$ , a significant increase in the viscosity of the monomer solution occurs. To maintain the interface in the center of the junction, the flow rate of glycerol is increased in 500  $\mu\text{L h}^{-1}$  steps and the flow rate of monomer is reduced in 10  $\mu\text{L h}^{-1}$  steps approximately every 30 s. After 6 minutes, the hot plate is switched off and the device is removed. To remove remaining unreacted monomer solution and glycerol, the device is flushed with deionized water for several minutes.

### **Other injection strategies for complex devices**

Our method can be used to pattern complex devices, including many drop makers connected together; however, there are other devices that are not as easily patterned. For example, to create W/O/W/O triple emulsions requires a device consisting of three flow-focus junctions in series, with a wettability pattern in which the first drop maker is hydrophobic, the second hydrophilic, and the third hydrophobic. This pattern cannot be easily created using flow-confinement as we present it in the communication. However, with simple modifications to the method, this pattern can also be created. The challenge is to make the central junction hydrophilic while leaving the upper and lower junctions hydrophobic; however, to functionalize the central junction, the reactive solution must be flowed past the upper or lower junction, resulting in the patterns hydrophilic/hydrophilic/hydrophobic, or hydrophobic/hydrophilic/hydrophilic, neither of which is suitable for forming triple emulsions. A simple solution is to add a channel to the central junction, to allow the reactive solution to be injected directly, bypassing the other junctions. Another option is to use a “forward-flow” approach, in which all fluids are injected into the inlets of the device and exit through the outlet. If the fluids are injected in the configuration inert/reactive/inert, this will produce the correct pattern to form the triple emulsions; however, a difference with this injection strategy is that the crossover lines will be V-shaped rather than flat.

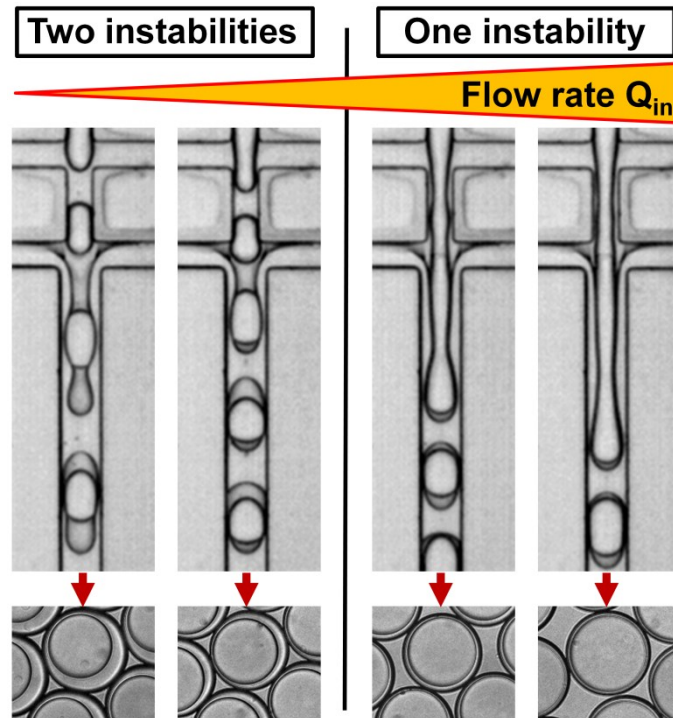
## One-Step Formation of Multiple Emulsions in Microfluidics

Adam R. Abate,<sup>‡</sup><sup>a</sup> Julian Thiele,<sup>‡</sup><sup>a,b</sup> David A. Weitz\*<sup>a</sup>

<sup>a</sup> School of Engineering and Applied Sciences/Department of Physics, Harvard University, Cambridge, Massachusetts, USA

<sup>b</sup> Institute of Physical Chemistry, University of Hamburg, Germany

<sup>‡</sup> Both authors contributed equally to this work.



Published in *Lab on a Chip* **2011**, *11*, 253-258.

### **Abstract**

We present a robust way to create multiple emulsions with controllable shell thicknesses that can vary over a wide range. We use a microfluidic device to create a coaxial jet of immiscible fluids; using a dripping instability, we break the jet into multiple emulsions. By controlling the thickness of each layer of the jet, we adjust the thicknesses of the shells of the multiple emulsions. The same method is also effective in creating monodisperse emulsions from fluids that cannot otherwise be controllably emulsified, such as, for example, viscoelastic fluids.

### **Introduction**

Multiple emulsions are drops containing smaller drops within them.<sup>1-3</sup> They are useful for making particles and capsules through a templating process.<sup>4-6</sup> Multiple emulsions can be formed with the desired structure using microfluidic devices;<sup>7-9</sup> by solidifying the drops, they can be transformed into particles or capsules whose properties are determined by those of the multiple emulsions. These capsules are useful because they provide a protective shell for active reagents; by tuning the properties of the shell, the capsules can be triggered to burst, to release their payloads under specific conditions of heat, pH, or physical stresses.<sup>2,10,11</sup> This makes capsules formed with microfluidics valuable for a range of active delivery applications, including for fragrances and enhancing enzymes in cosmetics, for pharmaceuticals, and for the controlled release of pesticides.<sup>12-15</sup>

However, current microfluidic techniques are limited because drops can be formed only with a narrow range of shell thicknesses. This limitation arises due to the mechanism of formation: in the best approach, the drops are formed by a multi-step mechanism; a series of drop makers are aligned end-to-end such that the output of one feeds the input of the next. Thus, the innermost drop is formed in the first drop maker and encapsulated in drops of increasing size in the next drop makers, producing the multiple emulsion in a stepwise process.<sup>16,17</sup> For example, to create a triple emulsion, the innermost drop is encapsulated in a larger drop to form a double emulsion, which is then encapsulated in a still larger drop to produce the triple emulsion. To produce monodisperse emulsions, the flow rates must be set to ensure that all junctions operate in the dripping regime.<sup>18</sup> This is



the regime in which monodisperse drops are formed at a periodic rate at a fixed location in the device. This limits the flow rates to a narrow range, and typically results in multiple emulsions with thick shells. However, many applications demand much thinner shells. Thus, a versatile method that can operate over a wide range of flow rates is essential.

In this paper we present a simple and robust technique to form multiple emulsions with a wide range of shell thicknesses. We use a microfluidic device consisting of a series of flow-focus junctions. By setting the flow rates such that all but the final junction are in the jetting regime, we produce a coaxial multiple jet of the fluids. The jet itself is broken into multiple emulsions using a dripping instability; a dripping instability is one in which a confined jet is broken into monodisperse drops at a periodic rate at a fixed location in the channel. This mechanism can thus operate at flow rates in which the inner phase is jetting, enabling production of multiple emulsions with a wider range of shell thicknesses. It can also create monodisperse drops from fluids that normally cannot be emulsified controllably, such as viscoelastic fluids. This is achieved by surrounding the viscoelastic fluid in a second fluid that is easier to emulsify; by inducing the outer fluid to pinch into drops, we also pinch the inner fluid into drops. The inner drops can be released by breaking the double emulsions, yielding a monodisperse emulsion of the viscoelastic fluid.

## Results and Discussion

We create our emulsions using a flow focusing geometry which consists of two channels that intersect to form a cross.<sup>19,20</sup> The dispersed phase is injected into the central inlet and the continuous phase into the side inlets. The fluids meet in the nozzle where drops are formed over a wide range of flow conditions, which can be described by two dimensionless numbers. The Weber number of the dispersed phase  $We_{in} = \rho v_{in}^2 l / \gamma$  relates the magnitude of inertial forces to surface forces;  $\rho$  and  $v_{in}$  are the density and velocity of the inner phase,  $l$  the diameter of the channel, and  $\gamma$  the surface tension of the jet.<sup>21</sup> The Capillary number of the outer phase  $Ca_{out} = \mu v_{out} / \gamma$  relates the magnitude of the shear on the jet, due to the continuous phase, to its surface tension;  $\mu$  and  $v_{out}$  are the viscosity and velocity of the outer phase.<sup>22</sup> For  $\{We_{in}, Ca_{out}\} > 1$ , the dispersed phase does not break into drops, whereas for  $\{We_{in}, Ca_{out}\} < 1$ , a dripping instability occurs, breaking the

dispersed phase into drops. Drop formation in microfluidics is usually classified as being shear dominated or pressure dominated. Shear dominated formation tends to occur in unconfined geometries, in which  $Ca \approx 1$ ,<sup>23</sup> whereas pressure dominated drop formation occurs in confined geometries in which  $Ca < 0.01$ . In our system,  $Ca > 0.01$ , but the flows are confined, precluding direct application of either formalism. Rather, in our system, the drop formation mechanism likely combines shear and pressure effects.

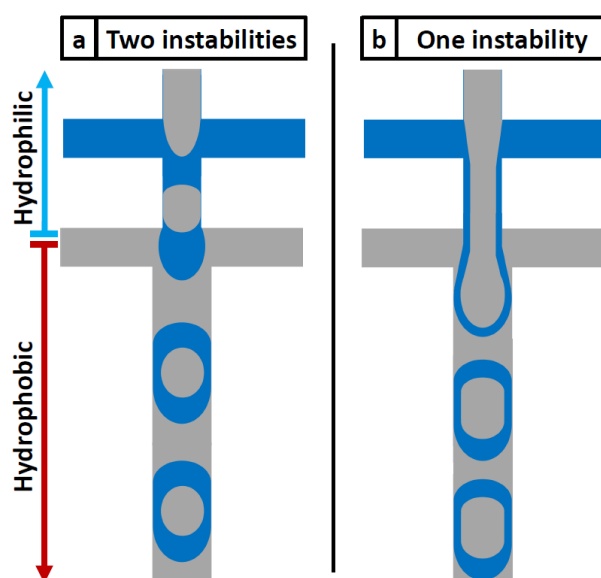


Figure 1: (a) Schematic of a double flow-focus device for double emulsion formation. The flow rates are normally set so that dripping instabilities are present in both junctions; this emulsifies the inner phase and then the outer phase, producing double emulsions in a two-step process. (b) By increasing flow rates the first instability can be removed, causing the inner phase to jet; this forms a double jet that can be broken into double emulsions in one step.

When forming double emulsions, two flow-focus junctions are used; the outlet of the first feeds the inlet of the next, as shown in Fig. 1a. Normally, dripping instabilities are present in both junctions. This produces double emulsions in a two-step process: the inner drop is formed in the first junction and encapsulated in the outer drop in the second.<sup>18,24–26</sup>

Double emulsions can also be formed in a one-step process by removing the first dripping instability, by increasing the flow rates in the first junction. This produces a jet of the inner phase that extends into the second junction. There, it is surrounded by a sheath of middle phase, producing a coaxial jet, as illustrated in Fig. 1b. If the flow rates in the

second junction are set to induce a dripping instability, the coaxial jet is pinched into double emulsions, as depicted in Fig. 1b. Thus, there are two distinct types of double emulsification: in two-step formation there are two regions in which drops are formed, whereas in one-step formation all drops form in a single region.

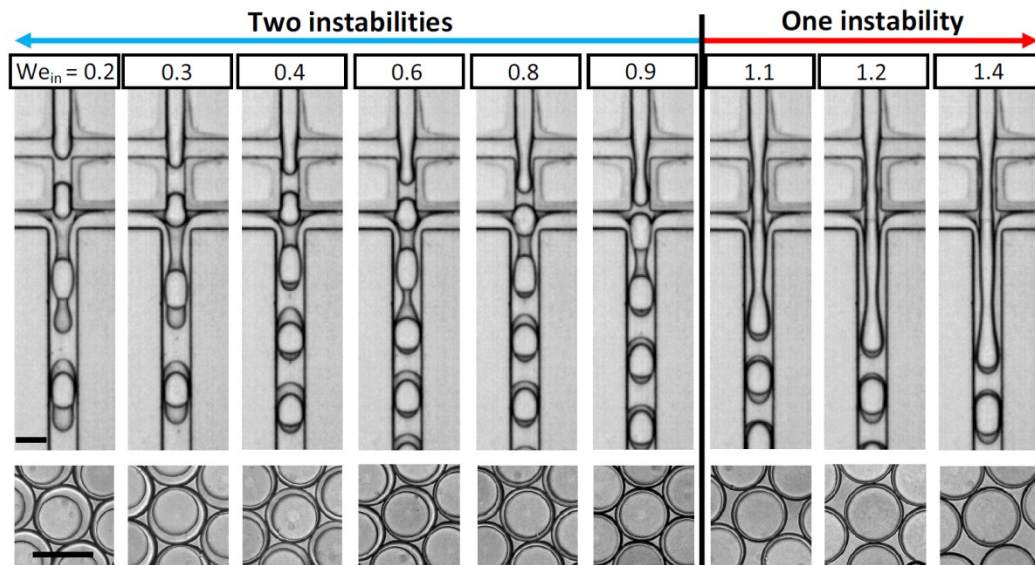


Figure 2: Double emulsion formation for different inner-phase Weber numbers,  $We_{in}$ . For low  $We_{in}$ , dripping instabilities are present in both junctions, forming double emulsions in a two-step process. When  $We_{in}$  is increased beyond one, the first instability is removed; this causes the inner phase to jet, forming a double jet that breaks in a one-step pinch off. The inner and continuous phases, injected into the first and third inlets, are composed of HFE-7500 with the ammonium salt of Krytox® FSL at 1.8% by weight; the middle phase, injected into the second inlet, is water with sodium dodecyl sulfate (SDS) at 0.5% by weight. The scale bars denote 80  $\mu\text{m}$ .

To demonstrate control over the formation process using dripping instabilities, we construct a double flow-focus device with a constant channel height of 50  $\mu\text{m}$ . The width of the nozzle channel in the first junction is 50  $\mu\text{m}$  and in the second junction 80  $\mu\text{m}$ . For the fluids, we use deionized water with sodium dodecyl sulfate (SDS) at 0.5% by weight, and HFE-7500 fluorocarbon oil with the ammonium carboxylate of Krytox® 157 FSL at 1.8% by weight as the surfactant. The density is 1614  $\text{kg m}^{-3}$  for HFE-7500 and 998.3  $\text{kg m}^{-3}$  for water. The viscosity is 0.77 cSt for HFE-7500 and 1.01 cSt for water. We estimate the surface tension between the dispersed and continuous phase to be

$1\text{-}5\text{ mN m}^{-1}$ . To form O/W/O double emulsions, we pattern the wettability of the device such that the first junction is hydrophilic and the second hydrophobic. We accomplish the patterning of the wettability using a flow-confinement technique.<sup>27</sup> Wettability patterning is needed for both two-step and one-step formation. In two-step formation it is necessary to form the inner and outer drops in two different junctions. In one-step formation, it is necessary to form the coaxial jets that are broken into double emulsions. An advantage with one-step formation is that the patterning does not have to be as precise as with two-step formation. This is because once the inner jet is formed it is surrounded by a protective sheath of the middle phase; this allows it to remain encapsulated even if the channel properties in that region favor wetting. This makes one-step formation easier to implement and, generally, more robust in practice.

We begin by forming double emulsions with the two-step process. This requires two dripping instabilities, one in each junction. We set flow rates to  $600\text{ mL h}^{-1}$  for the inner,  $1000\text{ mL h}^{-1}$  for the middle, and  $2500\text{ mL h}^{-1}$  for the continuous phase, ensuring that  $\{We_{in}, Ca_{out}\} < 1$  in both junctions. This causes the innermost phase to drip in the first junction, and the middle phase to drip in the second, forming double emulsions in a two-step process, as shown for  $We_{in} = 0.2$  in Fig. 2. As we increase  $We_{in}$ , the first flow-focus junction approaches the jetting transition, although the process remains two-step, as shown for  $We_{in} = 0.8$  in Fig. 2. As we increase  $We_{in}$  above 1, the inner phase begins to jet, producing a coaxial jet, as shown for  $We_{in} = 1.1$  in Fig. 2. Because  $\{We_{in}, Ca_{out}\} < 1$  in the second junction, a dripping instability breaks the coaxial jet into double emulsions, as shown in Fig. 2.

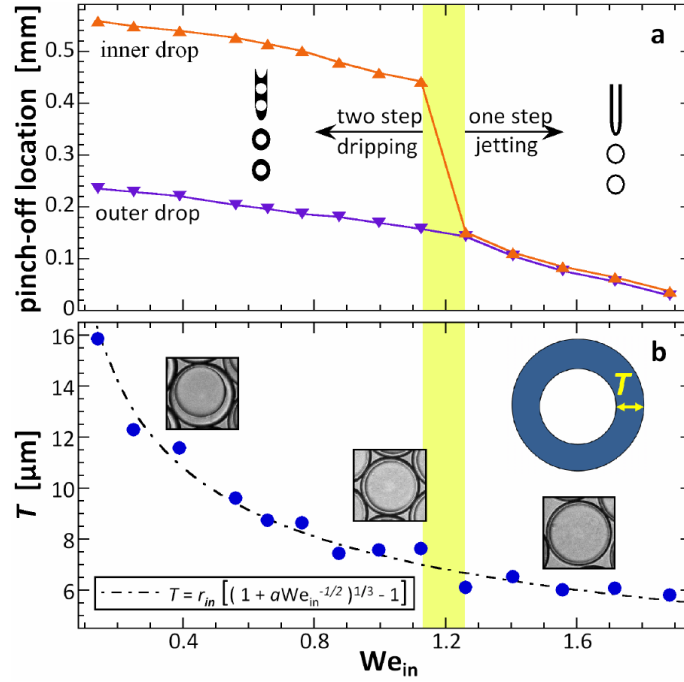


Figure 3: (a) Pinch-off locations of the inner and outer jets as a function of  $We_{in}$ . At low  $We_{in}$  dripping instabilities are present in both flow-focus junctions, so the inner and outer jets break at different locations. As  $We_{in}$  is increased beyond 1, the inner phase jets into the second junction; this causes the inner and outer phases to pinch off at the same place. (b) Because the first junction is not limited to the dripping regime, this allows double emulsions to be formed with thin shells. The function for  $T$  is derived by equating the volume of the shell to the volume of middle phase supplied over one drop formation cycle; it is plotted by inserting the inner drop radius  $r_{in}$  measured from the images, and the parameter  $a = U_{mid}(\rho/\gamma l^3)^{1/2} = 0.706$ , computed from known constants.

To quantify the transition between these formation processes, we measure the pinch-off locations of the drops. At low  $We_{in}$ , the inner and middle phases pinch off at different locations, because there are two separated dripping instabilities, as shown in Fig. 3a. As  $We_{in}$  is increased, both pinch-offs are displaced downstream due to the higher shear, though the process remains two-step, as shown in Fig. 3a. As  $We_{in}$  is increased beyond 1, the inner phase jets; the drops pinch off at the same place, as shown in Fig. 3a. The transition is sudden, due to the discontinuous nature of the dripping-to-jetting transition.<sup>28–30</sup> As the ratio of innermost to middle phase fluids increases, the shell thicknesses decrease, as shown in Fig. 3b. We measure the average shell thickness  $T$  by computing the difference in the radii of the outer and inner drops, measured optically. With two-step formation, shells thinner than 7  $\mu\text{m}$  cannot be formed because the requisite flow conditions do not allow dripping; by contrast, with one-step formation we operate in

the jetting regime, producing double emulsions with thin shells, as shown in Fig. 3b. To obtain the function for  $T$ , we equate the shell volume to the volume of middle phase supplied over a single drop cycle; this produces a function that depends only on  $We_{in}$  and the known constants,  $r_{in}$  the inner drop radius measured from the images, and  $a$ , a parameter equal to the product known constants; the function, if plotted without free-parameter, fit in Fig. 3b. The precision of the shell thickness measurement is limited by our ability to resolve the droplet interfaces, which for our images is  $\sim 1 \mu\text{m}$ .

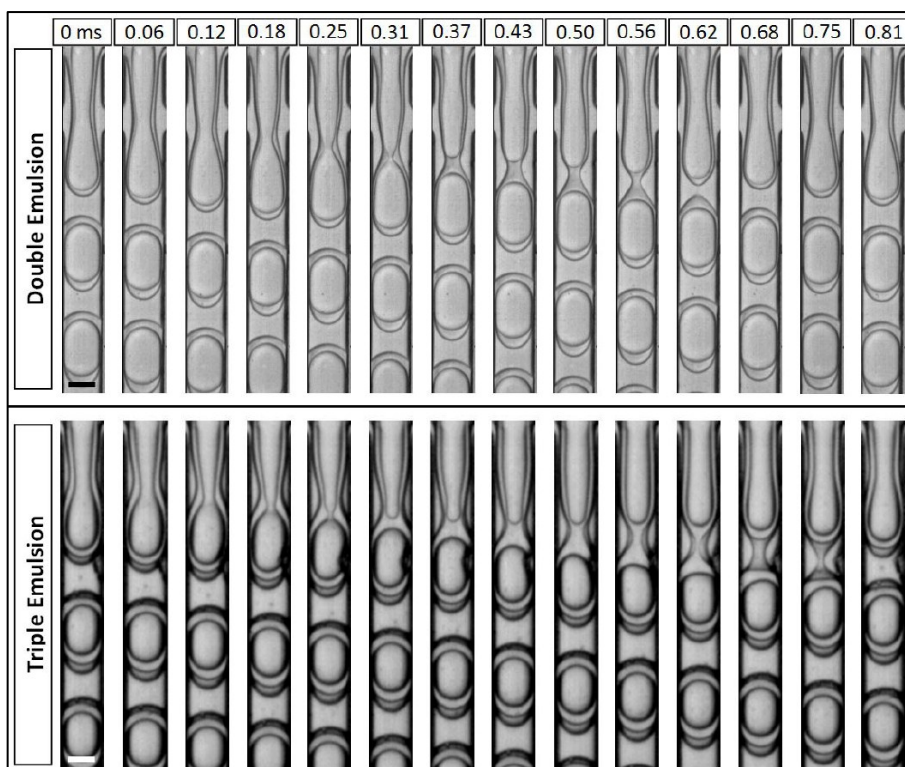


Figure 4: One-step formation of multiple emulsions. Double emulsions are formed by breaking a double jet, whereas triple emulsions are formed by breaking a triple jet. In these images, the inner jets break before the outer jets. As fluids for the double emulsions, we use HFE-7500 fluorocarbon oil with 1.8% of the ammonium salt of Krytox® 157 FSL (w/w) and deionized water with 0.5% SDS (w/w) as the surfactant. For the double emulsions, we inject oil, water, and oil into the first, second, and third inlets, respectively. To form triple emulsions, we inject water, oil, water, and oil into the first, second, third, and fourth inlets, respectively. The scale bar denotes 50  $\mu\text{m}$  for the upper row and 80  $\mu\text{m}$  for the lower row.

To visualize the dynamics of one-step formation, we record movies with a high-speed camera. Early in the cycle, the coaxial jet extends into the flow-focus junction, as shown for  $t = 0$  ms in Fig. 4. This allows the dripping instability to narrow the coaxial jet. Since the inner jet is thinner than the outer jet, it reaches an unstable width sooner; this causes it to pinch into a drop before the outer jet, as shown for  $t = 375$  ms. As the cycle progresses the outer jet continues to narrow and ultimately breaks, producing the double emulsion at  $t = 625$  ms.

One-step formation can also be used to create higher-order multiple emulsions. To illustrate this, we construct a triple emulsion device, consisting of three flow-focus junctions in series. To form W/O/W/O triple emulsions, we pattern the wettability to make the first junction hydrophobic, the second hydrophilic, and the third hydrophobic.

## 5 One-step formation of multiple emulsions

We inject water, HFE-7500, water, and HFE-7500, all with surfactants, into the first, second, third, and fourth inlets, respectively, at flow rates of  $4000 \text{ mL h}^{-1}$  for the innermost phase,  $3000 \text{ mL h}^{-1}$  for the first middle phase,  $3000 \text{ mL h}^{-1}$  for the second middle phase, and  $7500 \text{ mL h}^{-1}$  for the outermost phase. This ensures that  $\{We_{in}, Ca_{out}\} > 1$  for the first two junctions and  $\{We_{in}, Ca_{out}\} < 1$  for the third, so only one dripping instability is present. This creates a triple coaxial jet in the third junction, with a water jet surrounded by an oil sheath, surrounded by another water sheath, surrounded by the oil continuous phase, as shown in Fig. 4.

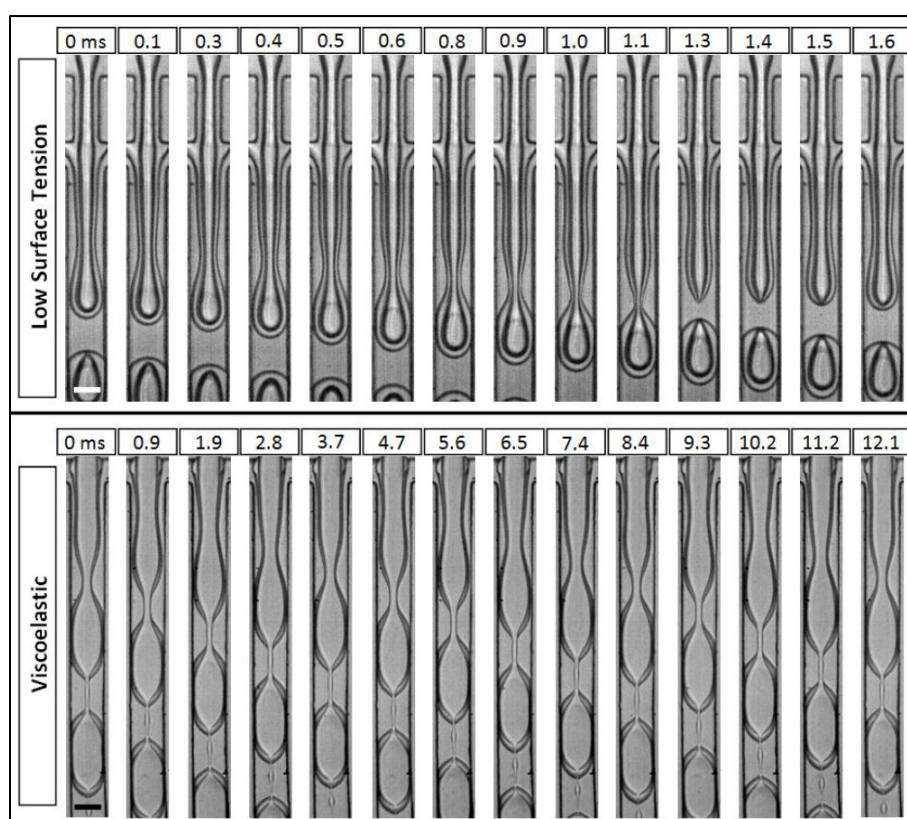


Figure 5: One-step formation of double emulsions in which the inner jet is composed of a fluid that does not easily break into drops. To form double emulsions from a fluid which has a very low interfacial tension with water, we inject octanol as the inner phase. To form double emulsions from a viscoelastic fluid, we inject poly(ethylene glycol) (mean  $M_w$  600000) in water at 10% by weight as the inner phase. In either case, HFE-7500 and water are injected as the middle and continuous phase, both with surfactants. The scale bars denote  $50 \mu\text{m}$ .



As with the double jet, the triple jet narrows when it enters the junction. This causes the inner jet to break,  $t = 250$  ms, then the middle jet to break,  $t = 625$  ms, then the outer jet to break,  $t = 750$  ms, producing a triple emulsion, as shown in Fig. 4. One-step formation of this type thus consists of a series of pinching events, one for each jet as it reaches an unstable width.

A different kind of one-step formation occurs when the inner jet is more stable than the outer jet. This occurs when the innermost phase is a fluid that forms very stable jets, such as a viscoelastic fluid or a fluid with a low surface tension. To demonstrate this, we replace the innermost phase with octanol, which has a low surface tension with water, resulting in a very stable jet, and making it difficult to emulsify using microfluidic techniques. By injecting octanol as the innermost phase, we produce a coaxial jet in which the inner jet is more stable than the outer jet, Fig. 5. As the outer jet pinches into a drop, it squeezes on the inner jet, pinching it into a drop as well. This produces a double emulsion with an octanol core, as shown in Fig. 5. Because a dripping instability is used, the double emulsions are monodisperse, as are the octanol cores. In essence, this enables a difficult fluid like octanol to be controllably emulsified, and provides a new way to create emulsions from such fluids. This method can also be applied to other difficult fluids, such as viscoelastic polymer fluids. These fluids are needed when templating particles or capsules from emulsions; however, due to their viscoelastic properties, they are extremely difficult to emulsify, because their elastic response under shear resists drop formation.<sup>31</sup> However, by surrounding the viscoelastic jet by an oil jet, it too can be controllably emulsified. We demonstrate this using a 10 wt% solution of poly(ethylene glycol) (PEG) (mean  $M_w$  600000) in water; frequency dependent shear behavior was probed at room temperature using a rheometer (ARES G2, Couette geometry). The viscous and elastic part of the complex shear modulus show scaling behavior according to the Maxwell model for viscoelastic fluids in the frequency range  $\omega = 0.01$ -100.<sup>32</sup> We determined the elastic modulus to be 1.5 Pa. As the water jet pinches into a drop, it also pinches the viscoelastic jet into a drop, as shown in Fig. 5. This produces double emulsions with viscoelastic cores. The cores can be released by breaking the double emulsions, yielding a monodisperse population of viscoelastic drops.

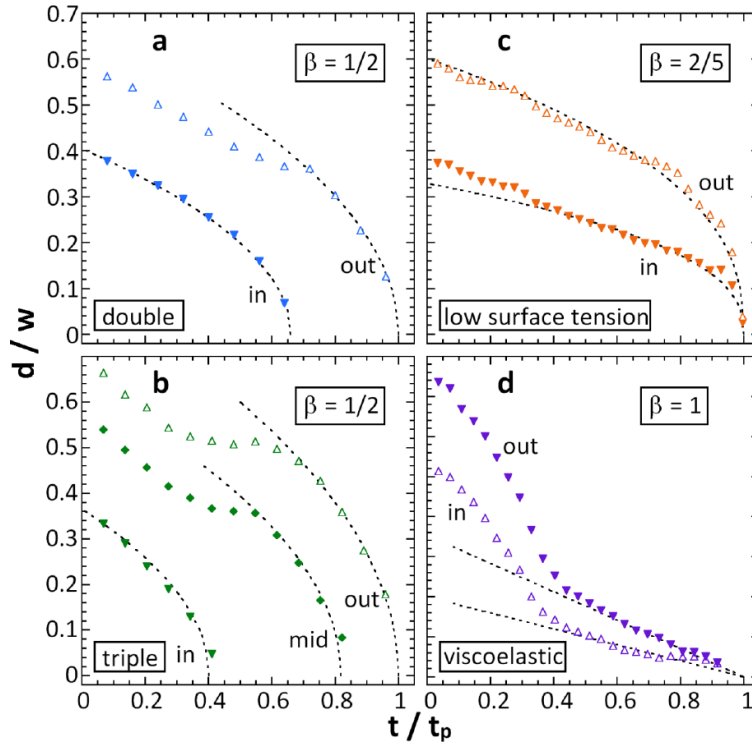


Figure 6: Jet diameter  $d$ , normalized by the channel width  $w$ , as a function of time during one-step formation  $t$ , normalized by the drop formation period  $t_p$  in (a) double emulsions and (b) triple emulsions; in these cases the inner jets break before the outer jets. When the inner phase is composed of a fluid that forms stable jets, the inner and outer phases break at the same time, as they do when the inner jet (c) has a low surface tension or (d) is viscoelastic. All collapses can be fit to power laws, but with different exponents depending on the physical properties of the fluids.

To quantify the dynamics of these breakups, we measure the jet widths as a function of time. Early in the process the inner and outer jets narrow in unison, as shown in Fig. 6a. When the inner jet reaches an unstable width, it breaks, rapidly narrowing and forming a drop. Interestingly, this coincides with a slight widening of the outer jet, showing that additional middle-phase fluid rushes into the void left by the collapse of the inner jet, as shown in Fig. 6a. Eventually, the outer jet also collapses, forming a double emulsion. In the case of the triple emulsion, this is followed by another widening and collapse of the third jet, as shown in Fig. 6b. The functional form of the collapse for the inner and outer jets is the same and can be fit to a power law with exponent  $1/2$ . This is consistent with the breakup of a single jet due to Rayleigh–Plateau instability. This similarity suggests that the jet breakup right at the moment of pinch-off for each of the nested jets is similar to that of a single jet.<sup>33,34</sup> When the inner jet is more stable than the outer one, the

pinching dynamics are different. With the octanol jet, there is a prolonged narrowing of both jets followed by a sudden collapse, as shown in Fig. 6c. The functional forms can also be fit to a power law, but with exponent  $2/5$ . This indicates that the pinching dynamics involve interactions between the jets. With the viscoelastic jet, the collapse is much slower. There is a prolonged narrowing followed by a very slow collapse; this is due to the viscoelasticity of the inner jet, as shown in Fig. 6d. These collapses can also be fit to power laws, with exponents of 1; unlike the other jets, these jets do not accelerate close to pinch off, as shown in Fig. 6d. Thus, although one-step formation can produce monodisperse double emulsions with different fluids, the pinching dynamics depend on the fluid properties.

## Conclusions

Microfluidic devices can form multiple emulsions in different processes by controlling dripping instabilities. If several instabilities are present, they are formed in a multi-step process, whereas if one is present, they are formed in a one-step process. The one-step process creates very thin-shelled multiple emulsions, which should be useful for capsule synthesis applications. It also enables difficult fluids, like viscoelastic fluids, to be emulsified controllably. This should be useful for synthesizing new kinds of particles requiring viscoelastic polymers.

## Acknowledgements

We thank Jim Wilking for assistance with rheological experiments and helpful discussions. This work was supported by the NSF (DMR-0602684), the Harvard MRSEC (DMR-0820484), and the Massachusetts Life Sciences Center. JT received funding from the Fund of the Chemical Industry (Germany) which is gratefully acknowledged.

## References

- (1) Bibette, J., Calderon, F. L., Poulin, P. *Rep. Prog. Phys.* **1999**, *62*, 969-1033.
- (2) Utada, A. S., Lorenceau, E., Link, D. R., Kaplan, P. D., Stone, H. A., Weitz, D. A. *Science* **2005**, *308*, 537-541.
- (3) Aserin, A. *Multiple Emulsion: Technology and Applications*, Wiley-VCH, **2007**.
- (4) Dendukuri, D., Doyle, P. S. *Adv. Mater.* **2009**, *21*, 1-16.
- (5) Fujiwara, M., Shiokawa, K., Tanaka, Y., Nakahara, Y. *Chem. Mater.* **2004**, *16*, 5420-5426.
- (6) Chen, C.-H., Shah, R. K., Abate, A. R., Weitz, D. A. *Langmuir* **2009**, *25*, 4320-4323.
- (7) Engl, W., Backov, R., Panizza, P. *Curr. Opin. Colloid Interface Sci.* **2007**, *13*, 206-216.
- (8) Chu, L.-Y., Utada, A. S., Shah, R. K., Kim, J.-W., Weitz, D. A. *Angew. Chem. Int. Ed.* **2007**, *46(47)*, 8970-8974.
- (9) Atencia, J., Beebe, D. J. *Nature* **2005**, *437*, 648-655.
- (10) Rojas, E. C., Staton, J. A., John, V. T., Papadopoulos, K. D. *Langmuir* **2008**, *24*, 7154-7160.
- (11) Livney, Y. D. *Curr. Opin. Colloid Interface Sci.* **2010**, *15*, 73-83.
- (12) Lee, M.-H., Oh, S.-G., Moon, S.-K., Bae, S.-Y. *J. Colloid Interface Sci.* **2001**, *240*, 83-89.
- (13) Khopade, A. J., Nandakumar, K. S., Jain, N. K. *J. Drug Targeting* **1998**, *6*, 285-292.
- (14) Özer, Ö., Özyazici, M., Tedajo, M., Taner, M. S., Köseoglu, K. *Drug Delivery* **2007**, *14*, 139-145.
- (15) El Shafei, G. M. S., El-Said, M. M., Attia, H. A. E., Mohammed, T. G. M. *Ind. Crops Prod.* **2009**, *31*, 99-106.
- (16) Seo, M., Paquet, C., Nie, Z., Xu S., Kumacheva, E. *Soft Matter* **2007**, *3*, 986-992.
- (17) Okushima, S., Nisisako, T., Torii, T., Higuchi, T. *Langmuir* **2004**, *20*, 9905-9908.
- (18) Abate, A. R., Weitz, D. A. *Small* **2009**, *5*, 2030-2032.
- (19) Anna, S. L., Bontoux N., Stone, H. A. *Appl. Phys. Lett.* **2003**, *82*, 364-366.
- (20) Gañán-Calvo, A. M., Gordillo, J. M. *Phys. Rev. Lett.* **2001**, *87*, 274501-1-274501-4.

- (21) Utada, A. S., Chu, L.-Y., Fernandez-Nieves, A., Link, D. R., Holtze, C., Weitz, D. A. *MRS Bull.* **2007**, *32*, 702-708.
- (22) Baroud, C. N., Willaime, H. *C. R. Phys.* **2004**, *5*, 547-555.
- (23) Utada, A. S., Fernandez-Nieves, A., Stone, H. A., Weitz, D. A. *Phys. Rev. Lett.* **2007**, *99*, 094502-1–094502-4.
- (24) Nisisako, T., Okushima, S., Torii, T. *Soft Matter* **2005**, *1*, 23-27.
- (25) Pannacci, N., Bruus, H., Bartolo, D., Etchart, I., Lockhart, T., Hennequin, Y., Willaime, H., Tabeling, P. *Phys. Rev. Lett.* **2008**, *101*, 164502–1-164502–4.
- (26) Barbier, V., Tatoulian, M., Li, H., Arefi-Khonsari, F., Ajdari A., Tabeling, P. *Langmuir* **2006**, *22*, 5230-5232.
- (27) Abate, A. R., Thiele, J., Weinhart M., Weitz, D. A. *Lab Chip* **2010**, *10*, 1774-1776.
- (28) Hong Y., Wang, F. *Microfluid. Nanofluid.* **2007**, *3*, 341-346.
- (29) Cramer, C., Fischer, P., Windhab, E. J. *Chem. Eng. Sci.* **2004**, *59*, 3045-3058.
- (30) Utada, A. S., Fernandez-Nieves, A., Gordillo, J. M., Weitz, D. A. *Phys. Rev. Lett.* **2008**, *100*, 014502-1-014502-4.
- (31) Arratia, P. E., Gollub, J. P., Durian, D. J. *Phys. Rev. E: Stat., Nonlinear, Soft Matter Phys.* **2008**, *77*, 036309–1-036309–6.
- (32) Ferry, J. D. *Viscoelastic Properties of Polymers*, Wiley, 3rd edn, **1980**.
- (33) Strutt, J. W., Rayleigh, L. *Philos. Mag. (1798–1977)* **1892**, *34*, 177-180.
- (34) Eggers, J., Villermaux, E. *Rep. Prog. Phys.* **2008**, *71*, 036601–1-036601–79.

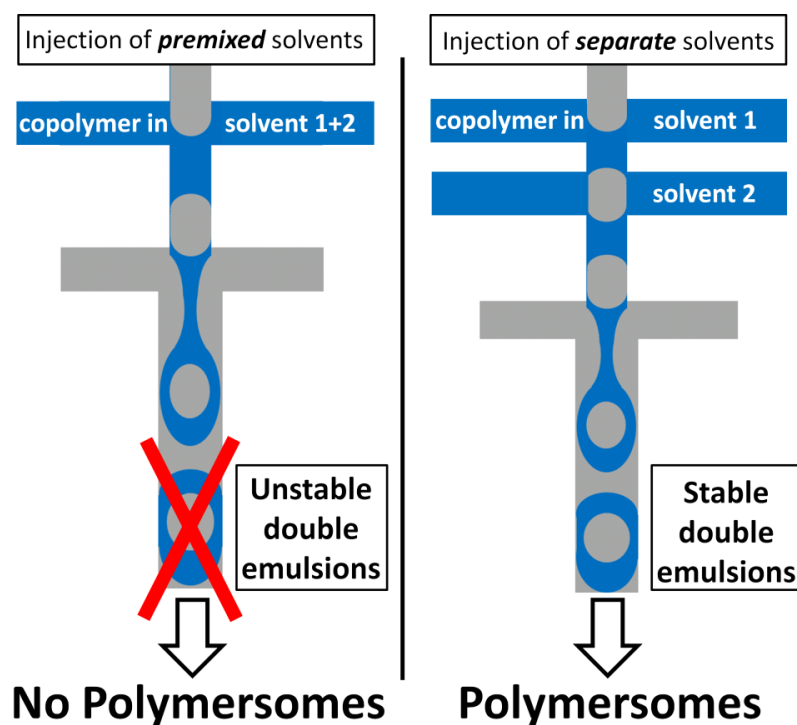
## Fabrication of Polymersomes using Double-Emulsion Templates in Glass-Coated Stamped Microfluidic Devices

Julian Thiele,<sup>a,b</sup> Adam R. Abate,<sup>a</sup> Ho Cheung Shum,<sup>a</sup> Simone Bachtler,<sup>a,c</sup> Stephan Förster,<sup>b</sup> David A. Weitz\*<sup>a</sup>

<sup>a</sup>School of Engineering and Applied Sciences/Department of Physics, Harvard University, Cambridge, MA 02138, USA

<sup>b</sup>Institute of Physical Chemistry, University of Hamburg, D-20146 Hamburg, Germany

<sup>c</sup>Hochschule Mannheim, University of Applied Sciences, D-68163 Mannheim, Germany



Published in *Small* **2010**, *6*(16), 1723-1727.

## Abstract

We present a versatile technique for fabricating polymersomes in glass-coated stamped microfluidic devices. We use templates comprised of double emulsions with a shell of block copolymers dissolved in organic solvents. The double emulsions direct the assembly of amphiphilic diblock copolymers into polymersomes during evaporation of the organic solvents. Our device consists of a single cross junction to make the core phase and two additional cross junctions to make the shell phase; this geometry allows us to inject two separate organic solvents to form the shell phase, greatly facilitating the formation of the polymersomes; by tuning their ratio of these two solvents, we control the rate at which the solvent mixture is evaporated. Moreover, this geometry also prevents fouling of the microfluidic device due to adsorption on the microchannel walls of poorly dissolved copolymers, allowing polymersomes to form.

## Introduction

Polymersomes are vesicular self-assemblies of amphiphilic diblock copolymers;<sup>1</sup> they consist of a spherical compartment enclosed by a macromolecular bilayer and have great potential as encapsulation and release systems.<sup>2-4</sup> They offer enhanced mechanical and structural stability as compared to vesicles made from phospholipids or detergents. By tailoring block lengths, block chemistry and functionalization of the copolymers, polymersomes with controlled biological, chemical, and physical properties can be formed.<sup>5,6</sup> Typically, polymersomes are formed by techniques such as film rehydration, electroformation, phase transfer, and ultrasonication. These techniques rely on the undirected self-assembly of the copolymers, and typically lead to polymersomes with broad size distributions and low encapsulation efficiency.<sup>7-9</sup> A promising alternative is the directed formation of polymersomes using copolymer-stabilized water/organic solvent/water (W/O/W) double emulsions in microfluidic devices.<sup>10,11</sup> The assembly of the copolymers is directed by the double-emulsion droplets during evaporation of the organic solvent in which the copolymer is dissolved. A crucial aspect of this technique is the choice of the organic solvent; it must be highly volatile and the diblock copolymer must be highly soluble within it. Moreover, the use of mixed solvents provides additional control over the interaction between the block copolymers in the bilayer.<sup>12</sup> However,

many organic solvents either evaporate too quickly causing the copolymers to form precipitates that eventually clog the microfluidic device, or the organic solvent takes too long to be completely evaporated. These problems can be addressed by using mixtures of organic solvents for dissolving the copolymers.

Organic solvents are typically premixed before injection into microfluidic devices for forming the double emulsion templates.<sup>10</sup> As the concentration of the copolymers and the composition of the premixed solvents cannot be tuned inside the device, any copolymer precipitates cannot be easily removed without disruption of the emulsion generation. Thus, the ability to inject additional solvents during the operation of the device would enable in-situ removal of precipitates and eliminate the problem of fouling. Therefore, a microfluidic design that combines the ability to form double emulsions with the ability to inject and mix two organic solvents is desirable. This goal is difficult to achieve using glass capillary microfluidic devices, as the channel design is not easily customized. These limitations can be overcome using lithographic fabrication techniques to produce more sophisticated microfluidic devices. A convenient fabrication technique is soft lithography using poly(dimethylsiloxane) (PDMS), which can be used to fabricate rather sophisticated devices;<sup>13,14</sup> unfortunately however, PDMS has a low chemical resistance, and swells when it comes in contact with most organic solvents.<sup>15</sup> The resistance of PDMS towards organic solvents can be significantly increased by depositing a glasslike coating using sol-gel chemistry.<sup>16</sup> While this approach has been successfully applied to generate single emulsion drops of organic solvents, its application to sophisticated devices for the fabrication of complex structures such as double emulsions has not been demonstrated. An optimal system for fabricating double emulsion-templated polymersomes would combine the versatility of stamped microfluidic devices with resistance against organic solvents.

In this paper, we report the formation of double-emulsion-templated polymersomes in stamped microfluidic devices. We coat the devices with a sol-gel to produce a durable glasslike layer with tailored surface properties; the coating is evenly distributed throughout the microfluidic device. This increases the resistance of the channel walls against organic solvents, thus enabling the use of organic solvents for dissolving the diblock copolymers. The device geometry allows us to inject two separate streams of organic solvents to form the shell of the double emulsion, and to control the rate at which



the solvents are injected. By tuning the ratio of the two organic solvents with different volatilities, the rate at which the solvent mixture is evaporated can be manipulated. The separate injection of the two organic solvents prevents the adsorption of poorly dissolved copolymers on the microchannel walls. Therefore, unlike conventional microfluidic devices using single injection of premixed solvents that fail due to clogging within seconds of operation, our device enables continuous generation of copolymer-stabilized double emulsion with a shell of organic solvents.

### Results and Discussion

In PDMS devices, double emulsions can be formed using a variety of channel geometries including T-junctions and flow focusing junctions.<sup>17-19</sup> In this work, we use a flow-focusing cross-junction geometry. Typically double emulsions are produced in an array of two cross junctions with different wettability. Drops formed in the first junction enter the second junction where they are encapsulated to create double emulsions.<sup>20,21</sup> However, this device geometry does not allow manipulation of the composition of the shell phase of double emulsions, which is important because mixtures of solvents are often used for dissolving block copolymers in fabricating polymersomes.<sup>10</sup> We therefore introduce a second cross junction for injecting an additional solvent in our device, as illustrated schematically in Figure 1.

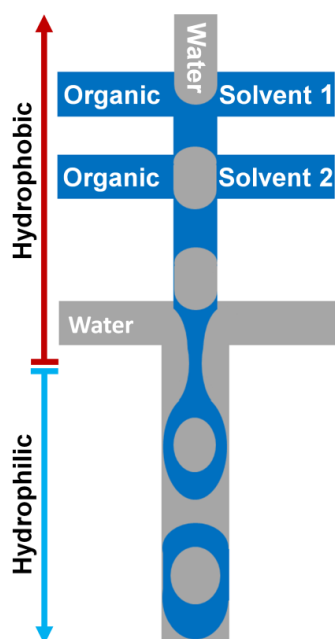


Figure 1: Schematic of a sol-gel-coated microfluidic device for forming double emulsions with a shell phase of organic solvents. The sol-gel coating in the upper half of the device is untreated and remains hydrophobic, while the coating in the lower part is rendered hydrophilic due to functionalization by grafted poly(acrylic acid). The device design enables separate injection and mixing of two organic solvents that form the shell of W/O/W double emulsions.

For the formation of copolymer-stabilized double emulsions, we dissolve a diblock polymer in the organic solvent stream injected at the first junction, and inject another organic solvent at the second cross junction, which is miscible with the copolymer-loaded solvent. The device geometry enables the two organic solvents to be injected in separate channels; moreover, it also allows us to control the flow rate of each solvent independently and tune the ratio of the two solvents in which the diblock copolymers are dissolved. To produce double emulsions with a shell of organic solvents, the PDMS devices must resist degradation and swelling due to the organic solvents. We achieve this by coating the PDMS devices using sol-gel chemistry to create a glasslike layer which is both durable and homogeneously distributed even on the rather complex devices, as shown in the scanning electron micrographs of the coated microchannels.<sup>22</sup> A second advantage of the glass coating is the ability to spatially control the wettability of the surface.<sup>23,24</sup> We achieve this by functionalizing the intrinsically hydrophobic sol-gel with photoreactive silanes. The surface can then be made hydrophilic with high spatial control through the use of a photochemical surface treatment.<sup>25,26</sup> In this fashion, we make the first and

second cross junctions hydrophobic while the third junction is made hydrophilic; this allows water drops to be dispersed in a continuous phase of organic solvents at the first and second junctions, while the continuous water phase required for the double emulsion is injected at the third, hydrophilic junction.

We demonstrate the concept to form poly(ethylene-glycol)-*b*-poly(lactid acid), PEG<sub>5000</sub>-*b*-PLA<sub>5000</sub>,<sup>27,28</sup> polymer vesicles. To form the double-emulsion templates, the diblock copolymer is first dissolved in an organic solvent, chloroform. However, the high density of chloroform causes the double emulsions to sediment, and subsequently wet the bottom of the collection vial, destabilizing the double emulsions. Thus, to lower the density of the organic phase, we add toluene to the copolymer-containing chloroform as a second organic solvent.<sup>10</sup> For the formation of stable polymer vesicles, the osmolarities of the inner and outer phases of the double-emulsion template must be balanced. Otherwise, the size of the polymersomes will change significantly during solvent evaporation due to osmotically driven diffusion of water. We balance the osmolarity by adding glucose to the inner phase and a polyvinyl alcohol (PVA) to the outer phase of our double emulsion.

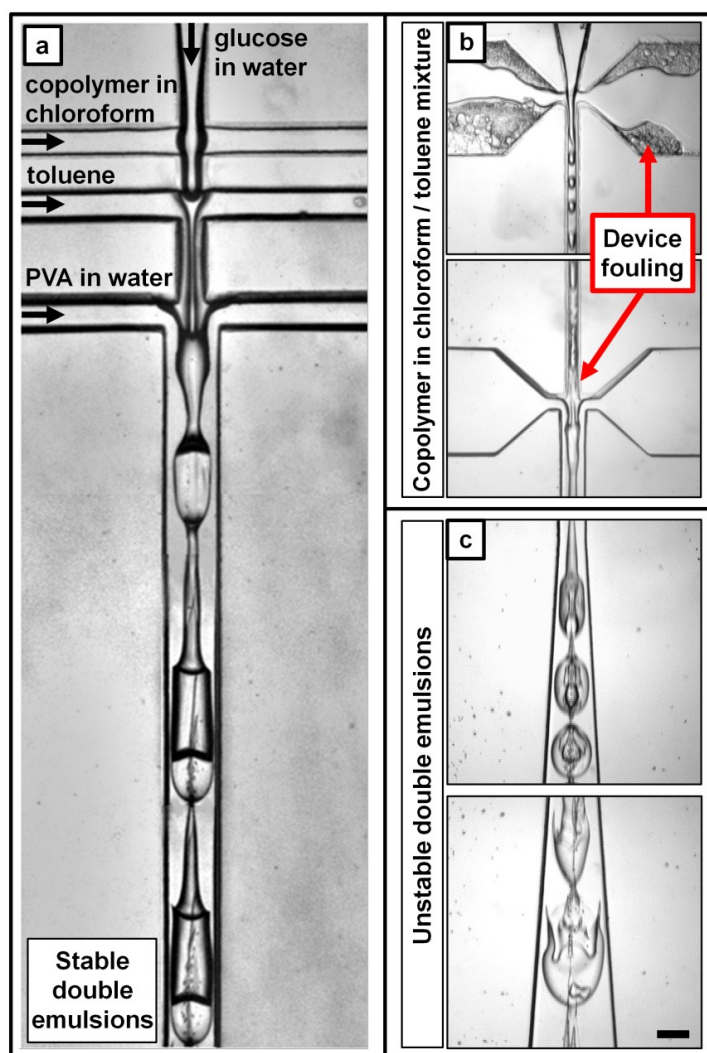


Figure 2: a) Microfluidic device forming diblock copolymer-stabilized W/O/W double emulsions. The channel width of the first and second dropmaker is 100 and 160  $\mu\text{m}$ , respectively; the channel height is 100  $\mu\text{m}$ . To maintain the stability of the polymersomes during the fabrication process, we balance the osmolarity of the inner and outer phase of the double emulsion by adding glucose to the inner phase and polyvinyl alcohol (PVA) to the outer phase. The non-Newtonian nature of the PVA solution causes the middle phase to develop a tail, which initially connects the double emulsions. However, the jet breaks up into double emulsion droplets approximately 1mm downstream in the outlet channel. b,c) Formation of diblock polymer-stabilized W/O/W double emulsions from premixed mixtures of chloroform and toluene in a conventional microfluidic device using two cross junctions. b) The diblock polymer forms precipitates after the more volatile chloroform starts to evaporate in the microfluidic device. The resultant precipitates adhere to the surface of the channels, leading to a thick layer of copolymers. c) Most of the copolymer precipitates before reaching the second junction to form double emulsions. Some of the precipitates are observed in the shell phase of the double-emulsion drops formed. Since the organic solvent phase is depleted of the block copolymers before the second junction, the two interfaces of the shell of the double emulsions formed are not sufficiently stabilized. Thus the double-emulsion drops burst downstream. Scale bar for all panels denotes 100  $\mu\text{m}$ .

The three phases are fed into the device shown in Figure 2a. Droplets of the innermost phase are emulsified by the copolymer-containing chloroform at the first droplet making junction. Toluene is added at the second droplet making junction. Finally, PVA solution is used for emulsifying the organic solvent phase that contains aqueous inner drops. However, due to the shear-thinning nature of the PVA solution,<sup>29</sup> its viscosity drops significantly when the middle jet with inner droplets flows through the third cross junction, where the PVA solution is squeezed between the middle jet and the channel wall. Instead of breaking up into double-emulsion droplets, the compound jet of middle phase with inner drops develops tails, initially connecting the inner drops along the jet, as shown in Figure 2a. However, the jet eventually breaks up into droplets downstream, forming the desired double-emulsion drops.

Although the sol-gel coating provides a rigid network which prevents swelling of the PDMS microfluidic device, sol-gel coatings often consist of a nanoporous structure that allows chloroform and toluene to penetrate the sol-gel barrier into the PDMS.<sup>30</sup> Due to a higher swelling ratio in PDMS, chloroform evaporates faster, resulting in a lower chloroform fraction in the solvent mixture. As the solubility of PEG-*b*-PLA in toluene is significantly lower than in chloroform, the diblock copolymer forms precipitates after the more volatile chloroform starts to evaporate in the microfluidic device. The precipitated copolymers adsorb onto the microchannels and foul the device if the composition of the solvent mixture cannot be maintained; this leads to a buildup of a thick layer of copolymers on the channel walls, as shown in Figure 2b. In this case the hydrophobic PLA-block adheres to the hydrophobic walls, leaving the hydrophilic PEG-block facing the flow within the channels. This results in an inversion of the wettability pattern of the channels and causes the water within the drops to wet the hydrophilic surface. Thus, the drops occasionally merge with other drops,<sup>31</sup> making the drop size ill-controlled, as shown in Figure 2b. As most of the copolymer in the organic solvent mixture precipitates before emulsification, only a small amount of the precipitates stay dissolved in the organic solvent phase, resulting in destabilization of the double-emulsion drops, as shown in Figure 2c. As the double emulsions are not sufficiently stabilized by copolymer molecules, they eventually burst as they flow downstream. With our new device geometry, we separately inject chloroform with PEG-*b*-PLA in the first cross junction and toluene in the second cross junction. Therefore, we can manipulate the composition of the solvent mixture by changing the flow rates of the two organic solvents; thus the loss of

chloroform due to evaporation into the PDMS can be compensated for. However, if sufficient diffusive mixing is allowed, precipitation of the copolymer can still take place at the chloroform/toluene interface.<sup>32</sup> We overcome this by using elevated flow rates, and by shortening the microchannel between the second nozzle, where toluene is injected, and the third cross junction, where the double emulsion is formed. This prevents the copolymer concentration at the chloroform/toluene interface to decrease below its solubility limit. In our experiments, we find flow rates of 1000 mL h<sup>-1</sup> for toluene and 500 mL h<sup>-1</sup> for chloroform to be optimal; this corresponds to a volumetric ratio of 2:1. Thereby we prevent precipitation of copolymers which otherwise causes failing of the microfluidic device within seconds after injection of copolymer-containing solvents. However, if the volumetric ratio of toluene to chloroform is higher, precipitation of copolymer in the microchannel between the second and third cross junction is observed. After double emulsions are formed at the third cross junction, local mixing in the drops leads to a homogeneous distribution of the copolymer in the shell of the double emulsion. Due to its surface activity, PEG-*b*-PLA adsorbs at the two interfaces of the shell and stabilizes the droplets. The stability can be further increased by adding a homo polymer, PLA<sub>5000</sub>, to the chloroform in the shell.

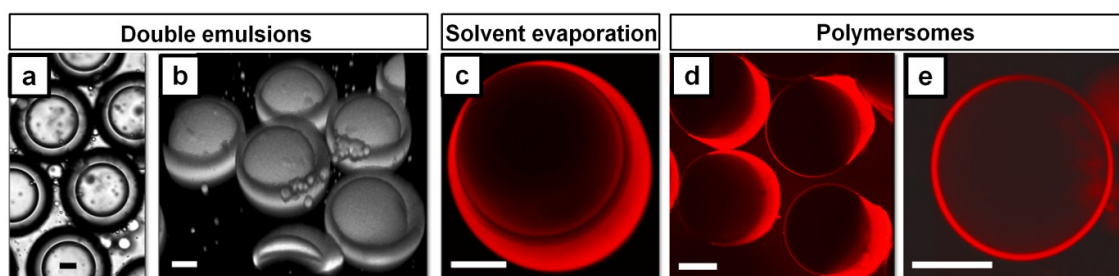


Figure 3: Formation of polymersomes from copolymer-stabilized W/O/W double emulsions. a) Bright-field microscope image and b) 3D reconstruction of stacks of confocal microscopy images. The double emulsion consists of aqueous drops wrapped in a shell of 120 mg mL<sup>-1</sup> PEG<sub>5000</sub>-*b*-PLA<sub>5000</sub> and 40 mg mL<sup>-1</sup> PLA<sub>5000</sub> dissolved in chloroform and toluene in a ratio of 1:2 by volume. The organic phase is labeled with Nile Red. c) The organic solvent from the shell starts to evaporate, leading to dewetting of the shell phase from the inner droplet. After evaporation of the organic solvents, aggregates of excess polymer either d) remain attached to the polymersomes, or e) occasionally detach from the polymersomes. Scale bars are 20  $\mu$ m.

During solvent evaporation, the PEG-*b*-PLA-stabilized double emulsions undergo a dewetting transition as the polymersomes are formed. The organic solvent mixture initially wets the entire inner drop and is homogeneously distributed on its surface, as shown in Figure 3a,b; it then dewets from the inner phase, as indicated in Figure 3c. The dewetting is driven by evaporation of the volatile organic solvents as well as by the relative high surface energy between the inner and outer phase.<sup>33</sup> The result is a state of partial wetting where the double emulsions adopt an acorn-like, asymmetric structure. However, if the volumetric ratio of toluene and chloroform in the initial double emulsions is between 1:1 and 2:1, stable double emulsions are formed, but the drops do not undergo dewetting. If the shell of the double emulsions contains an excess of chloroform, the double emulsions are destabilized due to the density mismatch of the inner drop and surrounding shell. With the optimized volumetric ratio of toluene and chloroform, the diblock copolymer molecules at the two interfaces of the shell self-assemble into a membrane, enclosing the inner phase. Upon dewetting, the bulb of the acorn-like dewetted drop which contains the excess diblock copolymer and homo polymer, remains on the surface of the polymersome. After evaporation of the organic solvents, a polymeric aggregate of these polymers remains attached to the surface of the polymersomes, as shown in Figure 3d. Occasionally, the aggregate detaches from the polymersome, as shown in Figure 3e. Since the volume of the inner drop remains unchanged during the dewetting transition, the polymersome size is only determined by the droplet size of the most inner fluid of the double-emulsion template, which can be controlled by tuning the dimension of the nozzle and the flow rate ratio of inner and middle phase.<sup>19,34</sup> With our microfluidic device we are able to form double-emulsion templates of approximately 100-150  $\mu\text{m}$  in diameter, corresponding with a polymersome diameter of approximately 50-100  $\mu\text{m}$ . However, the principles of polymersome formation should be applicable down to the smallest scale as limited by the feature size of the microfluidic device.

## Conclusions

Our new geometry in stamped microfluidic devices allows us to form polymersomes from copolymer-stabilized W/O/W double emulsions. In contrast to the limited flexibility using two cross junctions for fabricating double emulsions, our modified microfluidic device enables independent injection and mixing of two organic solvents, which form the

double-emulsion shell. This is useful for maintaining the ratios of the solvents specific to the diblock copolymers used, and prevents fouling of the channel walls which would cause instantaneous failure of the device. The control over the solvent mixture is important for ensuring continuous operation of the device, and for applying the double-emulsion approach for polymersomes to a wider range of polymers. As the solvent streams do not mix before emulsification, our modified device also enables the preparation of other core-shell structures from rapidly reacting solvent streams. Our approach should also be useful for forming Janus-like particles with freely tunable composition by using two curable monomer streams which can be solidified during emulsification. In addition, the ease of fabrication of stamped PDMS microfluidic devices should facilitate fabrication of highly parallelized devices for larger-scale production of polymersomes.

## Experimental Section

### Preparation of devices

The PDMS microfluidic devices are fabricated using soft lithography.<sup>13</sup> All channels have a fixed height of 100  $\mu\text{m}$ . The PDMS replica is bonded to a glass slide after oxygen plasma treatment. We then coat the PDMS device with a photoreactive sol-gel.<sup>26</sup> The sol-gel is intrinsically hydrophobic, but can be made hydrophilic using photolithographic techniques, though other surface treatments are possible.<sup>35</sup> We graft patches of hydrophilic poly(acrylic acid) onto the sol-gel using spatially patterned UV light in specific areas. All other parts of the device remain hydrophobic due to the default properties of the sol-gel coating. To form double emulsions with a shell of organic solvents, we pattern the first and second cross junction to remain hydrophobic and the third cross junction to be hydrophilic.

### Preparation of double-emulsion templates

All chemicals are obtained from Sigma-Aldrich Co. unless noted otherwise. PEG<sub>5000</sub>-*b*-PLA<sub>5000</sub> and PLA<sub>5000</sub> are obtained from Polysciences Inc. Water with a resistivity of



16.8 M $\Omega$  cm<sup>-1</sup> is prepared using a Millipore Milli-Q system. The osmolarities of the inner and continuous phase of the copolymer-stabilized double emulsions are measured with a micro osmometer (Advanced Instruments, Inc., Model 3300). The osmolarities are approximately 104 and 114 mOsm, respectively. We form copolymer-stabilized double emulsions in our modified PDMS microfluidic device by injecting an aqueous solution of glucose (100 mM) as the inner phase, chloroform with 120 mg mL<sup>-1</sup> diblock copolymer and 40 mg mL<sup>-1</sup> homopolymer as the first shell phase, toluene as the second shell phase and an aqueous solution of a polyvinyl alcohol (weight-averaged molecular weight,  $M_W$  13000-23000 g mol<sup>-1</sup>, 87–89 % hydrolyzed) at 3 % w/w as the continuous phase. A typical set of flow rates of the inner, first shell, second shell, and outer phases is 300, 1000, 500, and 3500 mL h<sup>-1</sup>, respectively.

### Formation of polymersomes

The copolymer-stabilized double emulsions are collected in a glass vial. We place single samples between a microscopy slide and a cover slip, separated by a silicone isolator, 0.5 mm in thickness. This reduces the rate at which the organic solvents evaporate and allows us to monitor the polymersome formation using optical microscopy. If the double emulsions are left in air, the organic solvents evaporate too quickly destabilizing the double emulsions.

### Keywords

double emulsions · glass-coatings · PDMS microfluidics · polymersomes

### References

- (1) Antonietti, M., Förster, S. *Adv. Mater.* **2003**, *15*, 1323-1333.
- (2) Discher, D. E., Ortiz, V., Srinivas, G., Klein, M. L., Kim, Y., David, C. A., Cai, S. S., Photos, P., Ahmed, F. *Prog. Polym. Sci.* **2007**, *32*, 838-857.
- (3) Li, S., Byrne, B., Welsh, J., Palmer, A. F. *Biotechnol. Prog.* **2007**, *23*, 278-285.

- (4) Reisch, M. *Chem. Eng. News* **2007**, *85*, 15-21.
- (5) Gan, Z., Jim, T., Li, M., Yuer, Z., Wang, S., Wu, C. *Macromolecules* **1999**, *32*, 590-594.
- (6) Meier, M., Aerts, S., Staal, B., Rasa, M., Schubert, U. S. *Macromol. Rapid. Commun.* **2005**, *26*, 1918-1924.
- (7) Discher, D. E., Eisenberg, A. *Science* **2002**, *297*, 967-973.
- (8) Discher, B. M., Won, Y. Y., Ege, D. S., Lee, J. C. M., Bates, F. S., Discher, D. E., Hammer, D. A. *Science* **1999**, *284*, 1143-1146.
- (9) Kita-Tokarczyk, K., Grumelard, J., Haefele, T., Meier, W. *Polymer* **2005**, *46*, 3540-3563.
- (10) Shum, H. C., Kim, J.-W., Weitz, D. A. *J. Am. Chem. Soc.* **2008**, *130*, 9543-9549.
- (11) Lorenceau, E., Utada, A. S., Link, D. R., Cristobal, G., Joanicot, M., Weitz, D. A. *Langmuir* **2005**, *21*, 9183-9186.
- (12) Shum, H. C., Bibette, J., Weitz, D. A. private communication.
- (13) Xia, Y., Whitesides, G. M. *Angew. Chem. Int. Ed.* **1998**, *37*, 550-575.
- (14) Duffy, D., McDonald, J., Schueller, O., Whitesides, G. M. *Anal. Chem.* **1998**, *70*, 4974-4984.
- (15) Lee, J. N., Park, C., Whitesides, G. M. *Anal. Chem.* **2003**, *75*, 6544-6554.
- (16) Abate, A. R., Lee, D., Do, T., Holtze, C., Weitz, D. A. *Lab Chip* **2008**, *8*, 516-518.
- (17) Okushima, S., Nisisako, T., Torii, T., Higuchi, T. *Langmuir* **2004**, *20*, 9905-9908.
- (18) Lao, K.-L., Wang, J.-H., Lee, G.-B. *Microfluid. Nanofluid.* **2009**, *7*, 709-719.
- (19) Abate, A. R., Poitzsch, A., Hwang, Y., Lee, J., Czerwinska, J., Weitz, D. A. *Phys. Rev. E* **2009**, *80*, 026310–1-026310–5.
- (20) Nisisako, T. *Chem. Eng. Technol.* **2008**, *31*, 1091-1098.
- (21) Abate, A. R., Weitz, D. A. *Small* **2009**, *5*, 2030-2032.
- (22) See supporting information.
- (23) Nisisako, T., Okushima, S., Torii, T. *Soft Matter* **2005**, *1*, 23-27.
- (24) Pannacci, N., Bruus, H., Bartolo, D., Etchart, I., Lockhart, T., Hennequin, Y., Willaime, H., Tabeling, P. *Phys. Rev. Lett.* **2008**, *101*, 164502–1-164502–4.
- (25) Seo, M., Paquet, C., Nie, Z. H., Xu, S. Q., Kumacheva, E. *Soft Matter* **2007**, *3*, 986-992.
- (26) Abate, A. R., Krummel, A. T., Lee, D., Marquez, M., Holtze, C., Weitz, D. A. *Lab Chip* **2008**, *8*, 2157-2160.
- (27) Elvassore, N., Bertucco, A., Caliceti, P. *J. Pharma. Sci.* **2001**, *90*, 1628-1636.

- (28) Ahmed, F., Pakunlu, R. I., Brannan, A., Bates, F. S., Minko, T., Discher, D. E. *J. Controlled Release* **2006**, *116*(2), 150-158.
- (29) Lazareva, T. G., Shinkareva, E. V. *Russ. J. Appl. Chem.* **2002**, *75*, 1722-1725.
- (30) Wu, G., Wang, J., Shen, J., Yang, T., Zhang, Q., Zhou, B., Deng, Z., Fan, B., Zhou, D., Zhang, F. *Mater. Res. Bull.* **2001**, *36*, 2127-2139.
- (31) Fidalgo, L. M., Abell, C., Huck, W. T. S. *Lab Chip* **2007**, *7*, 984-986.
- (32) Thiele, J., Steinhauser, D., Pfohl, T., Förster, S. *Langmuir* **2010**, *26*, 6860-6863.
- (33) Hayward, R. C., Utada, A. S., Dan, N., Weitz, D. A. *Langmuir* **2006**, *22*, 4457-4461.
- (34) Ward, T., Faivre, M., Abkarian, M., Stone, H. A. *Electrophoresis* **2005**, *26*, 3716-3724.
- (35) Abate, A. R., Thiele, J., Weinhart, M., Weitz, D. A. *Lab Chip* **2010**, *10*, 1774-1776.

## Supplemental information

This supplemental information contains the characterization of our sol–gel coated PDMS devices using scanning electron microscopy (SEM). In addition, we provide experimental details to demonstrate the resistance of our devices against organic solvents.

We coat our PDMS devices with a glass-like coating using sol–gel chemistry.<sup>1-2</sup> To illustrate the distribution and thickness of the coating, we image the coated microchannels using scanning electron microscopy (SEM) at three positions of the device indicated by the red lines in Fig. 1a, bottom left; the corresponding SEM images are shown in Fig. 1b. The micrographs show a homogenous distribution of the sol–gel coating throughout the device. We estimate the coating thickness to be 2-5  $\mu\text{m}$ . To demonstrate that our coated PDMS devices resist degradation due to organic solvents, we compare the swelling of a native PDMS device with a sol–gel coated PDMS device by flowing chloroform, which typically swells PDMS devices, into the channels.<sup>3</sup> We monitor the channels with optical microscopy as chloroform is injected into the microchannels. After 20 s, the microchannel width has decreased by an average of 40 % in the uncoated PDMS device, as shown in Fig. 1a, top right. In contrast, the sol–gel coated microchannels maintain the same channel width, as shown in Fig. 1a, bottom right. We observe similar trends for other

solvents including acetone, toluene and hexane. Thus sol–gel coatings can not only be used to coat PDMS microfluidic devices for forming single emulsion drops of organic solvents, but they can also be applied to complex microchannel structures such as those for forming double emulsions.

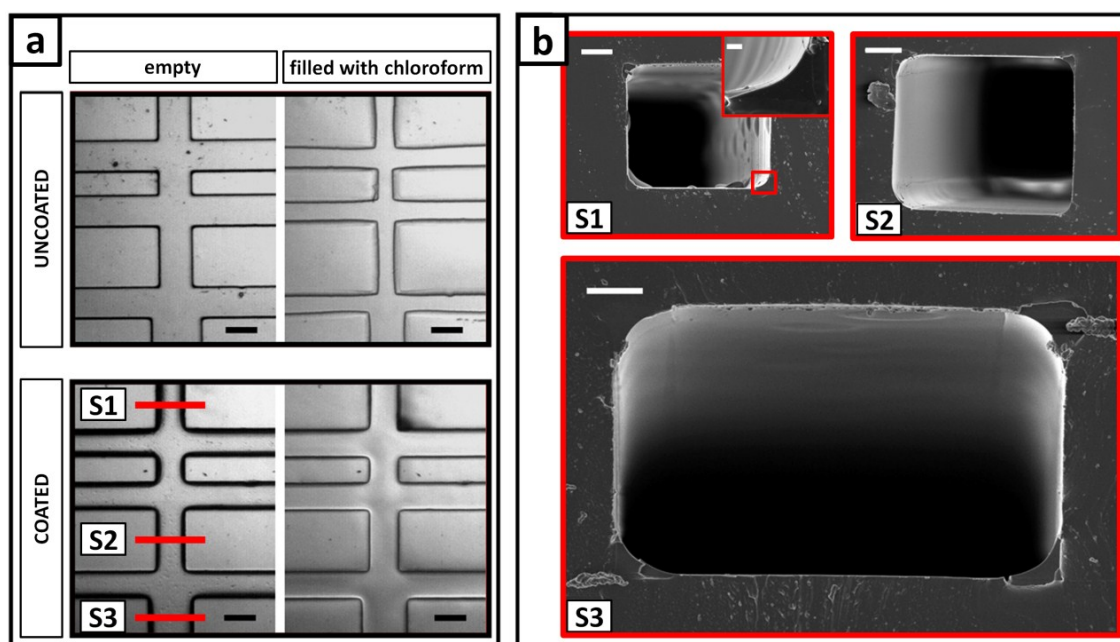


Figure 1: Swelling of uncoated and sol-gel coated microchannels in a PDMS microfluidic device filled with chloroform. The device geometry is designed to enable formation of double emulsions with a shell of organic solvents. While the coated microchannels are stable, uncoated channels swell quickly; scale bars are 100  $\mu\text{m}$ . (b) SEM images of channel cross sections (S1 to S3) showing a homogenous distribution of the coating on the microchannel walls throughout the device. Scale bars denote 20  $\mu\text{m}$ ; scale bar for the insert of S1 is 1  $\mu\text{m}$ .

## References

- (1) Abate, A. R., Lee, D., Do, T., Holtze, C., Weitz, D. A. *Lab Chip* **2008**, *8*, 516-518.
- (2) Abate, A. R., Krummel, A. T., Lee, D., Marquez, M., Holtze, C., Weitz, D. A. *Lab Chip* **2008**, *8*, 2157-2160.
- (3) Lee, J. N., Park, C., Whitesides, G. M. *Anal. Chem.* **2003**, *75*, 6544-6554.

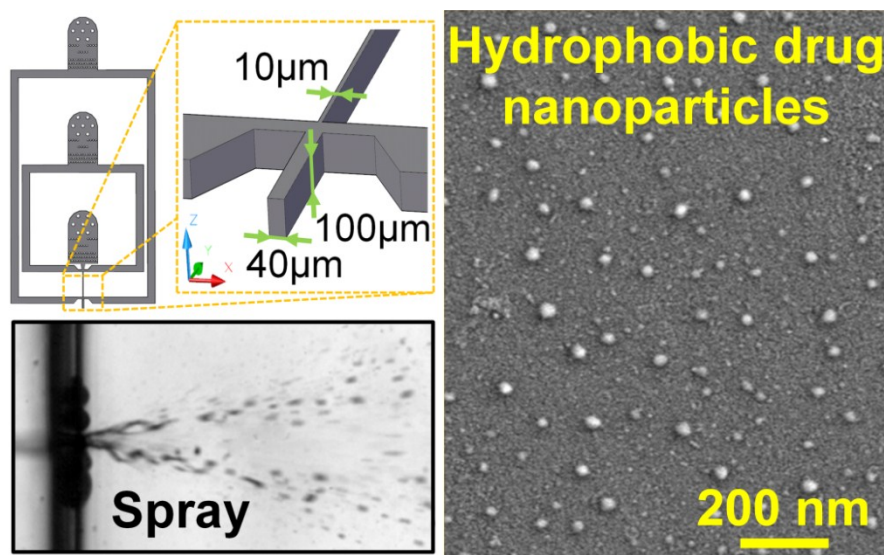
## Early development drug formulation on a chip: Fabrication of nanoparticles using a microfluidic spray dryer

Julian Thiele,<sup>a,b</sup> Maike Windbergs,<sup>a,c</sup> Adam R. Abate,<sup>a</sup> Martin Trebbin,<sup>b</sup> Ho Cheung Shum,<sup>a,c</sup> Stephan Förster,<sup>b</sup> David A. Weitz\*<sup>a</sup>

<sup>a</sup> School of Engineering and Applied Sciences/Department of Physics, Harvard University, Cambridge, MA 02138, USA

<sup>b</sup> Physical Chemistry I, University of Bayreuth, D-95447 Bayreuth, Germany

<sup>c</sup> Department of Mechanical Engineering, University of Hong Kong, Hong Kong



Published in *Lab on a Chip* **2011**, *11*, 2362-2368.

### **Abstract**

Early development drug formulation is exacerbated by increasingly poor bioavailability of potential candidates. Prevention of attrition due to formulation problems necessitates physicochemical analysis and formulation studies at a very early stage during development, where the availability of a new substance is limited to small quantities, thus impeding extensive experiments. Miniaturization of common formulation processes is a strategy to overcome those limitations. We present a versatile technique for fabricating drug nanoformulations using a microfluidic spray dryer. Nanoparticles are formed by evaporative precipitation of the drug-loaded spray in air at room temperature. Using danazol as a model drug, amorphous nanoparticles of 20-60 nm in diameter are prepared with a narrow size distribution. We design the device with a geometry that allows the injection of two separate solvent streams, thus enabling co-spray drying of two substances for the production of drug co-precipitates with tailor-made composition for optimization of therapeutic efficiency.

### **Introduction**

The development of novel pharmaceuticals is a challenging field involving cost-intensive research in combination with a high attrition rate of potential candidates.<sup>1,2</sup> Due to high-throughput technologies an increasing number of new chemical entities with potential therapeutic efficiency is identified.<sup>3,4</sup> Unfortunately, the molecular complexity of drugs has significantly increased over the last decade.<sup>5-7</sup> Although molecular complexity usually contributes to biological activity, it often causes poor solubility of drugs.<sup>6,8</sup> This limits their bioavailability in the human body, and the reason for attrition of pharmacologically promising substances can often be found in the failure to develop a suitable formulation for therapeutic application.<sup>9</sup> Prevention of failure due to formulation necessitates physicochemical analysis and formulation studies at a very early stage during development.<sup>10,11</sup> At this stage, the availability of the drug candidate is limited to small amounts, thus hampering extensive experiments.

One suitable approach to increase the bioavailability of a drug is to reduce the particle size, which increases the specific surface and, therefore, facilitates release and absorption

of the drug.<sup>12-15</sup> Furthermore, increased bioavailability can be achieved by amorphization of the sample. In this context, spray drying is a powerful technique enabling instantaneous drying of solutions, emulsions or suspensions in one step. The final product is a fine, often amorphous powder with a large surface. Pharmaceutical application of spray drying techniques are ubiquitous; their use ranges from the manufacture of dry plant extracts for avoiding decomposition of thermally degradable components, to the production of excipients for compression with improved binding characteristics.<sup>16-18</sup> Furthermore, the technique is successfully used for co-precipitation of a drug and another substance to increase the drug's bioavailability.<sup>19</sup> However unfortunately, in case of early stage formulation development the use of conventional spray drying setups is restricted. Conventional spray drying equipment requires large amounts of sample as the dead volume of the apparatus is rather large and a considerable portion of discard material is generated during the process. Furthermore, the optimization of processing parameters necessitates additional quantities of sample to receive a homogeneous product. Moreover, particle sizes below 100 nm, as often required for targeted drug delivery, are extremely hard to generate.<sup>20,21</sup> An appropriate application for spray drying in early development would require the miniaturization of the setup. These limitations can be overcome using microfluidic techniques.<sup>22-26</sup> Extremely small volumes can precisely be handled on microfluidic chips enabling the controlled generation of homogeneous product as well as a fast change of process conditions. It would be highly desirable to design a microfluidic chip which combines the versatility of microfluidics with the ability to process homogeneous spray dried particles with high accuracy.

In this paper, we present the first microfluidic spray dryer on a poly(dimethylsiloxane) (PDMS) chip.<sup>27-29</sup> We use the hydrophobic model drug danazol to test the new device. By controlling the collection distance of the spray, we can control the crystallinity of the product. Our microfluidic device enables fabrication of drug nanoparticles with sizes of less than 100 nm in diameter. The versatile device design also enables the formation of amorphous co-precipitates by co-spray drying two substances.

## Results and Discussion

In conventional spray dryers, a single liquid stream is typically vaporized by compressed air in a spray nozzle; the spray is then mixed with a heated gas stream in a drying chamber to evaporate the solvent and yield the dry product.<sup>21</sup> However, this setup only allows processing of single solvent systems or mixtures of premixed solvents. To process multiple separate solvent streams as required for solvent/antisolvent precipitation or rapidly reacting solvent streams, the spray dryer generally needs to be equipped with additional separate inlet channels.<sup>30</sup> In this work, we use a microfluidic device with an array of two flow-focusing cross junctions, as shown in Figure 1.

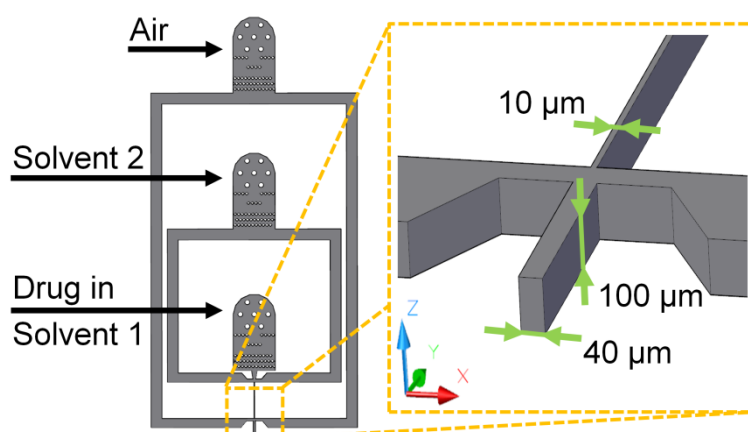


Figure 1: Schematic of a microfluidic device for forming nanoparticles from hydrophobic drugs by spray drying. The microfluidic device is rendered hydrophilic with an oxygen plasma treatment. The device geometry enables separate injection of two solvent streams of which the spray is formed.

The device enables separate injection of two solvents and provides a third inlet for compressed air to form the spray. For the formation of hydrophobic drug nanoparticles, we dissolve the hydrophobic drug danazol in an organic solvent injected into the first inlet, and inject the second fluid into the second inlet. The two solvents form a jet at the first cross junction, which extends into the second cross junction where compressed air is injected to form the spray. To process hydrophobic drugs, the PDMS device must resist fouling due to adsorption of drug crystals on the microchannel walls.<sup>31,32</sup> This is



especially crucial when starting up the device, as potential backflow of the drug-loaded solvent stream into the anti-solvent reservoir, and vice versa, can cause significant precipitation of the hydrophobic drug in the microchannels. To prevent adsorption of the drug on the microchannel walls, we treat the intrinsically hydrophobic PDMS device with oxygen plasma, as the plasma renders the walls of the device hydrophilic.<sup>33</sup> Although the hydrophilicity of the plasma treated device decreases over time, the channel surface can easily be regenerated in the same manner multiple times. However, for early drug formulation development, the amount of sample is extremely small thus being the limiting factor in such an experiment rather than the duration of a surface plasma treatment. In addition, we minimize the surface contact between the drug-loaded solvent stream and the channel walls. We achieve this by designing a device geometry with a high aspect ratio. The ratio  $h/w$  is 10:1 in the upper half of the device and 4:1 at the spray nozzle. Although high-aspect-ratio channel geometries are generally known to increase surface interactions,<sup>34</sup> microchannels with a high aspect ratio are less pressure-resistant than square channels, when fabricated in the rather soft PDMS; thus the operating spray dryer channels easily expand, as shown in Figure 2.

To determine the impact of the channel deformation on the flow profile, we process a typical solvent/antisolvent system in our spray dryer and compare the device deformation at low and high pressure. Our observations are supported by computational fluid dynamics (CFD) simulations coupled with fluid-structure interaction (FSI) using COMSOL 4.1.0.185. We design a 3D simulation model of the microfluidic spray dryer considering the solid mechanics of the device described by a linear elastic model and the fluid flow therein described by the Navier-Stokes equations. For the device building material PDMS, which is mixed from the pre-polymer and crosslinker in a ratio of 10:1, Young's modulus is approximately 4 MPa, the Poisson's Ratio is 0.42, and the density is  $920 \text{ kg m}^{-3}$ .<sup>35,36</sup> The model consists of 62713 finite elements with an average mesh quality of 0.8003 on a scale of 0 to 1, where 1 is the highest quality. The model is solved for 401878 degrees of freedom. A detailed discussion of the simulation model and its mathematical background is provided in the ESI<sup>†</sup> for this publication. For the spray experiment at low pressure, we inject isopropyl alcohol (IPA) as the solvent, water as the anti-solvent and compressed air into the first, second and third inlet, respectively, at flow rates of  $1 \text{ mL h}^{-1}$  for the inner phase and  $10 \text{ mL h}^{-1}$  for the middle phase. The air pressure is set to 0.34 bar. For the high-pressure experiment, we increase the flow rates of IPA and

water to  $5 \text{ mL h}^{-1}$  and  $50 \text{ mL h}^{-1}$ , respectively, and set the air pressure to 2.09 bar. At low pressure (0.34 bar), the PDMS device demonstrates minimal deformation and we observe a two dimensional focused flow pattern between the first and second cross junction. However, as we increase the pressure, the PDMS device responds to the internal stress and expands, as shown in the magnified view of Figure 2A. Due to the high aspect ratio, the largest expansion of the microchannels is observed in the side walls of the channels. Image analysis of microscope images shows that the microchannels widen by an average factor of two, as shown in the magnified views in Figure 2A. This deformation strongly influences the flow profile inside the spray dryer, as shown in the corresponding simulations in Figure 2B. As illustrated by the slice plot of the simulated velocity profile, the flow between the first and second cross junction adopts a three dimensional flow pattern, similar to that observed in microfluidic capillary devices.<sup>37</sup> Thereby, the inner phase is surrounded by a protective sheath of the middle phase, as shown in the magnified view of Figure 2A (right). This minimizes the surface contact of the solvent in which the hydrophobic drug is dissolved with the channel walls and prevents fouling of our device.

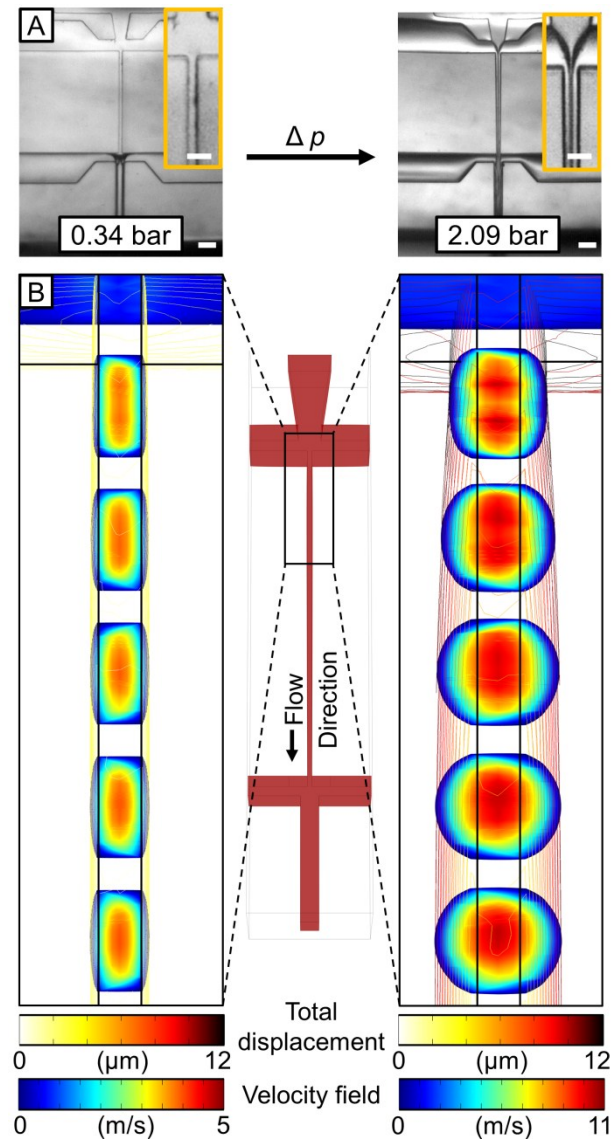


Figure 2: Pressure-induced deformation of the microfluidic spray dryer during operation. (A) Bright-field microscopy images of the microfluidic spray dryer at low pressure (left) and operating pressure (right). The dark fields in the microchannels indicate the curvature of the channel walls causing the light to scatter. The scale bars denote  $20\ \mu\text{m}$ . (B) The impact of the deformation on the flow profile is studied using CFD simulations based on the finite element method. The initial rectangular microchannels (left) expand and adopt a circular shape (right). This deformation changes the flow pattern from a two dimensional focused flow to an elliptic to coaxial flow, therefore reducing the contact between the drug-loaded solvent stream and the channels walls. To emphasize the deformation, the simulation model is viewed from an angle of approximately  $30^\circ$  above the second cross junction, and the original position of the microchannel walls is added as black lines to the simulation model.

When forming a spray, the spray shape and drop size are important factors influencing drying, particle size and morphology of the processed drug. To determine drop size and

spray shape, we visualize the spray formation in our spray dryer with a high-speed camera. We inject IPA into the first and second inlet at a total flow rate of  $55 \text{ mL h}^{-1}$ . At low air pressure, the solvent stream is not dispersed into a spray; instead, a jet of liquid is ejected from the spray nozzle and breaks into large droplets due to Rayleigh-Plateau instability, as shown in Figure 3A.<sup>37</sup> As the air pressure is increased beyond 0.5 bar, we observe the formation of a mixture of large drops and finely dispersed drops at the spray nozzle; the onset of spraying can be confirmed by the round full cone pattern adopted by the droplets formed, that appears as a triangular spray pattern in the side view of the high-speed camera. This precise pattern is formed due to turbulences imparted to the liquid prior to the orifice in the short outlet channel. To quantify the spray formation process, we measure the drop size  $d$  as a function of the air pressure  $p$ , as shown in Figure 3B. The drop size decreases linearly with increasing pressure to approximately  $4 \mu\text{m}$  in diameter at 2.1 bar, which is the maximum pressure our spray dryer can withstand without delamination of the plasma-bonded PDMS.

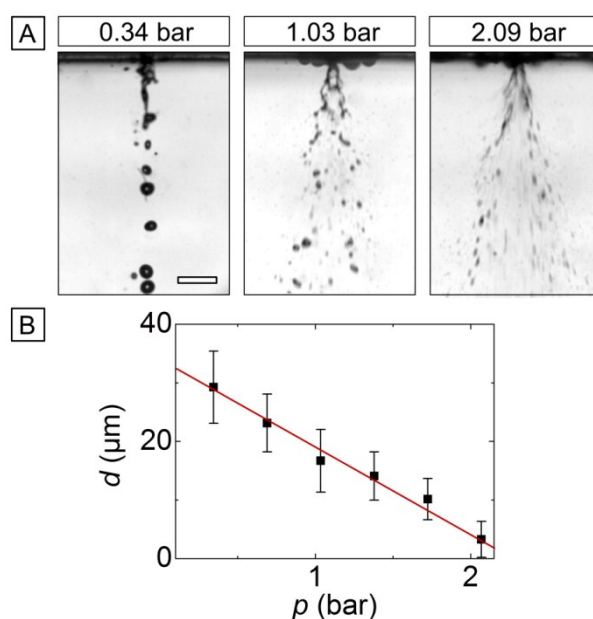


Figure 3: (A) Spray profile of the nozzle for different air pressures. IPA is injected into the spray dryer at  $50 \text{ mL h}^{-1}$ . At low pressure, a fluid jet is ejected from the nozzle which breaks into single droplets downstream. When the pressure is increased beyond 0.5 bar, the spray profile adopts a cone-like shape. The scale bar for all panels denotes  $100 \mu\text{m}$ . (B) Drop diameter as a function of  $p$ . With increasing pressure, the mean size of the droplets decreases linearly. At a pressure of 2.09 bar, the droplets are approximately  $4 \mu\text{m}$  in diameter. The red line is a guide to the eye.

We demonstrate the concept to form hydrophobic drug nanoparticles with our microfluidic spray dryer. Danazol is used as a model drug, which is an isoxazole derivative of testosterone and applied for the treatment of endometriosis and hereditary angioedema.<sup>23</sup> In general, a convenient method for processing hydrophobic drugs is liquid antisolvent precipitation (LASP), where the drug, dissolved in an alcohol, is precipitated by mixing the drug solution with water as the antisolvent.<sup>16,38</sup> We dissolve danazol in isopropyl alcohol and inject it together with water into the first cross junction. As we operate our microfluidic device in the laminar flow regime, only diffusion based mixing of the solvent streams is observed at their interfaces. To evaluate the effect of microfluidic processing alone on the particle size and morphology of the hydrophobic drug, no stabilizer or surfactant is added to influence the particle growth, nor do we use common co-solvents such as DMSO and benzyl alcohol. We set the flow rates to 5 mL h<sup>-1</sup> for danazol, and 50 mL h<sup>-1</sup> for water, which corresponds to a volumetric ratio of 1:10 and has been shown to yield danazol microparticles in conventional LASP processes.<sup>23</sup> The spray is suspended in air, thus ensuring that the product is dried upon collection. We examine the morphology and particle size of the processed drug using scanning electron microscopy (SEM). While unprocessed danazol is composed of particles with irregular shapes ranging from approximately 2 μm to 100 μm, the particle size is reduced significantly by processing the drug using our microfluidic spray dryer. As shown in Figure 4A, we yield danazol nanoparticles with a narrow particle size distribution (PSD) from 20 nm to 60 nm and, therefore, smaller than previously reported.<sup>7,23</sup>

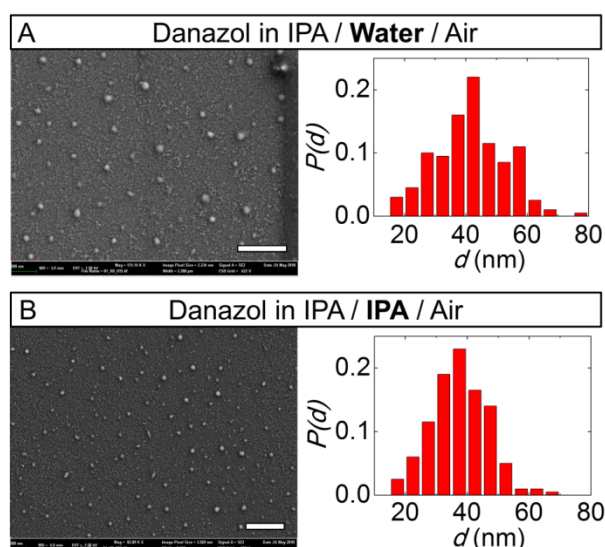
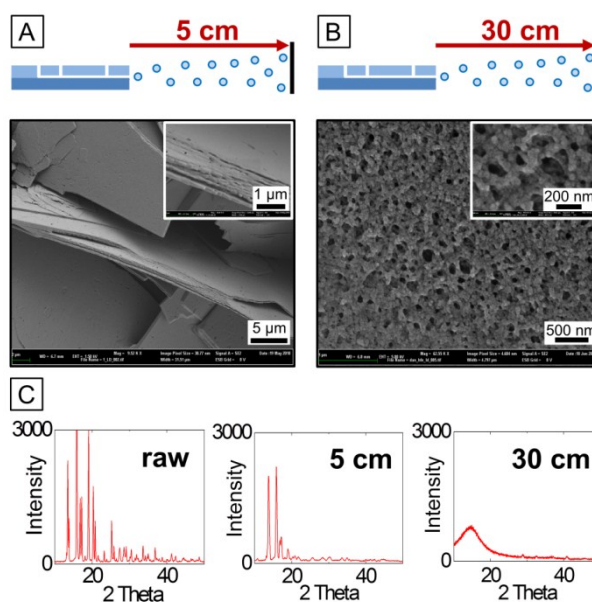


Figure 4: Effect of the solvent system on particle size and composition. Danazol in IPA is mixed with (A) water as the antisolvent, or (B) IPA as the solvent inside the microfluidic spray dryer. In either case, nanoparticles are produced with a narrow PSD and an average diameter of 20-60 nm. Scale bars denote 300 nm.

The formation of drug nanoparticles using LASP is driven by mixing of the drug solution with the antisolvent. Thus, the degree of supersaturation of the drug solution governs nucleation and growth of the drug nanoparticles.<sup>16</sup> However, sufficient mixing only occurs in the short outlet channel prior to the orifice of the spray nozzle in our microfluidic device. Since we use high flow rates to form a stable spray, the delay time of the fluids in the outlet channel should be too short to enable growth of the drug nuclei by mixing. To reveal the formation process, we replace the antisolvent with the solvent, and inject a solution of danazol in IPA and pure IPA into the first and second inlet, respectively. The formation of danazol nanoparticles of identical size and morphology in the absence of the antisolvent indicates that the particle formation is primarily driven by the evaporation of the spray and not by the formation of nuclei due to supersaturation, as shown in Figure 4B. Our hypothesis is further supported by using a microfluidic spray dryer with a longer channel between the first and second nozzle and thus increased time of diffusion, which does not have a significant influence on the particle properties.

Another crucial aspect of the spray drying process is the distance from the spray drying nozzle at which the final product is collected. While it is known that the morphology and size of hydrophobic drugs depends on the initial concentration of reactants, the choice of

additives and the ratio of solvent and antisolvent,<sup>39</sup> we find a significant dependence on the collection distance by performing spatial sampling of the spray. To illustrate this, we inject danazol and IPA as described above, but this time we collect the spray in steps of 5 cm from the spray nozzle. From our SEM analysis, two distinct product morphologies are revealed. At a collection distance of 5 cm, we observe an assembly of stacks of danazol; the thickness of each stack is about 60-80 nm, as shown in Figure 5A. These values are in good agreement with the size of single danazol nanoparticles, as shown in Figure 4A and 4B.



Spatial sampling of processed danazol. Depending on the collection distance, various morphologies are observed; (A) assembly of stacks with a thickness of 60-80 nm, and (B) nanoparticles, approximately 20 nm to 60 nm in diameter, assembled in a dense network. (C) XRD patterns of processed danazol collected at a distance of 5 cm and 30 cm from the spray nozzle, and unprocessed danazol as a reference.

However, as the time of flight is too short to allow for complete evaporation of the spray upon collection, the remaining solvent increases the mobility of danazol particles on the collection substrate, allowing them to fuse and reach an energetically more favourable state.<sup>16</sup> We therefore increase the collection distance to 30 cm; as the spray is completely evaporated, single nanoparticles are formed, that become densely packed over the long time of sample collection, as shown in Figure 5B. X-ray powder diffraction analysis

(XRD) is employed to determine the effect of spatial sampling on the crystallinity of danazol. We use the characteristic peaks at  $2\theta$  of 15.8, 17.1 and 19.0 in the XRD pattern of unprocessed danazol as reference. In processed danazol, the intensity of the characteristic peaks decreases as the collection distance of the spray is increased. This indicates that the initial crystallinity of the drug is not recovered, as shown in Figure 5C. The formation of amorphous danazol is of importance, as the difference in physicochemical properties of the amorphous form significantly increases the bioavailability of danazol.<sup>23</sup>

Another way to fabricate amorphous hydrophobic drug particles is to co-spray dry the drug and a crystallization inhibitor.<sup>40</sup> As a control experiment, we first co-spray dry danazol in IPA together with water and collect the spray at low distance. As shown before, the spray is not completely evaporated due to the short time of flight. This allows danazol to grow into star-shape crystalline aggregates, as shown in Figure 6A. We use poly(vinylpyrrolidone) (PVP) as a substance for co-spray drying with danazol to fabricate amorphous co-precipitates, as PVP is known to inhibit crystal growth in pharmaceutical formulations.<sup>41-44</sup> We process danazol in IPA together with a 1.5 wt% solution of PVP in water at equal flow rates of  $25 \text{ mL h}^{-1}$ . Again, the spray is collected at short distance. However, as the spray is dried, danazol precipitates from the spray in a combination with PVP without crystallization, thus no characteristic peaks are observed in the XRD pattern, as shown in Figure 6B.



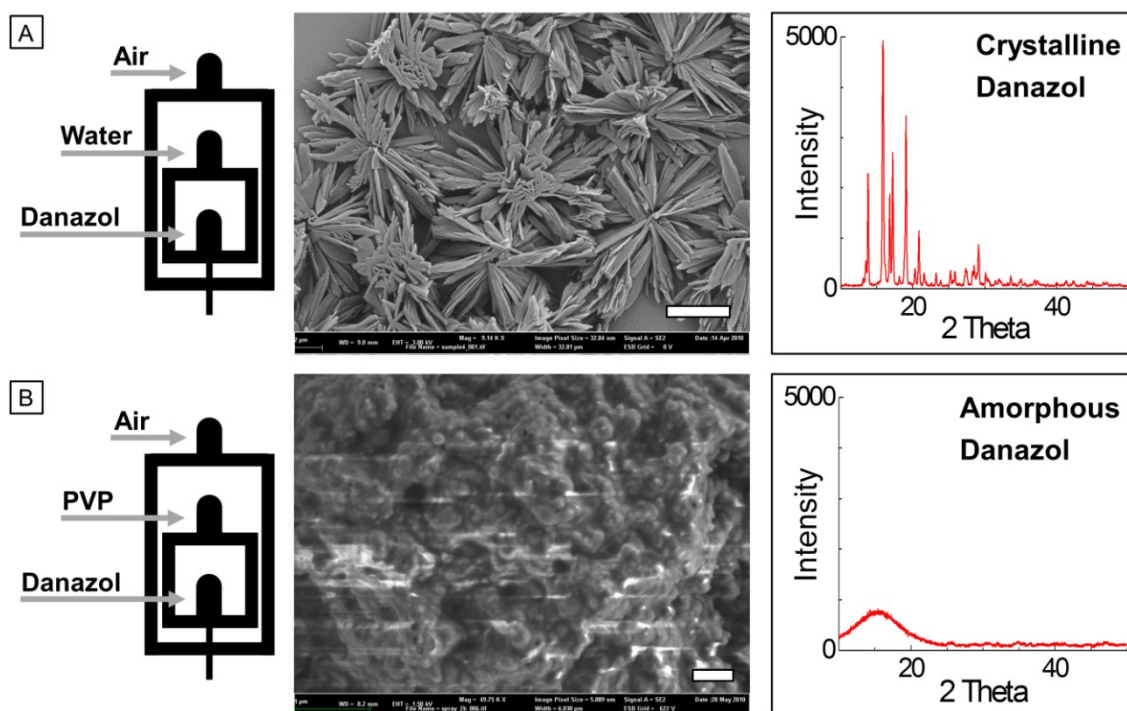


Figure 6: Inhibition of danazol crystallization by PVP. (A) Danazol in IPA is mixed with water inside the microfluidic device; the spray is collected at a distance of 1 cm from the nozzle, allowing danazol to grow into crystalline aggregates, as indicated by the XRD pattern. The scale bar is 5  $\mu\text{m}$ . (B) By processing danazol in IPA and an aqueous solution of PVP, which are injected separately into our spray dryer, amorphous co-precipitates are yielded, as indicated by the corresponding XRD pattern. Scale bar denotes 500 nm.

To relate the performance of our microfluidic spray dryer to conventional spray dryers, we perform spray drying experiments with the same formulations and compare the results by XRD and SEM. We use the well-established and widely known Mini Spray Dryer B-191 (Buechi, Germany) with a spray rate of  $10 \text{ mg min}^{-1}$ , and process a solution of danazol in IPA without and with PVP, respectively. In both cases, we yield particles ranging from approximately  $1 \mu\text{m}$  to  $5 \mu\text{m}$ , which are substantially larger than the danazol particles formed with our microfluidic spray dryer. Moreover, the degree of crystallinity of the resultant danazol particles without PVP is high, as shown in Figure 7A. We assume that the smaller drop and particle size is achieved due to the well-controllable flow conditions in the microfluidic device and the use of pulsation-free syringe pumps, which enable a degree of control over the spray formation and mixing prior to the nozzle that cannot be achieved in conventional macro-sized setups. Thereby, a higher degree of control over the early stage of nucleation and growth due to short mixing times in the

micron-sized environment of our device eventually leads to the formation of particles below 100 nm, as we have observed in our studies.

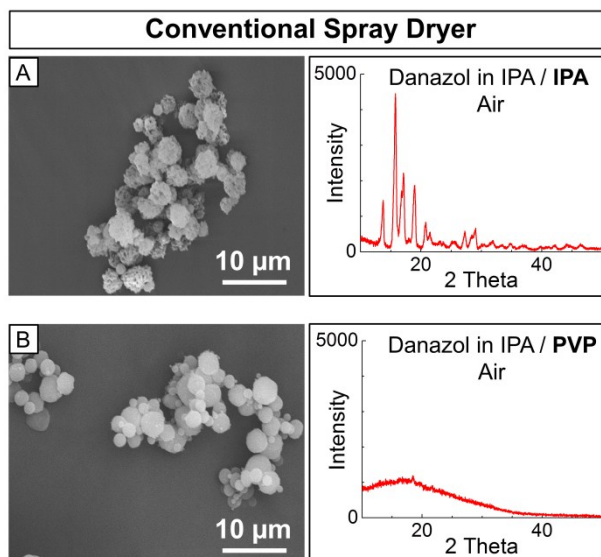


Figure 7: Fabrication of danazol particles and danazol/PVP co-precipitates in a conventional spray dryer using the same formulations as in our microfluidic device. (A) Instead of amorphous drug nanoparticles, crystalline particles, and (B) microscopic co-precipitates are yielded.

## Experimental

### Device Fabrication

The PDMS microfluidic devices are fabricated using soft lithography.<sup>27</sup> All channels have a fixed height of 100  $\mu\text{m}$ . The PDMS replica is bonded to a flat sheet of cured PDMS using oxygen plasma treatment. The plasma treatment renders the microchannels temporarily hydrophilic.<sup>33</sup> To retain the hydrophilic surface modification, suitable for handling hydrophobic drugs, the device is flushed with deionized water. The nozzle of the spray dryer is prepared by slicing the outlet channel of the stamped device with a razor blade. To achieve reproducible accuracy when slicing, we include a guide to the eye in the initial AutoCAD design of the spray dryer.

### **Spray drying experiments**

PVP (weight-averaged molecular weight, MW 10000 g mol<sup>-1</sup>) and all other chemicals are obtained from Sigma-Aldrich Co. unless noted otherwise. Danazol (99.9 %) is obtained from Selectchemie AG. Water with a resistivity of 16.8 MΩcm<sup>-1</sup> is prepared using a Millipore Milli-Q system. All solutions are filtered through a 0.2 μm PTFE filter (Millipore). We form danazol nanoparticles using our microfluidic spray dryer. To demonstrate long term stability of the process, each experiment is performed over a time period of 2 h. We inject a saturated solution of danazol in IPA into the first inlet and water or IPA into the second inlet at 5 mL h<sup>-1</sup> and 50 mL h<sup>-1</sup>, respectively. For the formation of co-precipitates, we inject PVP in water (1.5 % w/w) at 50 mL h<sup>-1</sup> into the second inlet. We fill the PE tubing that connects the syringe pumps with the device with pure IPA to prevent precipitation of the drug in the event of back flow of the drug-loaded solvent stream into the second solvent reservoir, and vice versa. To form the spray, air is injected into the third inlet at 2.09 bar. The spray is ejected into air and dried at room temperature. We image the spray using a Phantom v9.1 camera (Vision Research) at 64000 fps. The droplet size is obtained by measuring the size of at least 200 drops from high-speed camera images.

### **Product collection and characterization**

Processed danazol is collected at distances between 5 cm and 30 cm from the spray nozzle. For SEM analysis, the spray is collected on glass slides and coated with Pd/Pt. We use an Ultra55 Field Emission SEM (Zeiss). The size distribution of the nanoparticles is determined by image analysis of SEM photographs using a public domain, Java-based image processing program, ImageJ. For XRD analysis and long-term experiments, samples are collected in an aluminium box over which the spray dryer is mounted. Due to the full-cone spray pattern, the dried product assembles in a circular pattern solely on the bottom of the collection box from which it is recovered in 70 % to 95 % yield. XRD analysis is performed using a Scintag XDS2000 powder diffractometer (Scintag, Cupertino, California, USA) with Cu Kα radiation at 40 kV and 30 mA. The XRD patterns are taken at room temperature in the range of 10° ≤ 2θ ≤ 50° with a scan rate of 1° min<sup>-1</sup> and a step size of 0.02°.

## Conclusions

Our microfluidic spray dryer is a versatile novel tool for early formulation development of new drug candidates. Precisely controlled generation of amorphous drug nanoparticles can successfully be realized requiring only small quantities of sample. The particles exhibit narrow size distribution and low mean particle sizes. By independent injection of two solvent streams, drug co-precipitates can be prepared as well. Our approach should also be useful for forming composite nanoparticles with freely tunable composition. As the spray is dried at room temperature, our microfluidic device also enables processing of thermally degradable materials. In addition, nanosuspensions, which can greatly enhance the dissolution rate and bioavailability of hydrophobic drugs, can be easily prepared by spraying the nanoparticles into a stabilizer solution. Therefore, our approach not only enables the formation of nanoprecipitates with a small particle size, but also improves the versatility of spray drying for manipulating the composition of the resultant nanoparticles. Design and fabrication of spray drying devices is easy and inexpensive, thereby allowing customized design for each formulation and disposal of the whole chip after use. As drug candidates during their early development phase lack a complete toxicological profile, this aspect is more than valuable contributing to safety and protection during development of new pharmaceuticals.

## Acknowledgements

We thank Christian Holtze and Jim Wilking for helpful discussions and COMSOL AB for technical support. This work was supported by BASF, the NSF (DMR-0602684), the Harvard MRSEC (DMR-0820484), and the Massachusetts Life Sciences Center. Experiments were performed in part at the Center for Nanoscale Systems (CNS), which is supported by the NSF (ECS-0335765). JT received funding from the Fund of the Chemical Industry (Germany) and MW was funded by the German Academic Exchange Service.

## References

- (1) Masi, J. A., Hansen, R. W., Grabowski, H. G. *J. Health Econ.* **2003**, *22*, 151-185.
- (2) Kola, I., Landis, J. *Nature Rev. Drug Discov.* **2004**, *3*, 711-715.
- (3) Kubinyi, H. *Nat. Rev. Drug Discov.* **2003**, *2*, 665-668.
- (4) Chen, X. Q., Autnan, M. D., Gesenberg, C., Gudmundsson, O. S. *AAPS PharmSciTech* **2006**, *8*, E402-208.
- (5) Chen, X., Vaughn, J. M., Yacaman, M. J., Williams III, R. O., Johnston, K. P. *J. Pharm. Sci.* **2004**, *93*, 1867-1878.
- (6) Rabinow, B. E. *Nat. Rev. Drug Discovery* **2004**, *3*, 785-796.
- (7) Panagiotou, T., Mesite, S. V., Fisher, R. J. *Ind. Eng. Chem. Res.* **2009**, *48*, 1761-1771.
- (8) Schuffenhauer, A., Brown, N., Selzer, P., Ertl, P., Jacoby, E. *Ind. Eng. Chem. Res.* **2006**, *46*, 525-535.
- (9) Venkatesh, S., Lipper, R. A. *J. Pharm. Sci.* **2000**, *89*, 145-154.
- (10) Lipinski, C. A., Lombardo, F., Dominy, B. W., Feeney, P. J. *Adv. Drug Del. Rev.* **1997**, *23*, 3-25.
- (11) Huang, L. F., Tony, W. Q. *Adv. Drug Del. Rev.* **2004**, *56*, 321-334.
- (12) Costa, P., Lobo, J. M. S. *Eur. J. Pharm. Sci.* **2001**, *13*, 123-133.
- (13) Gao, L., Zhang, D., Chen, M. *J. Nanopart. Res.* **2008**, *10*, 845-862.
- (14) Merisko-Liversidge, E., Liversidge, G. G., Cooper, E. R. *Eur. J. Pharm. Sci.* **2003**, *18*, 113-120.
- (15) Kesisoglou, F., Panmai, S., Wu, Y. *Adv. Drug Delivery Rev.* **2007**, *59*, 631-644.
- (16) Vehring, R. *Pharm. Res.* **2008**, *25*, 999-1022.
- (17) Chiou, D., Langrish, T. A. G., Braham, R. *J. Food Eng.* **2008**, *86*, 288-293.
- (18) Gonnisson, Y., Goncalves, S. I., Remon, J. P., Vervaet, C. *Drug Dev. Ind. Pharm.* **2008**, *34*, 248-257.
- (19) Paudel, A., Van Humbeeck, J., Van den Mooter, G. *Mol. Pharm.* **2010**, *7*, 113-1148.
- (20) Gao, H., Shi, W., Freund, L. B. *Proc. Natl. Acad. Sci. U.S.A.* **2005**, *102*, 9469-9474.
- (21) Li, X., Anton, N., Arpagaus, C., Belleteix, F., Vandamme, T. F. *J. Controlled Release* **2010**, doi:10.1016/j.jconrel.2010.07.113.
- (22) Ali, H. S. M., York, P., Blagden, N. *Int. J. Pharm.* **2009**, *375*, 107-113.

- (23) Zhao, H., Wang, J.-X., Wang, Q.-A., Chen, J.-F., Yun, J. *Ind. Eng. Chem. Res.* **2007**, *46*, 8229-8235.
- (24) Tetradis-Meris, G., Rossetti, D., de Torres, C. P., Cao, R., Lian, G., Janes, R. *Ind. Eng. Chem. Res.* **2009**, *48*, 8881-8889.
- (25) Miller, P. W., Jennings, L. E., deMello, A. J., Gee, A. D., Long, N. J., Vilar, R. *Adv. Synth. Catal.* **2009**, *351*, 3260-3268.
- (26) Utada, A. S., Lorenceau, E., Link, D. R., Kaplan, P. D., Stone, H. A., Weitz, D. A. *Science* **2005**, *308*, 537-541.
- (27) Xia, Y., Whitesides, G. M. *Angew. Chem. Int. Ed.* **1998**, *37*, 550-575.
- (28) Peterson, S. L., McDonald, A., Gourley, P. L., Sasaki, D. Y. *J. Biomed. Mater. Res. Part A* **2004**, *72A*, 10-18.
- (29) Weibel, D. B., Whitesides, G. M. *Curr. Opin. Chem. Biol.* **2006**, *10*, 584-591.
- (30) Ozeki, T., Beppu, S., Mizoe, T., Takashima, Y., Yuasa, H., Okada, H. *Pharm. Res.* **2006**, *23*, 177-183;
- (31) Mayer, P., Vaes, W. H. J., Hermens, J. L. M. *Anal. Chem.* **2000**, *72*, 459-464.
- (32) Honest, M., Jin, H. K., Kwansseop, L., Nokyoung, P., Jong, H. H. *Electrophoresis*, **2003**, *24*, 3607-3619.
- (33) Kim, B., Peterson, E. T. K., Papautsky, I. *Proc. 26<sup>th</sup> Annu. Int. Conf. IEEE EMBS*, San Francisco **2004**, 5013-5016.
- (34) Mao, P., Han, J. *Lab Chip* **2009**, *9*, 586-591.
- (35) Deuschle, J. K., Buerki, G., Deuschle, H. M., Enders, S., Michler, J., Arzt, E. *Acta Mater.* **2008**, *56*, 4390-4401.
- (36) Armani, D., Liu, C., Aluru, N. *12<sup>th</sup> Int. Conf. IEEE MEMS* **1999**, 222-227.
- (37) Utada, A. S., Chu, L.-Y., Fernandez-Nieves, A., Link, D. R., Holtze, C., Weitz, D. A. *Mater. Res. Soc. Bull.* **2007**, *32*, 702-708.
- (38) Zhang, J.-Y., Shen, Z.-G., Zhong, J., Hu, T.-T., Chen, J.-F., Ma, Z.-Q., Yun, J. *Int. J. Pharm.* **2006**, *323*, 153-160.
- (39) Škapin, S. D., Matijević, E. *J. Colloid Interface Sci.* **2004**, *272*, 90-98.
- (40) Wong, S. M., Kellaway, I. W., Murdan, S. *Int. J. Pharm.* **2006**, *317*, 61-68.
- (41) Sekikawa, H., Nakano, M., Arita, T. *Chem. Pharm. Bull.* **1978**, *26*, 118-126.
- (42) Yoshioka, M., Hancock, B. C., Zografí, G. *J. Pharm. Sci.* **1995**, *84*, 983-986.
- (43) Taylor, L. S., Zografí, G. *Pharm. Res.* **1997**, *14*, 1691-1698.
- (44) Kim, J.-H., Choi, H.-K. *Int. J. Pharm.* **2002**, *236*, 81-85.

## Supplemental information

This supplemental information contains details of the simulation model that has been developed to study the deformation of the channel geometry of our microfluidic spray dryer and its impact on the flow profile inside the device.

Analysis of the flow pattern of a flow-focused aqueous solution of Rhodamine B in a microfluidic device shows that the surface contact between the dye solution and the channel walls decreases with increasing channel height, as shown in Figure S1.

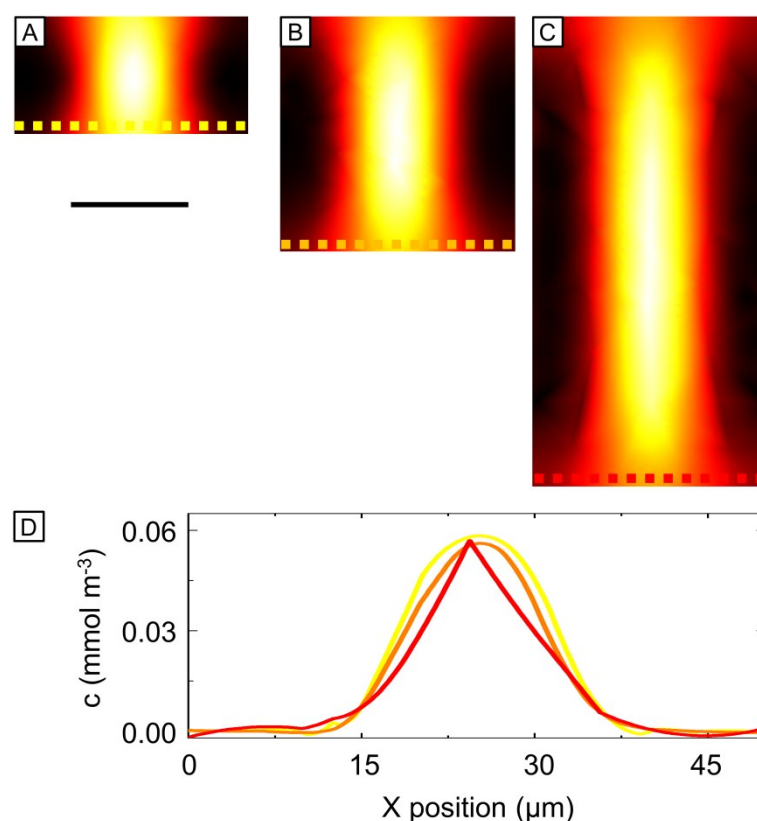


Figure S1: Finite element simulation of a flow-focused fluid stream of Rhodamine B in water in microchannels with a constant width of 50 μm and varying heights of (A) 25 μm, (B) 50 μm and (C) 100 μm. The plane-cuts, which show the concentration profile of Rhodamine B, and (D) the corresponding line scans reveal that the surface contact between the substance and the microchannel walls decreases from low to high aspect ratios. The scale bar denotes 25 μm.

We analogously develop a device with a high aspect ratio to minimize the surface contact of the danazol-loaded solvent stream with the channel walls. Thus, fouling of the device due to adsorption of the hydrophobic drug on the microchannel walls can be prevented.

However, PDMS microchannels with a high-aspect ratio are less pressure-resistant than squared channels and expand at high flow rates and high air pressure. To study the impact of the channel deformation on the flow profile, we use COMSOL Multiphysics v4.1.0.185, which allows simulating coupled multiphysics problems, such as the solid mechanics of PDMS that are coupled with the fluid dynamics in the case at hand. The tasks for developing the simulation model are illustrated in Figure S2.

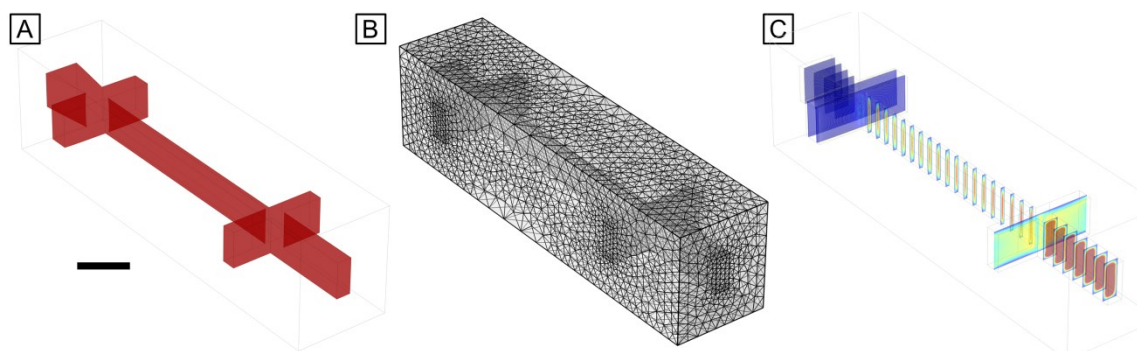


Figure S2: Towards the simulation of the fluid flow inside the microfluidic spray dryer at low flow rates and low air pressure: (A) Import of the 3D device geometry drawn in AutoCAD 2011, (B) mesh generation and (C) solution of the model. The scale bar denotes 100  $\mu\text{m}$ .

In a first step, a model of the device section of interest, which we design using AutoCAD 2011, is imported to COMSOL. Thereafter, the boundary conditions are assigned to the microchannel walls, the inlets and the outlet of the device assuming stationary conditions. Thereby, the fluid dynamics are described by the Navier-Stokes equations which can be simplified assuming incompressible fluids, thus  $\rho = \text{const.}$ <sup>1</sup>

$$\rho \nabla \cdot \mathbf{u} = 0$$

$$\rho \frac{\partial \mathbf{u}}{\partial t} + \rho (\mathbf{u} \cdot \nabla) \mathbf{u} = \nabla \cdot [-p \mathbf{I} + \mu (\nabla \mathbf{u} + \nabla \mathbf{u}^T)] + \mathbf{F}$$

with the density of the fluid  $\rho$ , the pressure  $p$ , the identity matrix  $\mathbf{I}$ , the dynamic viscosity of the fluid  $\mu$ , the velocity field  $\mathbf{u}$  and the volume force  $\mathbf{F}$ . The deformation of PDMS is simulated using COMSOL's linear elastic model which involves the following equations:<sup>1</sup>



$$-\nabla \cdot \boldsymbol{\sigma} = \mathbf{F}_v$$

$$\boldsymbol{\sigma} = (\mathbf{S} \cdot (\mathbf{I} + \nabla \mathbf{u}))$$

$$\mathbf{S} - \mathbf{s}_0 = \mathbf{C} : (\boldsymbol{\varepsilon} - \alpha(T - T_{\text{Ref}}) - \boldsymbol{\varepsilon}_0)$$

$$\boldsymbol{\varepsilon} = \frac{1}{2} (\nabla \mathbf{u}^T + \nabla \mathbf{u} + \nabla \mathbf{u}^T \nabla \mathbf{u})$$

with the stress tensor  $\mathbf{S}$ , the strain tensor  $\boldsymbol{\varepsilon}$ , the 4th order elasticity tensor  $\mathbf{C}$ , the initial stresses  $\mathbf{s}_0$ , the initial strains  $\boldsymbol{\varepsilon}_0$ , the thermal expansion tensor  $\alpha$  and the (reference) temperature  $T$  ( $T_{\text{Ref}}$ ). The specific material properties are then defined, as listed in Table S1.

Name	Value
Young's modulus ( $E_{\text{PDMS}}$ ) <sup>2</sup>	4 MPa
Poisson's ratio ( $\nu_{\text{PDMS}}$ ) <sup>2</sup>	0.42
Density of PDMS ( $\rho_{\text{PDMS}}$ ) <sup>3</sup>	920 kg m <sup>-3</sup>
Density of water ( $\rho_{\text{Water}}$ ) <sup>4</sup>	998.2 kg m <sup>-3</sup>
Dynamic viscosity ( $\eta_{\text{Water}}$ ) <sup>4</sup>	1.002 · 10 <sup>-3</sup> kg m <sup>-1</sup> s <sup>-1</sup>
Main channel inlet ( $v_{\text{MC,slow}}$ )	0.02867 m s <sup>-1</sup>
Side channel inlet ( $v_{\text{SC,slow}}$ )	0.2525 m s <sup>-1</sup>
Pressure ( $p_{\text{slow}}$ )	0.34 bar
Main channel inlet ( $v_{\text{MC,fast}}$ )	0.1434 m s <sup>-1</sup>
Side channel inlet ( $v_{\text{SC,fast}}$ )	1.263 m s <sup>-1</sup>
Pressure ( $p_{\text{fast}}$ )	2.09 bar

Table S1: Material properties used in the simulation model.

The model is solved for 62713 finite elements and 401878 degrees of freedom using a multifrontal massively parallel solver (MUMPS). The average element quality of the mesh is 0.8003 on a scale from 0 to 1, where 1 is the highest quality; the minimal element quality is 0.3903. Using a Windows 7 x64 machine with two quad-core Intel® Xeon® E5440 processors operating at 2.83 GHz and an internal memory of 32 GB RAM, the less complex model of the microfluidic spray dryer at low flow rates and low pressure is solved in 1307 s, and the model of the microfluidic device operating at high flow rates and high air pressure is solved in 2700 s.

### References

- (1) COMSOL AB *MEMS Module User's Guide*, COMSOL AB, Version 4.1, **2010**, 174-184; 279-321.
- (2) Deuschle, J. K., Buerki, G., Deuschle, H. M., Enders, S., Michler, J., Arzt, E. *Acta Mater.* **2008**, *56*, 4390-4401.
- (3) Armani, D., Liu, C., Aluru, N. *12<sup>th</sup> Int. Conf. IEEE MEMS*, **1999**, 222-227.
- (4) Weast, R., Astle, M. *Handbook of Chemistry and Physics*, CRC Press, Boca Raton, 60<sup>th</sup> edn., **1979**, F-11, F-49.

## 8 List of Publications

1. U. E. A. Fittschen, F. Meirer, C. Strelt, P. Wobrauschek, J. Thiele, G. Falkenberg, G. Pepponi, *Spectrochim. Acta, Part B* **2008**, *63*, 1489-1495.  
“Characterization of atmospheric aerosols using Synchrotron radiation total reflection X-ray fluorescence and Fe K-edge total reflection X-ray fluorescence-X-ray absorption near-edge structure”
2. U. E. A. Fittschen, N. H. Bings, S. Hauschild, S. Förster, A. F. Kiera, E. Karavani, A. Frömsdorf, J. Thiele, G. Falkenberg, *Anal. Chem.* **2008**, *80*, 1967-1977.  
“Characteristics of Picoliter Droplet Dried Residues as Standards for Direct Analysis Techniques”
3. H. C. Shum, J. Thiele, S.-H. Kim, *Advances in Transport Phenomena, Vol. 3*, L. Wang (Ed.), Springer, **2011**, submitted.  
“Microfluidic fabrication of vesicles”

The following papers and communications have been published or submitted during the course of this thesis.

4. H. C. Shum, A. R. Abate, D. Lee, A. Studart, B. Wang, C. Chen, J. Thiele, R. K. Shah, A. Krummel, D. A. Weitz, *Macromol. Rapid Commun.* **2010**, *31*, 108-118.  
“Droplet Microfluidics for Fabrication of Non-Spherical Particles”
5. J. Thiele, D. Steinhauser, T. Pfohl, S. Förster, *Langmuir* **2010**, *26*, 6860-6863.  
“Preparation of Monodisperse Block Copolymer Vesicles via Flow Focusing in Microfluidics”
6. A. R. Abate, J. Thiele, M. Weinhart, D. A. Weitz, *Lab Chip* **2010**, *10*, 1774-1776.  
“Patterning microfluidic device wettability using flow confinement”

7. S. Seiffert, J. Thiele, A. R. Abate, D. A. Weitz, *J. Am. Chem. Soc.* **2010**, *132*, 6606-6609.  
“Smart Microgel Capsules from Macromolecular Precursors”
8. J. Thiele, A. R. Abate, H. C. Shum, S. Bachtler, S. Förster, D. A. Weitz, *Small* **2010**, *6*, 1723-1727.  
„Fabrication of Polymersomes using Double-Emulsion Templates in Glass-Coated Stamped Microfluidic Devices”
9. A. R. Abate, J. Thiele, D. A. Weitz, *Lab Chip* **2011**, *11*, 253-258.  
“One-step formation of multiple emulsions in microfluidics”
10. A. R. Abate, A. Rotem, J. Thiele, D. A. Weitz, *Phys. Rev. E: Stat. Nonlinear Soft Matter Phys.* **2011**, *84*, 031502-1-031502-5.  
“Efficient encapsulation with plug-triggered drop formation”
11. J. Thiele, M. Windbergs, A. R. Abate, M. Trebbin, H. C. Shum, S. Förster, D. A. Weitz, *Lab Chip* **2011**, *11*, 2362-2368.  
“Early development drug formulation on a chip: Fabrication of nanoparticles using a microfluidic spray dryer”
12. J. Thiele, S. Seiffert, *Lab Chip* **2011**, *11*, 3188-3192.  
“Double Emulsions with Controlled Morphology by Microgel Scaffolding”
13. T. Liu, S. Seiffert, J. Thiele, A. R. Abate, D. A. Weitz, W. Richtering, *Proc. Natl. Acad. Sci. USA* **2011**, accepted.  
“Non-Coalescence of Oppositely Charged Droplets in Stimuli-Sensitive Emulsions”
14. J. Thiele, M. Trebbin, J. Perlich, D. Steinhauser, S. Förster, in preparation.  
“Perpendicular orientation of cylinder micelles in microchannels”

## 8.1 Non-peer-reviewed publications

1. A. R. Abate, S. Seiffert, A. S. Utada, A. Shum, R. Shah, J. Thiele, W. J. Duncanson, A. Abbaspourad, M. H. Lee, I. Akartuna, D. Lee, A. Rotem, D. A. Weitz,  
[http://weitzlab.seas.harvard.edu/publications/Bookchapter\\_Microfluidic\\_techniques.pdf](http://weitzlab.seas.harvard.edu/publications/Bookchapter_Microfluidic_techniques.pdf)  
“Microfluidic techniques for synthesizing particles”
2. D. A. Weitz, J. Thiele, A. R. Abate, Pub. No. WO/2011/028764.  
“Multiple Emulsions Created Using Jetting and Other Techniques”
3. A. R. Abate, J. Thiele, D. A. Weitz, C. Holtze, M. Windbergs, U.S. Patent Application Serial No. 61/485026, filed 05/11/11 (not yet published).  
“Spray Drying Techniques”
4. J. Thiele, M. Trebbin, S. With, V. Körstgens, M. Rawolle, G. Benecke, G. Herzog, M. Schwartzkopf, A. Buffet, J. Perlich, P. Müller-Buschbaum, S. V. Roth and S. Förster, *HASYLAB Annual Report 2011*, submitted.  
“Shear orientation in microfluidic channels investigated at the microfocus beamline MiNaXS/P03 at PETRA III”
5. M. Rawolle, V. Körstgens, M. A. Ruderer, E. Metwalli, S. Guo, M. Trebbin, S. With, J. Thiele, G. Herzog, G. Benecke, M. Schwartzkopf, A. Buffet, J. Perlich, S. V. Roth, P. Lellig, J. S. Gutmann, and P. Müller-Buschbaum, *HASYLAB Annual Report 2011*, submitted.  
“Comparison of grazing incidence small angle X-ray scattering of a titania thin film sponge structure at BW4 (DORIS III) and P03 (PETRA III)”
6. V. Körstgens, M. Rawolle, A. Buffet, G. Bennecke, G. Herzog, J. Perlich, M. Schwartzkopf, M. Trebbin, J. Thiele, S. With, F. J. de Jong, M. Schlüter, S. V. Roth, S. Förster, and P. Müller-Buschbaum, *HASYLAB Annual Report 2011*, submitted.

## 8.1 Non-peer-reviewed publications

---

“Flow induced surface attachment of gold nanoparticles - an in situ x-ray investigation with micro-fluidic cell”

7. M. Rawolle, V. Körstgens, M. Trebbin, S. With, J. Thiele, G. Herzog, G. Benecke, M. Schwartzkopf, A. Buffet, J. Perlich, S. V. Roth, T. Fröschl, N. Hüsing and P. Müller-Buschbaum, *HASYLAB Annual Report 2011*, submitted.  
“In-situ sol-gel templating in a micro-fluidic cell probed at beamline P03 (PETRA III)”

## 8.2 Conference presentations

1. J. Thiele  
“Polymersome formation in glass-coated PDMS microfluidics”  
Oral presentation at “Annual meeting of the FCI fellows”, October 09, 2009, Oldenburg (GER).
2. J. Thiele, M. Trebbin, S. Förster  
“Preparation of monodisperse block copolymer vesicles via flow focusing in microfluidics”  
Poster presentation at “44<sup>th</sup> Meeting of the German Colloid Society”, September 28-30, 2009, Hamburg (GER).
3. J. Thiele, H. C. Shum, S. Förster, D. A. Weitz  
“Polymersome formation in glass-coated PDMS microfluidics”  
Poster presentation at “APME 2009”, October 4-7, 2009, Dresden (GER).
4. M. Windbergs, J. Thiele, D. A. Weitz  
“Controlled coalescence as an approach to formulate monodisperse hydrogel particles with high drug load”  
Poster presentation at “AAPS Annual Meeting and Exposition and FIP Pharmaceutical Sciences World Congress”, November 14-18, 2010, New Orleans (USA).
5. J. Thiele, M. Trebbin, S. With, J. Perlich, S. Förster  
“Shear orientation in microfluidic channels”  
Poster presentation at “Makromolekulares Kolloquium 2011”, February 23-26, 2011, Freiburg (GER).

## 9 Acknowledgements

I thank all the people who contributed to this work. First and foremost, I express my sincere gratitude to my supervisors *Prof. Stephan Förster* and *Prof. David A. Weitz* for giving me the opportunity to work on both interesting and challenging topics, whilst leaving me the freedom needed for the implementation of this thesis. I very much appreciate their contributions of time and funding, not to forget their guidance in scientific writing. It has been a real pleasure working with them. I am also indebted to *Dr. Adam Abate* who guided my first steps at Harvard University. His never-ending willingness to provide help and advice are gratefully acknowledged, as is his careful proof-reading of the manuscripts.

In addition, I thank my close colleagues and coworkers at the School of Engineering and Applied Sciences/Department of Physics (Harvard University), at the Max-Planck-Institute for Dynamics and Self-Organization (Göttingen), at the Institute of Physical Chemistry (University of Bayreuth) for providing support and a pleasant atmosphere as well as for sharing their knowledge and scientific expertise. In particular, I thank *Sebastian With* who contributed to this work as an undergraduate student, all other members of the research group of Prof. Förster in Bayreuth and, especially, *Stephan Hauschild*. Past group members that I have had the pleasure to work with or alongside at the Institute of Physical Chemistry in Hamburg are *Christine Barkmann*, *Melanie “Melle” Benken*, *Stephanie Domes*, *Volkan Filiz*, *Steffen Fischer*, *Martin Kehden*, *Ulf König*, *Isabell Mattern*, *Andreas Meyer*, *Jasmin Nitsche*, *Carsten Schellbach*, *Nina Schober*, *Kathrin Zielske* and – finally – *Sigrid “Sigi” Zeckert* who managed my university business and kept me updated during my time in the Weitz lab.

I am particularly thankful to my colleagues and friends *Simone Bachtler*, *Maike Windbergs* and *Sebastian Seiffert* for their ongoing support, encouragement and scientific guidance - not to forget the lasting memories from our time in the U.S. Lastly, I express my deepest gratitude to my family and friends for their continuous support during all those years. I truly appreciate everything you have done for me!

Parts of the present work were funded by the German Academic Exchange Service (DAAD) and the Fund of the Chemical Industry (FCI), which is gratefully acknowledged.

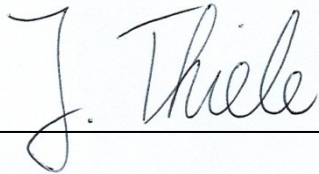


## 10 Declaration / Erklärung

I hereby declare that I am the sole author of this doctoral thesis; no other sources have been used in this work than those stated above. This work has neither previously been submitted to the Faculty of Biology, Chemistry and Earth Sciences at the University of Bayreuth nor to any other scientific institution for the purpose of a doctoral thesis.

Hiermit versichere ich, dass ich die vorliegende Arbeit selbständig und ausschließlich unter Verwendung der angegebenen Hilfemittel und Quellen angefertigt habe. Diese Arbeit wurde bisher weder an der Fakultät für Biologie, Chemie und Geowissenschaften der Universität Bayreuth noch an einer anderen wissenschaftlichen Einrichtung zum Zwecke der Promotion eingereicht.

Bayreuth, den 15.04.2011



A handwritten signature in black ink, reading "J. Thiele", is written over a horizontal line. The signature is cursive and appears to be on a light blue background.